

Analysis of a model microswimmer with applications to blebbing cells and mini-robots

Qixuan Wang · Hans G. Othmer

October 7, 2018

Contents

1	Introduction	2
2	Swimming at low Reynolds number	5
3	The solitary PMPY swimmer	6
3.1	Scaling the PMPY problem	7
3.2	The reflection method and the Rotne-Prager-Yamakawa approximation	8
3.3	Power expenditure and the performance of a PMPY	12
3.4	A comparison of the solutions	14
4	A PMPY swimmer in the presence of a passive buoyant obstacle	16
4.1	The linear and angular velocities after the first reflection	16
4.2	Accuracy of the system	18
4.3	Chasing an object	19
4.4	Tracer trajectories	20
5	Swimming with a friend	25
5.1	Preliminary analysis of the two-swimmer system	27
5.2	Hydrodynamic interactions between two PMPY swimmers on a line	29
5.3	Hydrodynamic interaction between two PMPY models swimming in a plane	32
6	Extended scallop theorem and mixed controls	35
7	Discussion	37
	Appendices	38
A	Newtonian flow produced by the translation and radial expansion of a sphere	38

Supported in part by NSF Grants DMS 0817529 and 1311974 and a grant from the Simons Fdn to H. G. Othmer, and by NIH grant R01GM107264 and NSF grant DMS1562176 to Qing Nie

Qixuan Wang
540R Rowland Hall
University of California, Irvine
Tel.: (949) 824-3217
E-mail: qixuanw@uci.edu

Hans G. Othmer
School of Mathematics, 270A Vincent Hall
University of Minnesota
Tel.: (612) 624-8325
Fax: (612) 626-2017
E-mail: othmer@math.umn.edu

B	Accuracy of $U_i^{(e)}$ after incorporating the second reflection	39
C	Calculation of $\Omega_{3,i}^{(1)}$	41
D	Numerical scheme of two PMPY models	41
E	Asymptotic analysis of the three systems consisting of two hobbled PMPYs	43
E.1	System A (two dumb-bells) with controls in $(\dot{l}_I, \dot{l}_{II})$	43
E.2	System B with controls in (\dot{R}_1, \dot{R}_3)	45
E.3	System C with controls in (\dot{l}_I, \dot{R}_3)	47

Abstract Recent research has shown that motile cells can adapt their mode of propulsion depending on the environment in which they find themselves. One mode is swimming by blebbing or other shape changes, and in this paper we analyze a class of models for movement of cells by blebbing and of nano-robots in a viscous fluid at low Reynolds number. At the level of individuals, the shape changes comprise volume exchanges between connected spheres that can control their separation, which are simple enough that significant analytical results can be obtained. The goal is to understand how the efficiency of movement depends on the amplitude and period of the volume exchanges when the spheres approach closely during a cycle. Previous analyses were predicated on wide separation, and we show that the speed increases significantly as the separation decreases due to the strong hydrodynamic interactions between spheres in close proximity. The scallop theorem asserts that at least two degrees of freedom are needed to produce net motion in a cyclic sequence of shape changes, and we show that these degrees can reside in different swimmers whose collective motion is studied. We also show that different combinations of mode sharing can lead to significant differences in the translation and performance of pairs of swimmers.

Keywords Low Reynolds number swimming · Self-propulsion · Amoeboid swimming · Robotic swimmers · *pushmepullyou* · reflection method

1 Introduction

Locomotion of cells, both individually and collectively, is an important process in development, tissue regeneration, the immune response, cancer metastasis, and wound healing. The motion of an individual cell is classified as either mesenchymal or amoeboid, depending on how it interacts mechanically with its environment (Binamé *et al.* 2010). The mesenchymal mode is used by cells such as fibroblasts that have a well-organized cytoskeleton, which comprises the actin filaments, intermediate filaments, and microtubules, and use strong adhesions to transmit force to their surroundings via integrin-mediated adhesion complexes. Mesenchymal movement usually involves the extension of broad flat lamellipodia and/or pseudopodia and is driven by actin polymerization at the leading edge. Amoeboid motion involves a less structured cytoskeleton and weaker surface interactions, and leads to speeds up to forty times faster than those resulting from mesenchymal motion (Renkawitz & Sixt 2010). In this mode cells may use pseudopodia, but can also use protrusions such as blebs (Figure 1) which involve blister-like extensions of the membrane. Leukocytes, which normally use the mesenchymal mode in the extracellular matrix (ECM), can migrate *in vivo* in the absence of integrins, using a ‘flowing and squeezing’ mechanism (Lämmermann *et al.* 2008). Cells of the slime mold *Dictyostelium discoideum* (Dd) can move either by extending pseudopodia or by blebbing, and they monitor the stiffness of their surroundings to determine the mode: pseudopodia in a compliant medium and blebbing in stiffer media (Zatulovskiy *et al.* 2014). Furthermore, blebbing cells are efficient in their chemotactic response to cyclic-AMP, producing nearly all of their blebs up-gradient. In certain tumor cells, knockdown of secreted MMPs, which are enzymes that degrade the ECM, produces only a small reduction in speed because cells compensate for the decreased proteolysis by undergoing a ‘mesenchymal-to-amoeboid transition (MAT) (Wolf *et al.* 2003, Friedl & Wolf 2003). The MAT can also be triggered by changes in the

adhesiveness of the ECM (Friedl & Alexander 2011, van Zijl *et al.* 2011). Moreover, cells such as Dd and neutrophils can swim in a fluid environment (Barry & Bretscher 2010), and a model of swimming by such cells appears in Wang & Othmer (2016). In fact, some cells move only by blebbing. Certain carcinoma cells in suspension spontaneously polarize and forms blebs at the leading edge, and while they cannot move on 2D substrates, they can move in 3D (Bergert *et al.* 2012).

Thus numerous cell types display enormous plasticity in the choice of locomotory mode, in that they sense the mechanical properties of the environment and adjust the balance between the modes by adjusting the balance between signal transduction pathways that control the structure of the cytoskeleton (Renkawitz *et al.* 2009, Bergert *et al.* 2012, Fackler & Grosse 2008). Crawling and swimming are the extremes on a continuum of strategies, but cells sense their environment and use the most efficient strategy in a given context. While blebbing is frequently thought of as a 'push-pull' mechanism in which a cell expands at the front, followed by contraction at the rear, another type of blebbing called 'stable-bleb migration', has recently been observed in progenitor cells of the gastrulating zebrafish embryo (Maiuri *et al.* 2015, Ruprecht *et al.* 2015). In this mode cells form a balloon-like protrusion at their front, and these cells can move more rapidly than other cells in the embryo.

The fact that some cells can use very complicated shape changes for locomotion leads to a question posed by experimentalists, which is 'How does deformation of the cell body translate into locomotion?' (Renkawitz & Sixt 2010). Two examples are shown in Fig. 1. In (a) is shown a cell that blebs and moves very little, and in (b) is a Dd cell that uses a combination of blebs at the front and contraction at the rear to move in a tissue-like environment. Fig. 1 (c) shows the different modes used by cells in different environments. In this paper we analyze a simple model of the push-pull type for movement in a fluid by blebbing, motivated by the recent experimental findings mentioned above. Protrusions and other shape changes require forces that must be correctly orchestrated in space and time to produce net motion – protrusions on cells in (a) are not, while those in (b) are – and to understand this orchestration one must couple the cellular dynamics with the dynamics of the surrounding fluid or ECM.

At the spatial scale of cells and the speeds at which they move, the exterior fluid problem is a low Reynolds number (LRN) flow. LRN flows have been extensively studied in the context of bacterial and sperm movement. Taylor (1952) treated the flagellum as an infinite cylinder executing small-amplitude oscillations, and Hancock (1953) developed a large-amplitude theory using singular solutions to the Stokes equations situated along the center line of a flagellum, to describe the motion in three dimensions. This 'slender-body theory' was further developed by Higdon (1979) to account for hydrodynamic interactions between the flagellum and the cell head, and Phan-Thien *et al.* (1987) used the boundary-element method to allow for non-spherical heads and non-slender flagella. The current state of knowledge is reviewed in Elgeti *et al.* (2015).

A separate path in cell locomotion at LRN was stimulated by Purcell's seminal article (Pur-

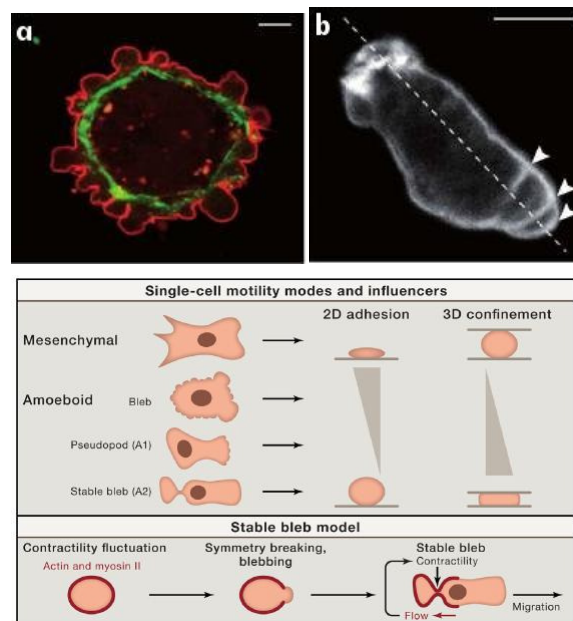


Fig. 1.1 (a) Blebbing on a melanoma cell: myosin (green) localizes under the blebbing membrane (red) (b) The actin cortex of a blebbing Dd cell migrating to the lower right. Arrowheads indicate the successive blebs and arcs of the actin cortex (from Charras & Paluch (2008)). (c) A schematic of the various modes of movement (from Welch (2015)).

cell 1977) and by interest in mini-robots. Several models of LRN swimmers that do not rely on slender-body theory exist. There is *Purcell's two-hinge swimmer*, the Najafi-Golestanian *accordion* model in which three spheres of fixed size are connected by movable links (Najafi & Golestanian 2004, Alexander *et al.* 2009), the *push-me-pull-you* swimmer (PMPY) (Avron *et al.* 2005), in which two spheres that can expand or contract radially are connected by an extensible arm, and a three-sphere volume-exchange or *breather* model in which the spheres are linked by rigid connectors but exchange volume (Wang *et al.* 2012). In Wang & Othmer (2015) we compared the performance of these models, and showed that generally the PMPY model is the most efficient.¹

However, in all analyses of two- or three-sphere models to date, the spheres were treated as point particles that generate point forces, which in effect means that the separation between them is large enough that hydrodynamic interactions between the spheres can be neglected. Thus the conclusions reached in these analyses are not directly applicable to models of cells that swim by blebbing, nor to realistic robotic swimmers. Hydrodynamic interactions between spheres of fixed size have been studied for almost a century, and analytical results are available for a pair of spheres connected by a rigid rod (a dumbbell) (Stimson & Jeffery 1926). Approximation methods for other configurations center on either a truncated multipole expansion of the Green's function or on the method of reflections, both described in Kim & Karrila (1991).

In this paper we use the basic PMPY swimmer as a model of blebbing or for mini-robots to study the swimming behaviors of solitary and group swimmers at LRN. Our objective is to understand the effect of higher-order hydrodynamic interactions between spheres in a PMPY swimmer, and for this we use the reflection method (Kim & Karrila 1991). In section 3 we investigate the difference between the higher-order solution and the asymptotic solution both analytically and numerically, and show that the asymptotic solution may severely underestimate the effectiveness of a PMPY swimmer. There we also compare its swimming behavior to existing experimental data on swimming *Dd* amoebae. In section 4 we apply the reflection method to a system consisting of one active PMPY swimmer and a passive buoyant object. We discuss the hydrodynamic effect of the velocity field generated by the PMPY swimmer on the passive object and vice versa, we numerically investigate how effectively the swimmer can pursue the passive object, and we study the higher-order hydrodynamic effects on a tracer trajectory. In section 5 we apply the reflection method to a system of two PMPY models, one in which the swimmers are collinear and the other a planar system, and we discuss the higher-order hydrodynamic interactions between the two active swimmers. In section 6 we review the *scallop theorem*, which is the fundamental principle of LRN swimming, and discuss how this extends to the hydrodynamic interactions amongst several swimmers, each unable to swim on its own. We also discuss how different combinations of shape change modes affect the collective swimming behavior of such swimmers. Throughout we only consider the regime in which there is sufficient spacing between units so as to justify the neglect of the lubrication effects that arise when objects in relative motion are in close proximity. Such effects are discussed by various authors (Brenner 1961, Cooley & O'Neill 1969b;a) in other contexts.

¹ The measures of performance that are used here and in the literature do not include the work needed to move material between spheres in the PMPY and breather models, and thus the accordion model suffers by comparison in this respect.

2 Swimming at low Reynolds number

Hereafter we suppose that the swimmer is immersed in an infinite, incompressible fluid of density ρ and viscosity μ , that is at rest at infinity. The Navier-Stokes equations for the fluid velocity \mathbf{u} are (Childress 1977)

$$\rho \frac{\partial \mathbf{u}}{\partial t} + \rho(\mathbf{u} \cdot \nabla) \mathbf{u} = \nabla \cdot \mathbb{T} + \mathbf{f}_{\text{ext}} = -\nabla p + \mu \Delta \mathbf{u} + \mathbf{f}_{\text{ext}}, \quad (2.1)$$

$$\nabla \cdot \mathbf{u} = 0 \quad (2.2)$$

where

$$\mathbb{T} = -p \boldsymbol{\delta} + \mu(\nabla \mathbf{u} + (\nabla \mathbf{u})^T)$$

is the Cauchy stress tensor and \mathbf{f}_{ext} is the external force field. We further assume that the swimmer is self-propelled and does not rely on any exterior force, and therefore we require that $\mathbf{f}_{\text{ext}} = \mathbf{0}$ throughout. Either the swimmer is neutrally buoyant or the gravitational force is included in the pressure.

When converted to dimensionless form and the symbols re-defined, these equations read

$$\text{ReSl} \frac{\partial \mathbf{u}}{\partial t} + \text{Re}(\mathbf{u} \cdot \nabla) \mathbf{u} = -\nabla p + \mu \Delta \mathbf{u}, \quad \nabla \cdot \mathbf{u} = 0, \quad (2.3)$$

where the Reynolds number based on a characteristic length scale L and a characteristic speed scale U is $\text{Re} = \rho L U / \mu$. In addition, $\text{Sl} = \omega L / U$ is the Strouhal number and ω is a characteristic frequency of the shape changes. When $\text{Re} \ll 1$ the convective momentum term in equation (2.3) can be neglected, but the time variation requires that $\text{ReSl} = \omega \rho L^2 / \mu$. When both terms are neglected, which we assume throughout, the low Reynolds number (LRN) flow is governed by the Stokes equations

$$\mu \Delta \mathbf{u} - \nabla p = \mathbf{0}, \quad \nabla \cdot \mathbf{u} = 0. \quad (2.4)$$

Throughout we consider small cells such as Dd, whose small size and low speeds lead to LRN flows (Wang & Othmer 2015), and in this regime time does not appear explicitly, there are no inertial effects, and bodies move by exploiting the viscous resistance of the fluid. As a result, time-reversible deformations produce no motion, which is known as the "scallop theorem" (Purcell 1977). Under the assumptions of an infinite fluid domain with $\mathbf{u} = \mathbf{0}$ at infinity and the absence of external forces, there is no net force or torque on a self-propelled swimmer in the Stokes regime, and therefore movement is a purely geometric process: the net displacement of a swimmer during a stroke is independent of the rate at which the stroke is executed, as long as the Reynolds number remains small enough.

Let $D(t) \subset \mathbb{R}^3$ be a closed, compact set occupied by the swimmer at time t , and let $\partial D(t)$ denote its prescribed time-dependent boundary. In reality amoeboid swimming cells may take up or release fluid, but we assume that the prescribed motion of the boundary is such that the volume of the swimmer is conserved under all deformations. A *swimming stroke* is specified by a time-dependent sequence of shapes, and it is *cyclic* if the initial and final shapes are identical, i.e., $\partial D(0) = \partial D(T)$, where T is the period. The swimmer's boundary velocity \mathbf{V} relative to fixed coordinates can be written as a part \mathbf{v} that defines the intrinsic shape deformations, and a rigid motion part $\mathbf{U} + \boldsymbol{\Omega} \times \mathbf{x}$, where $\mathbf{U}, \boldsymbol{\Omega}$ are the rigid translation and rotation, resp.. If \mathbf{u} denotes the velocity field in the fluid exterior to D , then a standard LRN self-propulsion problem is: *given a cyclic shape deformation specified by \mathbf{v} , solve the Stokes equations (2.4) subject to*

$$\int_{\partial D} \boldsymbol{\sigma} \cdot \mathbf{n} = \mathbf{0}, \quad \int_{\partial D} \mathbf{x} \times (\boldsymbol{\sigma} \cdot \mathbf{n}) = \mathbf{0}, \quad \mathbf{u}|_{\mathbf{x} \in \partial D} = \mathbf{V} = \mathbf{v} + \mathbf{U} + \boldsymbol{\Omega} \times \mathbf{x}, \quad \mathbf{u}|_{\mathbf{x} \rightarrow \infty} = \mathbf{0}$$

where \mathbf{n} is the exterior normal, and the integrals are the force- and torque-free conditions.

3 The solitary PMPY swimmer

The simplest PMPY model consists of two spheres that can expand or contract radially, and an extensible, massless rod connecting them (Figure 3.1). The standard assumptions on the domain and the fluid, which

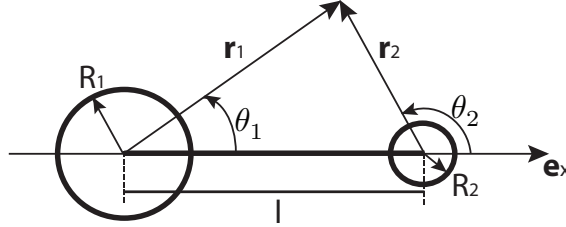


Fig. 3.1 Geometry of the pushpull model.

is described by the Stokes' equations (2.4), apply here. Let $R_i(t)$ be the radius of the i th sphere ($i = 1, 2$) and $l(t)$ the length of the rod. The prescribed motion of each sphere consists of two parts: a rigid translation along the x -axis at velocity $\mathbf{U}_i = U_i \mathbf{e}_x$, and a radial expansion or contraction: \dot{R}_i . Thus the no-slip boundary conditions on the surfaces of the two spheres can be expressed as:

$$\mathbf{u}(\mathbf{r}_i; t) = U_i(t) \mathbf{e}_x + \dot{R}_i(t) \hat{\mathbf{r}}_i \quad \text{at} \quad |\mathbf{r}_i| = R_i(t), \quad i = 1, 2 \quad (3.1)$$

where \mathbf{r}_i is the radius vector with origin at the center of the i th sphere (Figure 3.1) and $\hat{\mathbf{r}}_i$ is the outward unit vector along the \mathbf{r}_i direction. The instantaneous velocity of the swimmer is defined as the average of the velocities of the two spheres

$$\bar{\mathbf{U}} = \frac{\mathbf{U}_1 + \mathbf{U}_2}{2} = \frac{U_1 + U_2}{2} \mathbf{e}_x, \quad (3.2)$$

although other measures such as the velocity of the center of mass could also be used. The instantaneous velocity would change in the latter case, but the net translation during a cycle would not.

The rate of change of the length of the connecting rod is $\dot{l}(t)$, and thus the velocities of the two spheres are related by:

$$U_2 - U_1 = \dot{l}. \quad (3.3)$$

We assume that the total volume $V_1 + V_2 \equiv V_T$ is conserved during the motion, and thus the radii of the spheres satisfy the constraint

$$R_1^3(t) + R_2^3(t) \equiv \frac{3}{4\pi} V_T \quad (3.4)$$

In addition, the PMPY swimmer is force- and torque-free, and while the swimmer's linear geometry automatically guarantees that it is torque-free in the absence of asymmetric shear forces, the force-free constraint is non-trivial. Let $\mathbf{F}_i(t)$ be the hydrodynamic force due to drag and expansion exerted on the i th sphere at time t – then the constraint is that

$$\sum_{i=1,2} \mathbf{F}_i(t) \equiv \mathbf{0}. \quad (3.5)$$

It is clear that extension and contraction of the rod produces a direct effect on the translation of either sphere, whereas the expansion only has an indirect effect. If sphere one expands this has no direct effect on its movement since the expansion is radially symmetric, but the flow generated affects the second sphere. Simultaneously, the conservation of volume condition produces a reduction in size of the second sphere, which induces a flow that affects the first sphere. In the LRN regime these effects are felt instantaneously.²

The shape changes for a PMPY swimmer are described by \dot{l}, \dot{R}_1 and \dot{R}_2 , but in view of (3.4) two degrees of freedom define its motion. A cyclic stroke of a PMPY swimmer is determined by a periodic profile $(\dot{l}(t), \dot{R}_1(t))$ for $t \in [0, T]$, and a solution of the swimmer problem entails finding the relation between the swimmer's velocity $\bar{\mathbf{U}}$ and the controls (\dot{l}, \dot{R}_1) . In the general analysis that follows we assume that the controls are chosen so that the motion is not time reversible. An example of how the choice of phase difference between $\dot{l}(t)$ and $\dot{R}_1(t)$ affects the efficiency when both vary sinusoidally is given later.

3.1 Scaling the PMPY problem

The PMPY model contains three length scales: the radii of the spheres R_1, R_2 and the length of the connecting arm l . The geometry of the model requires that the two spheres never overlap, hence $R_1 + R_2 < l$. As previously defined, $Re = \rho LU / \mu \ll 1$, and therefore all lengths in the model must be small enough to ensure that

$$R_1, R_2, l \ll \frac{\mu}{\rho V}$$

However even if this LRN pre-condition is satisfied, the relations among the lengths R_1, R_2, l are also crucial in the swimming problem, and different relations may lead to different regimes of interaction (Kim & Karrila 1991). We assume that the radii of the two spheres are comparable, i.e., $O(R_1) \sim O(R_2)$, which rules out the possibility of interactions between a large sphere and a very small one (this case is discussed in Kim & Karrila (1991)). This leaves three major scenarios: the spheres are in close proximity in part of the cycle, i.e., $R_1(t) + R_2(t) \sim l(t)$ in part of the cycle; the spheres are widely-separated spheres throughout the cycle, where $R_1(t) + R_2(t) \ll l(t)$, and an intermediate regime. In the first regime the flow in the gap region dominates when the spheres nearly touch in part of the cycle, and the lubrication approximation provides the leading terms in an asymptotic expansion (Kim & Karrila 1991). If the spheres are also well-separated in part of the cycle this leads to a difficult matching problem that is not attempted here. We only consider the intermediate regime in which the separation never enters the lubrication regime, but is also not in the infinitely-separated regime throughout the cycle, as this has been studied previously (Avron *et al.* 2005). Our objective is to use the reflection method to determine corrections to the problem with very large separation.

Since the length scales involved are time-dependent, some care is needed in setting an appropriate scaling for the lengths. The primary criterion that must be met is that $(R_1(t) + R_2(t))/l(t) < 1$ throughout the cycle. Define

$$R_M = \max_t \{R_i(t)\}_{i=1,2}, \quad L_m = \min_t \{l(t)\}$$

and

$$\delta = R_M/L_m,$$

² The reader can easily show that in the absence of volume exchange the net translation after a periodic extension and contraction of the rod produces no motion. This provides the simplest example of the scallop theorem discussed later.

We then nondimensionalize the radii and rod lengths by R_M and L_m , resp.,

$$\hat{R}_i = \frac{R_i}{R_M} \leq 1, \quad \hat{l} = \frac{l}{L_m} \geq 1, \quad (3.6)$$

and we assume that the amplitudes of both rod displacement and radius changes are of the same order of R_M . Thus we let $\xi = \hat{l}$ and $\zeta_i = \hat{R}_i$, and apply the following scaling:

$$\hat{\xi} = \frac{T}{R_M} \xi, \quad \hat{\zeta}_i = \frac{T}{R_M} \zeta_i$$

Next, we nondimensionalize other length scales by R_M as well, and time by the period T to obtain

$$\hat{\mathbf{x}} = \frac{\mathbf{x}}{R_M}, \quad \hat{\nabla} = R_M \nabla, \quad \hat{t} = \frac{t}{T}, \quad \hat{\mathbf{u}} = \frac{T}{R_M} \mathbf{u}, \quad \hat{\mathbf{U}}_i = \frac{T}{R_M} \mathbf{U}_i, \quad \hat{\boldsymbol{\Omega}}_i = T \boldsymbol{\Omega}_i.$$

Finally, the drag force \mathbf{F} exerted on a sphere of radius R is related to the sphere velocity \mathbf{U} via $\mathbf{F} = 6\pi\mu R\mathbf{U}$, which leads to the following scaling for forces:

$$\hat{\mathbf{F}} = \frac{T}{6\pi\mu R_M^2} \mathbf{F} = \hat{R}\hat{\mathbf{U}}. \quad (3.7)$$

3.2 The reflection method and the Rotne-Prager-Yamakawa approximation

In previous analyses of the PMPY swimmer the spheres are infinitely-separated, and thus treated as the source of point forces. The free space Green's function, or Stokeslet, for the Stokes problem is

$$\mathbf{G}(\mathbf{x}, \mathbf{x}_0) = \frac{1}{r} \left[\mathbf{I} + \frac{\mathbf{r}\mathbf{r}}{r^2} \right] = \frac{1}{r} \left[\mathbf{I} + \hat{\mathbf{r}}\hat{\mathbf{r}} \right]. \quad (3.8)$$

Here \mathbf{I} is the unit second-rank tensor, $\mathbf{r} = \mathbf{x} - \mathbf{x}_0$, $r = |\mathbf{x} - \mathbf{x}_0|$ and $\hat{\mathbf{r}} = \mathbf{r}/|\mathbf{r}|$. Thus the velocity field generated at a point \mathbf{x} by a point force \mathbf{F} at \mathbf{x}_0 is

$$\mathbf{u}(\mathbf{x}) = \frac{\mathbf{G}(\mathbf{x}, \mathbf{x}_0)}{8\pi\mu} \cdot \mathbf{F}(\mathbf{x}_0). \quad (3.9)$$

When combined with the flow field generated by expansion of the spheres (*cf.* Appendix A), this leads to the following approximation for the velocity of the swimmer (Avron *et al.* 2005).

$$\bar{\mathbf{U}} = \frac{R_1 - R_2}{2(R_1 + R_2)} \dot{l} + \left(\frac{R_1}{l} \right)^2 \dot{R}_1 \quad (3.10)$$

The first and second terms are the leading order terms that result from the cyclic change of the rod length and the contraction and expansion of the spheres, resp.. If we nondimensionalize this solution we obtain

$$\hat{\bar{\mathbf{U}}} = \frac{\hat{R}_1 - \hat{R}_2}{2(\hat{R}_1 + \hat{R}_2)} \hat{\xi} + \left(\frac{\hat{R}_1}{\hat{l}} \right)^2 \delta^2 \hat{\zeta}_1. \quad (3.11)$$

Here we see that the first term in equation (3.10) is $O(1)$ while the second is $O(\delta^2)$. Therefore we expect that at least the $O(\delta)$ and $O(\delta^2)$ terms that result from the movement of the spheres should be taken into account. Said otherwise, equation (3.10) is only accurate to $O(1)$.

One approach to obtaining the higher-order effects of the interactions between the spheres in the PMPY model, both from their relative motion and the volume changes, is the reflection method (Kim & Karrila 1991). A general description of the the algorithm underlying this method is as follows.

- **The 0-th reflection.** The 0-th reflection for either sphere is simply the superposition of this sphere alone in whatever background flow, call it \mathbf{u}_∞ , exists. In another words, in this step no interactions between the spheres are taken into consideration. We denote the velocity field that results from translation and expansion/contraction of the i -th sphere by $\mathbf{u}_i^{(0)}(\mathbf{x})$, and the sum of these is the new field $\mathbf{u}^{(0)}(\mathbf{x})$. This step leads to the $O(1)$ term in (3.10).
- **The 1st reflection.** However, in the combined field $\mathbf{u}^{(0)}(\mathbf{x})$ the no-slip boundary conditions on each sphere are not met and to correct this one computes a new field by solving two new Stokes problems: one with the boundary value $-\mathbf{u}_1^{(0)}(\mathbf{x})$ on sphere 2, and one with the value $-\mathbf{u}_2^{(0)}(\mathbf{x})$ on sphere 1. This leads to two new fields $\mathbf{u}_{12}^{(1)}(\mathbf{x})$ and $\mathbf{u}_{21}^{(1)}(\mathbf{x})$, and the first reflection field is $\mathbf{u}^{(1)}(\mathbf{x}) = \mathbf{u}_{12}^{(1)}(\mathbf{x}) + \mathbf{u}_{21}^{(1)}(\mathbf{x})$.
- **The 2nd reflection.** In the second reflection two new corrections that satisfy $-\mathbf{u}_{12}^{(1)}(\mathbf{x})$ and $-\mathbf{u}_{21}^{(1)}(\mathbf{x})$, on sphere 1 and 2, respectively, are computed, and are called $\mathbf{u}_{121}^{(2)}(\mathbf{x})$, and $\mathbf{u}_{212}^{(2)}(\mathbf{x})$. The resulting second reflection field is $\mathbf{u}^{(2)}(\mathbf{x}) = \mathbf{u}_{121}^{(2)}(\mathbf{x}) + \mathbf{u}_{212}^{(2)}(\mathbf{x})$.
- Repeat until the desired accuracy is achieved.

This process has been proven to converge very rapidly for finite domains (Luke 1989).

In a LRN self-propulsion problem the flows vanish at infinity and the velocity generated by a sphere of radius R , centered at \mathbf{x}_0 , subject to a force \mathbf{F} , and ‘expanding’ at the rate $\dot{R} = dR/dt$ is (Appendix A):

$$\mathbf{u}(\mathbf{r}; R, \mathbf{F}, \dot{R}) = \frac{1}{24\pi\mu r} \left[\left(3 + \frac{R^2}{r^2}\right)\mathbf{F} + 3\left(1 - \frac{R^2}{r^2}\right)(\mathbf{F} \cdot \hat{\mathbf{r}})\hat{\mathbf{r}} \right] + \dot{R} \left(\frac{R}{r}\right)^2 \hat{\mathbf{r}}. \quad (3.12)$$

The first term and second terms in equation (3.12) result from the drag force \mathbf{F} and the radial change \dot{R} , resp., and we denote them by $\mathbf{u}\{\mathbf{F}\}$ and $\mathbf{u}\{\dot{R}\}$:

$$\begin{aligned} \mathbf{u}(\mathbf{r}; R, \mathbf{F}, \dot{R}) &= \mathbf{u}\{\mathbf{F}\}(\mathbf{r}; R) + \mathbf{u}\{\dot{R}\}(\mathbf{r}; R) \\ \mathbf{u}\{\mathbf{F}\}(\mathbf{r}; R) &= \frac{1}{24\pi\mu r} \left[\left(3 + \frac{R^2}{r^2}\right)\mathbf{F} + 3\left(1 - \frac{R^2}{r^2}\right)(\mathbf{F} \cdot \hat{\mathbf{r}})\hat{\mathbf{r}} \right] \\ \mathbf{u}\{\dot{R}\}(\mathbf{r}; R) &= \dot{R} \left(\frac{R}{r}\right)^2 \hat{\mathbf{r}}. \end{aligned}$$

The symmetric geometry of the PMPY model implies that the angular velocities $\boldsymbol{\Omega}_1$ and $\boldsymbol{\Omega}_2 = \mathbf{0}$ both vanish, while each reflection contributes to the translational velocity. We denote the translational velocity of sphere i that results from the n -th reflection as $\mathbf{U}_i^{(n)}$. In the zeroth reflection, i.e., when we consider the i th sphere ($i = 1, 2$) of the PMPY model alone immersed in the fluid, the radial expansion will not result in any rigid motion, but the drag force \mathbf{F}_i leads to the translational component

$$\mathbf{U}_i^{(0)} = \frac{1}{6\pi\mu R_i} \mathbf{F}_i \quad (3.13)$$

The first reflection is computed as follows. Given the velocity of sphere j , we have to find the solution of a Stokes problem with velocity $-\mathbf{u}_j^{(0)}$ on the surface of sphere i and vanishing at infinity, and from that compute the translational and rotational velocities at the first reflection. We use the reciprocal theorem as used in (Stone & Samuel 1996) to do this. Let $(\mathbf{U}_i^{(1)}, \mathbb{T}_i^1)$ be the first-reflection translational velocity of, and

stress on, sphere i , and similarly for sphere j . Then a version of the reciprocal theorem used here states that $\nabla \cdot \mathbb{T}_j^0 \cdot \mathbf{U}_i^1 = \nabla \cdot \mathbb{T}_i^1 \cdot \mathbf{u}_j$ and from this and a similar equivalence for the torques it follows that

$$\mathbf{U}_i^{(1)} = \frac{1}{4\pi R_i^2} \int_{S_i} \mathbf{u}_j^{(0)}(\mathbf{x}) \, dS(\mathbf{x}) \quad (3.14)$$

$$\boldsymbol{\Omega}_i^{(1)} = \frac{3}{8\pi R_i^3} \int_{S_i} \mathbf{n} \times \mathbf{u}_j^{(0)}(\mathbf{x}) \, dS(\mathbf{x}). \quad (3.15)$$

Since we are considering spheres, equivalent expressions obtained by use of Faxén's law (Kim & Karrila 1991) are

$$\mathbf{U}_i^{(1)} = \left(1 + \frac{R_i^2}{6} \nabla^2\right) \mathbf{u}_j^{(0)} \Big|_{\mathbf{x}=\mathbf{x}_i} \quad (3.16)$$

$$\boldsymbol{\Omega}_i^{(1)} = \frac{1}{2} \nabla \times \mathbf{u}_j^{(0)} \Big|_{\mathbf{x}=\mathbf{x}_i} \quad (3.17)$$

Once again, $\boldsymbol{\Omega}_i^{(1)} = \mathbf{0}$ due to the symmetry of the model, and by using (3.12) in (3.14), the translational component is

$$\mathbf{U}_i^{(1)} = \frac{1}{4\pi R_i^2} \int_{S_i} \mathbf{u}_j^{(0)} \, dS = \frac{1}{4\pi R_i^2} \int_{S_i} \mathbf{u}\{\mathbf{F}\}(\mathbf{r}; R) \, dS + \frac{\dot{R}_j}{4\pi} \left(\frac{R_j}{R_i}\right)^2 \int_{S_i} \frac{\mathbf{x} - \mathbf{x}_j}{|\mathbf{x} - \mathbf{x}_j|^3} \, dS(\mathbf{x}) \quad (3.18)$$

We denote the first and second terms in equation (3.18) as $\mathbf{U}_i^{(1,f)}$ and $\mathbf{U}_i^{(1,e)}$, resp., and then equation (3.18) can be written as

$$\mathbf{U}_i^{(1)} = \mathbf{U}_i^{(1,f)} + \mathbf{U}_i^{(1,e)}$$

$\mathbf{U}_i^{(1,f)}$ is the result of the drag force \mathbf{F}_j , and it has been well studied. The result is given by the Rotne-Prager-Yamakawa (RPY) approximation (Yamakawa 1970, Wajnryb *et al.* 2013, Zuk *et al.* 2014, Liang *et al.* 2013):

$$\mathbf{U}_i^{(1,f)} = \frac{1}{8\pi\mu l} \left[\left(1 + \frac{R_1^2 + R_2^2}{3l^2}\right) \mathbf{I} + \left(1 - \frac{R_1^2 + R_2^2}{l^2}\right) \frac{(\mathbf{x}_i - \mathbf{x}_j) \otimes (\mathbf{x}_i - \mathbf{x}_j)}{|\mathbf{x}_i - \mathbf{x}_j|^2} \right] \mathbf{F}_j \quad (3.19)$$

and together with the relations $\mathbf{U}_i^{(1,f)} = U_i^{(1,f)} \mathbf{e}_x$ and $\mathbf{F}_j = F_j \mathbf{e}_x$, we find that

$$\mathbf{U}_i^{(1,f)} = \frac{1}{4\pi\mu l} \left[1 - \frac{R_1^2 + R_2^2}{3l^2} \right] F_j. \quad (3.20)$$

In principle, the RPY approximation is a first order correction to the Oseen hydrodynamic interaction tensor, and thus allows for closer separation of the spheres. However, since the idea of the RPY approximation comes from the reflection method (Kim & Karrila 1991), the distance between any two spheres should still be kept within the regime in which the method can be applied.

$\mathbf{U}_i^{(1,e)}$ is due to the expansion \dot{R}_j , which can be calculated directly (Appendix B) or by Faxen's law,

$$\mathbf{U}_i^{(1,e)} = (-1)^i \dot{R}_j \left(\frac{R_j}{l}\right)^2 \mathbf{e}_x \quad (3.21)$$

which is precisely the radial expansion term in Avron's solution (equation (3.10)). This completes the first reflection, and equations (3.13, 3.20, 3.21) give the following approximation of the translational velocities of the spheres after one reflection

$$U_i \sim U_i^{(0)} + U_i^{(1)} = \frac{F_i}{6\pi\mu R_i} + \frac{F_j}{4\pi\mu l} \left(1 - \frac{R_1^2 + R_2^2}{3l^2}\right) + (-1)^i \dot{R}_j \left(\frac{R_j}{l}\right)^2. \quad (3.22)$$

Using the nondimensionalization given earlier, the nondimensional version of equation (3.22) is:

$$\hat{U}_i \sim \frac{\hat{F}_i}{\hat{R}_i} + \frac{3}{2} \delta \frac{\hat{F}_j}{\hat{l}} \left(1 - \delta^2 \frac{\hat{R}_1^2 + \hat{R}_2^2}{3\hat{l}^2}\right) + (-1)^i \delta^2 \left(\frac{\hat{R}_j}{\hat{l}}\right)^2 \hat{\zeta}_j \quad (3.23)$$

together with the equations (3.5, 3.3) we obtain the following closed system:

$$\begin{pmatrix} -1 & 0 & \frac{1}{\hat{R}_1} & \Gamma \\ 0 & -1 & \Gamma & \frac{1}{\hat{R}_2} \\ 1 & -1 & 0 & 0 \\ 0 & 0 & 1 & 1 \end{pmatrix} \begin{pmatrix} \hat{U}_1 \\ \hat{U}_2 \\ \hat{F}_1 \\ \hat{F}_2 \end{pmatrix} = \begin{pmatrix} \Gamma_2 \\ -\Gamma_1 \\ -\hat{\zeta} \\ 0 \end{pmatrix} \quad (3.24)$$

where

$$\Gamma \equiv \delta \frac{3}{2\hat{l}} \left(1 - \delta^2 \frac{\hat{R}_1^2 + \hat{R}_2^2}{3\hat{l}^2}\right) \quad \text{and} \quad \Gamma_i \equiv \delta^2 \left(\frac{\hat{R}_i}{\hat{l}}\right)^2 \hat{\zeta}_i.$$

It is easy to see that the matrix in (3.24) is non-singular and can be inverted explicitly. Therefore the solution of (3.24) can be expressed as a power series in δ , and since this solution represents an approximation stemming from the first reflection, we must determine how accurate it is and whether further reflections are justified. If we compute a second reflection, the translational velocity that results from drag forces from the 0^{th} up to the 2^{nd} reflections for sphere 1 is found to be (Kim & Karrila 1991):

$$\sum_{n=0}^2 U_1^{(n,f)} = \frac{F_1}{6\pi\mu R_1} \left(1 - \frac{15R_1R_2^3}{4l^4}\right) + \frac{F_2}{4\pi\mu l} \left(1 - \frac{R_1^2 + R_2^2}{3l^2}\right) + O\left(\frac{1}{l^5}\right), \quad (3.25)$$

and after nondimensionalization this reads

$$\sum_{n=0}^2 \hat{U}_1^{(n,f)} = \frac{\hat{F}_1}{\hat{R}_1} \left(1 - \frac{15}{4} \delta^4 \frac{\hat{R}_1 \hat{R}_2^3}{\hat{l}^4}\right) + \frac{3}{2} \delta \frac{\hat{F}_2}{\hat{l}} \left(1 - \delta^2 \frac{\hat{R}_1^2 + \hat{R}_2^2}{3\hat{l}^2}\right) + O(\delta^5). \quad (3.26)$$

One can show that a second reflection for the component due to radial expansion will lead to the correction $U_i^{(2,e)}$ of $O(\delta^5)$ (cf Appendix B). Hence with one reflection, the solution is accurate up to $O(\delta^4)$.

The perturbation expansions of the solution to equation (3.24) to $O(\delta^4)$ order are:³

$$U_1 \sim -\frac{R_2}{R_1+R_2}\xi + \delta \frac{3R_1R_2(R_1-R_2)}{2(R_1+R_2)^2l}\xi + \frac{\delta^2}{l^2} \left[\frac{9R_1^2R_2^2(R_1-R_2)}{2(R_1+R_2)^3}\xi - R_2^2\zeta_2 \right] \\ + \delta^3 \frac{R_1R_2(R_1-R_2)}{2(R_1+R_2)^4l^3} \left(25R_1^2R_2^2 - R_1^4 - R_2^4 - 2R_1^3R_2 - 2R_1R_2^3 \right) \xi + O(\delta^4) \quad (3.27)$$

$$U_2 \sim \frac{R_1}{R_1+R_2}\xi + \delta \frac{3R_1R_2(R_1-R_2)}{2(R_1+R_2)^2l}\xi + \frac{\delta^2}{l^2} \left[\frac{9R_1^2R_2^2(R_1-R_2)}{2(R_1+R_2)^3}\xi + R_1^2\zeta_1 \right] \\ + \delta^3 \frac{R_1R_2(R_1-R_2)}{2(R_1+R_2)^4l^3} \left(25R_1^2R_2^2 - R_1^4 - R_2^4 - 2R_1^3R_2 - 2R_1R_2^3 \right) \xi + O(\delta^4) \quad (3.28)$$

$$-F_1 = F_2 \sim \frac{R_1R_2}{R_1+R_2}\xi + 3\frac{\delta}{l} \left(\frac{R_1R_2}{R_1+R_2} \right)^2 \xi + 9\frac{\delta^2}{l^2} \left(\frac{R_1R_2}{R_1+R_2} \right)^3 \xi \\ + \frac{\delta^3}{l^3} \frac{(R_1R_2)^2}{(R_1+R_2)^4} \left(25R_1^2R_2^2 - R_1^4 - R_2^4 - 2R_1^3R_2 - 2R_1R_2^3 \right) \xi + O(\delta^4) \quad (3.29)$$

Finally, the velocity of the PMPY model, correct to $O(\delta^3)$, and subject to the pair of controls (ξ, ζ_1) , is

$$\bar{U} = \frac{R_1-R_2}{2(R_1+R_2)} \left[1 + 3\frac{\delta}{l} \frac{R_1R_2}{R_1+R_2} + 9\frac{\delta^2}{l^2} \left(\frac{R_1R_2}{R_1+R_2} \right)^2 \right. \\ \left. + \frac{\delta^3}{l^3} \left(\frac{R_1R_2}{R_1+R_2} \right)^3 \left(25 - \frac{R_1^2}{R_2^2} - \frac{R_2^2}{R_1^2} - 2\frac{R_1}{R_2} - 2\frac{R_2}{R_1} \right) \right] \xi + \delta^2 \left(\frac{R_1}{l} \right)^2 \zeta_1 + O(\delta^4). \quad (3.30)$$

If we compare equation (3.30) with equation (3.11), we see that the earlier analysis ignores all effects due to finite separation of the spheres, and thus (3.11) is only valid to zeroth-order in δ .

3.3 Power expenditure and the performance of a PMPY

Next we consider the power $P(t)$ required to propel the swimmer. For a PMPY model, the power P comprises two parts: P_D that results from the drag force on the spheres, and P_V that results from the radial expansion of the spheres. P_D is given by

$$P_D = F_1U_1 + F_2U_2$$

which can be simplified by the force-free condition (equation 3.5) and the geometric relation between the two spheres (equation 3.3) to the form

$$P_D = F_2(U_2 - U_1) = F_2\dot{l}.$$

The stress on the surface of a sphere expanding at the rate $\dot{R}(t)$ in a Newtonian fluid is obtained as follows (Brennen 2013). The continuity equation in the exterior fluid implies that the radial velocity $v_r = dR/dt$ has the form

$$v_r = \frac{F(t)}{r^2}.$$

³ In the remainder we omit the $\hat{\cdot}$ on nondimensionalized quantities for simplicity, but since δ appears in the equations this should not lead to any confusion.

The forces per unit area on the sphere acting at the sphere-fluid interface are the interior pressure p_i , the fluid stress force

$$\mathbb{T}_{rr} = \left(-p + 2\mu \frac{\partial v_r}{\partial r} \right) \Big|_{r=R}$$

due to the exterior fluid motion, and a tension T due to interfacial forces equal to

$$\frac{2T}{R}.$$

We neglect both the pressure difference across the interface and the interfacial tension, and therefore the force is

$$\mathbb{T}_{rr} = 2\mu \frac{\partial v_r}{\partial r} = -4 \frac{\mu}{R} \frac{dR}{dt}.$$

Therefore the power required to expand a sphere is

$$- \int_S \mathbb{T}_{rr} v_r ds = 16\pi\mu R \dot{R}^2$$

Therefore for the PMPY model we have

$$P_V = 16\pi\mu (R_1 \dot{R}_1^2 + R_2 \dot{R}_2^2)$$

and thus the the power expended to propel a PMPY at time t is

$$P = P_D + P_V = F_2 \dot{l} + 16\pi\mu (R_1 \dot{R}_1^2 + R_2 \dot{R}_2^2). \quad (3.31)$$

We nondimensionalize P as

$$\hat{P} = \frac{1}{6\pi\mu} \frac{T^2}{R_M^3} P$$

so that while $P = FU$ in dimensional form, after nondimensionalization we also have $\hat{P} = \hat{F}\hat{U}$. Thus the nondimensional version of equation (3.31) is

$$P = F \xi^2 + \frac{8}{3} (R_1 \zeta_1^2 + R_2 \zeta_2^2) \quad (3.32)$$

with hat notation omitted. While P_V is determined, P_D depends on the perturbation, which in turn depends on δ . A first order approximation to P is given in Avron *et al.* (2005), which after nondimensionalization reads

$$P = \frac{R_1 R_2}{R_1 + R_2} \xi^2 + \frac{8}{3} (R_1 \zeta_1^2 + R_2 \zeta_2^2) + O(\delta) \quad (3.33)$$

while higher-order approximations can be obtained by substituting the results of F obtained from equations (3.24) or (3.29) into equation (3.32).

Finally we define the performance \mathcal{P} of a stroke as the ratio of the translation per cycle to the energy expended in a cycle, *viz.*

$$\mathcal{P} = \frac{\left| \int_0^T \bar{U}(t) dt \right|}{\int_0^T P(t) dt}. \quad (3.34)$$

which has the units of $force^{-1}$. \mathcal{P} measures the energy required for the PMPY to swim a certain distance in a cycle, and a large value of \mathcal{P} indicates an energy-saving stroke. The nondimensional form of \mathcal{P} is

$$\hat{\mathcal{P}} = \frac{6\pi\mu R_M^2}{T} \mathcal{P} = \frac{\left| \int_0^1 \hat{U} d\hat{t} \right|}{\int_0^1 \hat{P} d\hat{t}}$$

3.4 A comparison of the solutions

Next we compare the asymptotic solution given by Eq. (3.10), the solution obtained by the reflection method (equation 3.24) and the solution that results from the $O(\delta^3)$ order approximation to the latter, given by (equation (3.30)), for a prescribed loop in the control space described by (\hat{l}, \hat{R}_1) . We use the sinusoidal circuits

$$R_1(t) = 2 + \sin 2\pi t, \quad R_2(0) = 3, \quad l = l_0 + \cos 2\pi t, \quad \text{for } t \in [0, 1] \quad (3.35)$$

with typical length unit μm and time unit min – these set the length and time scales for biological LRN swimmer, such as Dd amoebae (Van Haastert 2011), as will be seen later in this section. Thus the nondimensionalization is given by:

$$R_M \sim 3.24\mu\text{m}, \quad L_m = (l_0 - 1)\mu\text{m}, \quad \delta \sim \frac{3.24}{l_0 - 1}, \quad T = 1 \text{ min}$$

The results for scaled translation $\hat{X}(\hat{t}) = \int_0^{\hat{t}} \hat{U} d\hat{t}$ and scaled power $\hat{P}(\hat{t})$ in a period for different values of l_0 are shown in Figure 3.2a – e, and the relation between the scaled performance $\hat{\mathcal{P}}$ and l_0 is given in Figure 3.2f.

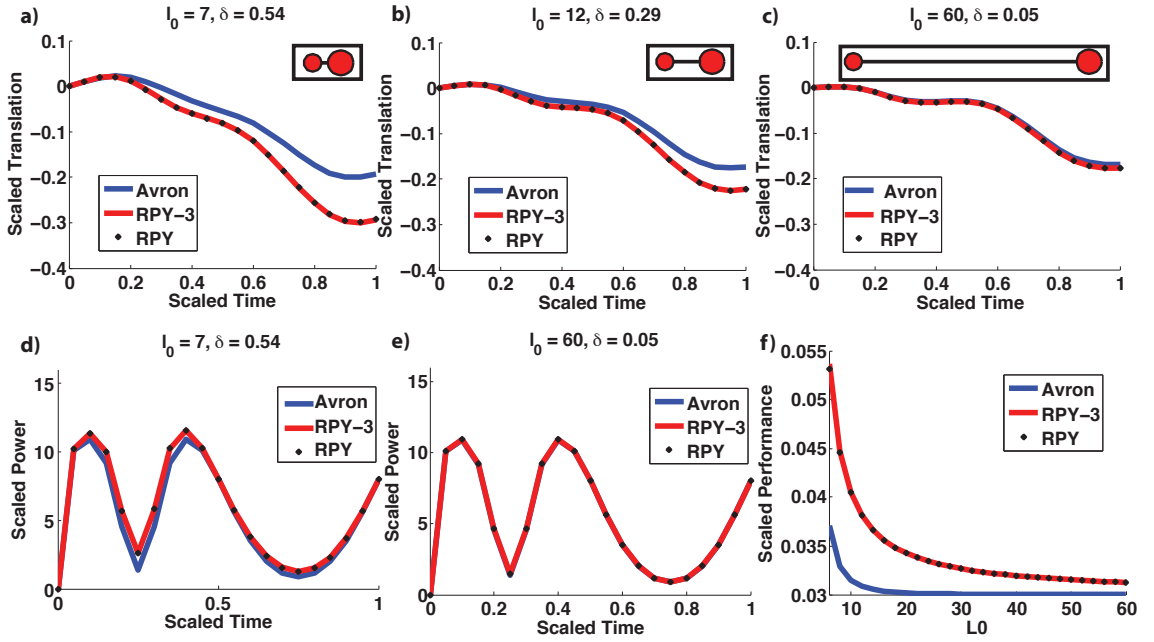


Fig. 3.2 A comparison of the asymptotic Avron solution (blue lines), the solution obtained by the reflection method (black dots) and its perturbation analysis up to the $O(\delta^3)$ order (red lines). (a-c) The scaled translation $\hat{X}(\hat{t}) = \int_0^{\hat{t}} \hat{U} d\hat{t}$ within a period for $l_0 = 7, 12, 60$. The initial profile of the swimmer is shown in the box. (d,e) The scaled power $\hat{P}(\hat{t})$ within a period, with $l_0 = 7, 60$. (f) The scaled performance $\hat{\mathcal{P}}$ of PMPY with respect to l_0 .

To maintain the correct geometry, the relation $l > R_1 + R_2$ must hold at all times. In Figure 3.2 we see that both the scaled translation \hat{X} and the power \hat{P} computed via the first reflection and its $O(\delta^3)$ approximation

(black dots and red solid lines, resp.) agree very well. On the other hand, the asymptotic approximation for the translation given by Eq. (3.10) and shown in Figure 3.2a-c, (blue lines) deviates from them significantly when l_0 is small. The scaled power of the Avron approximation coincides closely with that of the higher-order approximations (Figure 3.2d-e). As a result, the scaled performance deviates from the reflection results significantly when the spheres are relatively close (Figure 3.2f).

As pointed out earlier (Wang & Othmer 2015), PMPY adopts a mixed control strategy in (\dot{l}, \dot{R}) , which makes it superior to other linked-sphere models that adopt combinations of a single type of control. In fact, PMPY is the only model studied there for which the net translation $\hat{X} = \int_0^1 \hat{U} dt \sim O(1)$ over a period. This can be seen in Figures 3.2a-c, in that the net translation \hat{X} does not vanish as the length of the connecting rod increases. For $l \rightarrow \infty$, we have $\delta \rightarrow 0$, and equation (3.30) gives the estimate

$$\lim_{\delta \rightarrow 0} \hat{U} = \frac{\hat{R}_1 - \hat{R}_2}{2(\hat{R}_1 + \hat{R}_2)} \hat{\xi} \sim O(1), \quad \lim_{\delta \rightarrow 0} \hat{X} = \lim_{\delta \rightarrow 0} \int_0^T \hat{U}(t) dt \sim O(1)$$

For the stroke prescribed by equation (3.35), we have the estimate $\hat{X} \sim -0.17$ as $l_0 \rightarrow \infty$, $\delta \rightarrow 0$. On the other hand, the power \hat{P} does not change much as l_0 changes, and taken together, we have the estimate for the performance of PMPY in the limit $l_0 \rightarrow \infty$, $\delta \rightarrow 0$ of about $\hat{\mathcal{P}} \sim 0.03$.

Finally, we check if the flow regime for the PMPY model computations satisfies $\text{Re} \ll 1$ and $\text{ReSl} \ll 1$, which is required for a LRN swimmer. We assume that the medium is water ($\rho \sim 10^3 \text{kg} \cdot \text{m}^{-3}$, $\mu \sim 10^{-3} \text{Pa} \cdot \text{s}$), and test two sets of L and U from our simulations ($L = 6\mu\text{m}$, $U \sim -1.2\mu\text{m}/\text{min}$ from Figure 3.2a, or $L = 60\mu\text{m}$, $U \sim -0.6\mu\text{m}/\text{min}$ from Figure 3.2c). In either case we have $\text{Re} \ll 1$ and $\text{ReSl} \ll 1$ ($\text{Re} \sim O(10^{-6})$, $\text{ReSl} \sim O(10^{-6})$ in Figure 3.2a, and $\text{Re} \sim O(10^{-6})$, $\text{ReSl} \sim O(10^{-5})$ in Figure 3.2c).

The foregoing results are for a fixed phase difference, and next we investigate the effect of changing the phase difference between the two controls \dot{l} and \dot{R}_1 . We consider the following type of sinusoidal cycles

$$R_1(t) = 2 + \sin 2\pi t, \quad R_2(0) = 3, \quad l = l_0 + \sin(2\pi t + \phi), \quad \text{for } t \in [0, 1]$$

where $\phi \in [0, 2\pi]$ is the phase difference. The scaled net translation and performance with respect to ϕ is shown in Figure 3.3, from which we see that the maxima of both scaled net translation and performance are reached at a phase difference of $\phi = k\pi + \pi/2$, $k \in \mathbb{Z}$. In contrast, when $\phi = k\pi$, $k \in \mathbb{Z}$, the net translation after one cycle equals zero, which naturally leads to zero performance as well. This stems from the fact that in these cases the shape deformation become time reversible, and according to the scallop theorem, no net translation results.

To compare our analysis with experimental observations, we use the data on swimming amoebae from Van Haastert (2011), where it is reported that Dd amoebae move in a fluid environment by side protrusions. Typically the cell body is elongated, and single or multiple protrusions cyclically propagate along the cell Wang & Othmer (2016). Although the shape deformation mode of these amoebae cell is not exactly the same as a PMPY model, however similar to a PMPY, such a traveling protrusion mode does exploit mass transfer along an elongated body. It is reported that amoebae using this swimming mode have maximum cell body length $\sim 25\mu\text{m}$, average cell body width $\sim 6\mu\text{m}$, a typical stroke has period ~ 1 min, and a typical swimming velocity $\sim 3\mu\text{m}/\text{min}$. Using this data, we approximate

$$L \sim 25\mu\text{m}, \quad T \sim 1 \text{ min}, \quad R \sim 6\mu\text{m}, \quad U \sim 3\mu\text{m}/\text{min}$$

thus $\delta \sim R/L \sim 0.24$, $\hat{U} \sim TU/R \sim 0.5$ and the scaled net translation within a period $\hat{X} = X/R \sim 0.5$, which is about the same as for a PMPY. In fact, as can be seen from Figure 3.2a, if the spheres are not too separated in the model, the scaled net translation of a PMPY can reach $\hat{X} \sim 0.3$. On the other hand, other linked-sphere models that also have elongated shape and adopt large scale of shape deformations can only

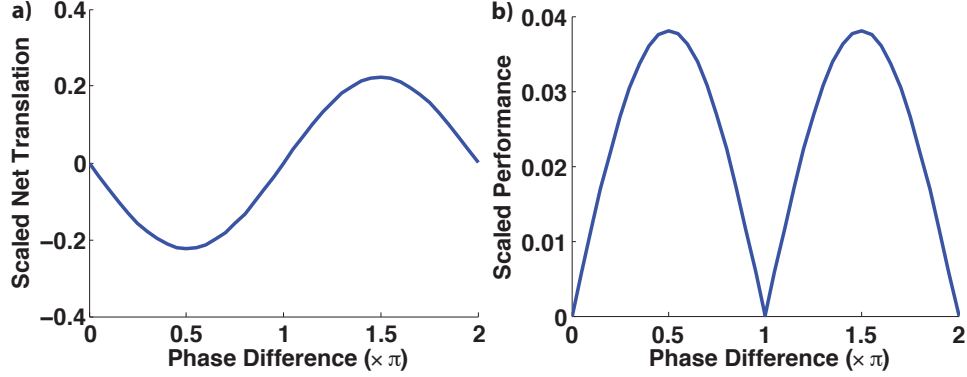


Fig. 3.3 The scaled net translation (a) and performance (b) with respect to phase difference between the two controls \hat{l} and \hat{R}_1 , with $l_0 = 12$, simulated by the RPY approximation.

result in $\hat{X} \sim O(\delta^2)$ (Wang & Othmer 2015), which is far less than a PMPY or a swimming amoebae as observed. Hence we believe the PMPY model is suitable in the study of swimming cells at LRN.

4 A PMPY swimmer in the presence of a passive buoyant obstacle

In an extension of the previous results that leads to several interesting applications, we next analyze a PMPY swimmer that interacts with an untethered, passive, neutrally-buoyant object nearby. To simplify the computation of the interaction, we suppose that the object is a rigid sphere, and that there is no external force or torque imposed on it. The geometry of the system is shown in Figure 4.1, where one sees that there are six characteristic lengths: the radius of each sphere (R_i , $i = 1, 2, 3$) and the lengths between any pair of spheres: (l_{ij} , $i, j = 1, 2, 3$). For scaling purposes we define

$$R_M = \max_i \{R_i(t)\}_{i=1,2,3}, \quad L_m = \min_i \{l_{12}(t)\}, \quad \delta = \frac{R_M}{L_m}$$

To apply the reflection method to this system, we require that $\delta < 1$ as before, and in addition, we only consider the regime $l_{13}, l_{23} > L_m$. Thus all non-dimensionalization relations in section 3.1 apply. The following discussion is similar to that in section 3.2, except that one more sphere is now involved in the system. We assume that the centers of all three spheres lies in the xy -plane, and that the active swimmer moves along the x -axis (Figure 4.1) initially. In this configuration the torque and angular velocities must be taken into account unless the three spheres are co-linear. However, the motion of the spheres will remain in the plane defined by their initial positions since the axis of rotation of a sphere is orthogonal to that plane. Thus the problem remains effectively two-dimensional, but this plays no role in the analysis.

4.1 The linear and angular velocities after the first reflection

At the zeroth-order reflection, in which no hydrodynamic interactions between the spheres are considered, the results for the swimmer are the same as in the absence of a passive object, and the velocity field for each sphere is given by equations (3.12, 3.13). At this order the linear and angular velocities of sphere 3 are

$$\mathbf{U}_3^{(0)} = \boldsymbol{\Omega}_3^{(0)} = \mathbf{0}, \quad \mathbf{u}_3^{(0)} \equiv \mathbf{0} \quad (4.1)$$

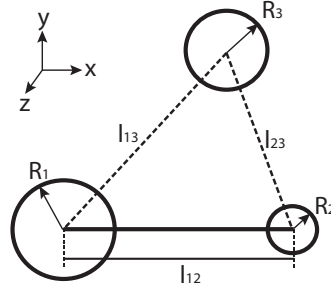


Fig. 4.1 The geometry of the system of a PMPY swimmer and a passive, neutrally-buoyant spherical object.

At the first reflection, each sphere is subject to the flows generated by the other spheres. Since $\mathbf{u}_3^{(0)} \equiv \mathbf{0}$, the calculation of rigid motions for sphere 1 and 2 in the first reflection are identical to section 3.2 – thus we have:

$$\begin{aligned} \mathbf{U}_1^{(1)} &= \left(1 + \frac{R_1^2}{6} \nabla^2\right) (\mathbf{u}_2^{(0)} + \mathbf{u}_3^{(0)}) \Big|_{\mathbf{x}=\mathbf{x}_1} = \frac{\mathbf{F}_2}{4\pi\mu l_{12}} \left(1 - \frac{R_1^2 + R_2^2}{3l_{12}^2}\right) - \dot{R}_2 \left(\frac{R_2}{l_{12}}\right)^2 \\ \boldsymbol{\Omega}_1^{(1)} &= \frac{1}{2} \nabla \times (\mathbf{u}_2^{(0)} + \mathbf{u}_3^{(0)}) \Big|_{\mathbf{x}=\mathbf{x}_1} = \mathbf{0} \\ \mathbf{U}_2^{(1)} &= \left(1 + \frac{R_2^2}{6} \nabla^2\right) (\mathbf{u}_1^{(0)} + \mathbf{u}_3^{(0)}) \Big|_{\mathbf{x}=\mathbf{x}_2} = \frac{\mathbf{F}_1}{4\pi\mu l_{12}} \left(1 - \frac{R_1^2 + R_2^2}{3l_{12}^2}\right) + \dot{R}_1 \left(\frac{R_1}{l_{12}}\right)^2 \\ \boldsymbol{\Omega}_2^{(1)} &= \frac{1}{2} \nabla \times (\mathbf{u}_1^{(0)} + \mathbf{u}_3^{(0)}) \Big|_{\mathbf{x}=\mathbf{x}_2} = \mathbf{0}. \end{aligned}$$

From this one sees that at the first reflection, the presence of the passive sphere at a sufficient distance does not affect the swimmer, but the converse is not true – the effect of the swimmer on the passive sphere is non-zero after the first reflection. Its translational velocity $\mathbf{U}_3^{(1)}$ is given by the sum of the contributions from translation and expansion of the swimmer's spheres, *viz.*,

$$\mathbf{U}_3^{(1)} = \sum_{i=1,2} \mathbf{U}_{3,i}^{(1,f)} + \mathbf{U}_{3,i}^{(1,e)} \quad (4.2)$$

where

$$\mathbf{U}_{3,i}^{(1,f)} = \left(1 + \frac{R_3^2}{6} \nabla^2\right) \mathbf{u}\{\mathbf{F}_i\} \Big|_{\mathbf{x}=\mathbf{x}_3} = \frac{1}{8\pi\mu l_{i3}} \left[\left(1 + \frac{R_i^2 + R_3^2}{3l_{i3}^2}\right) \mathbf{F}_i + \left(1 - \frac{R_i^2 + R_3^2}{l_{i3}^2}\right) (\mathbf{F}_i \cdot \mathbf{d}_{i3}) \mathbf{d}_{i3} \right] \quad (4.3)$$

$$\mathbf{U}_{3,i}^{(1,e)} = \frac{1}{2} \nabla \times \left(R_i^2 \dot{R}_i \frac{\mathbf{x} - \mathbf{x}_i}{|\mathbf{x} - \mathbf{x}_i|^3} \right) \Big|_{\mathbf{x}=\mathbf{x}_3} = \dot{R}_i \left(\frac{R_i}{l_{i3}}\right)^2 \mathbf{d}_{i3} \quad (4.4)$$

and

$$\mathbf{d}_{i3} = \frac{\mathbf{x}_3 - \mathbf{x}_i}{|\mathbf{x}_3 - \mathbf{x}_i|}, \quad l_{i3} = |\mathbf{x}_3 - \mathbf{x}_i|.$$

Although sphere 1 and 2 are rotation-free after the first reflection, one finds that the translation of sphere 1 and 2 contributes to the rotation of $\boldsymbol{\Omega}_3^{(1)}$, while their expansion has no effect on $\boldsymbol{\Omega}_3^{(1)}$. The detailed calculation

of $\boldsymbol{\Omega}_3^{(1)}$ is straightforward and is given in Appendix C. The result is that

$$\boldsymbol{\Omega}_3^{(1)} = \sum_{i=1,2} \frac{F_i}{8\pi\mu l_{i3}^3} [(\mathbf{x}_3 - \mathbf{x}_i) \cdot \mathbf{e}_y] \mathbf{e}_z. \quad (4.5)$$

To summarize the analysis for the first reflection, we first solve for the motion of the swimmer and the forces it exerts using the system (3.24), and use the results in equations (4.2, 4.5) to obtain the motion of sphere 3.

4.2 Accuracy of the system

For the PMPY, as we mentioned earlier, up to the first reflection, the passive buoyant sphere 3 has no effect on the PMPY model. It follows from section 3.2, that after the first reflection the translational velocities of the two spheres of the PMPY (U_1, U_2), together with the translational velocity of the PMPY ($\bar{\mathbf{U}}$), is accurate up to the δ^3 order. The leading order of $\hat{\bar{\mathbf{U}}}$ is of $O(1)$, as shown by equation (3.30). Because $\boldsymbol{\Omega}_{1,2}^{(0)} = \boldsymbol{\Omega}_{1,2}^{(1)} = \mathbf{0}$, we neglect the rotation effect of the PMPY.

Similar to the analysis of the PMPY, neglecting the second and higher reflections for the passive sphere 3 results in the translational velocity $\mathbf{U}_3 \sim \mathbf{U}_3^{(0)} + \mathbf{U}_3^{(1)}$ accurate up to order δ^3 . Moreover, the effects from the self-deformable PMPY model on sphere 3 starts to show up from the first reflection ($\mathbf{U}_3^{(0)} = \mathbf{0}$), thus an estimate of the leading term of $\hat{\mathbf{U}}_3$ is

$$\sum_{i=1,2} \frac{3}{4} \frac{\hat{\mathbf{F}}_i + (\hat{\mathbf{F}}_i \cdot \mathbf{d}_{i3}) \mathbf{d}_{i3}}{\hat{l}_{i3}} \delta \sim O(\delta)$$

For the angular velocity we have $\boldsymbol{\Omega}_3 \sim \boldsymbol{\Omega}_3^{(0)} + \boldsymbol{\Omega}_3^{(1)} = \boldsymbol{\Omega}_3^{(1)}$, and thus the leading order of $\hat{\boldsymbol{\Omega}}_3$ can be estimated as follows:

$$\sum_{i=1,2} \frac{3\hat{\mathbf{F}}_i}{4\hat{l}_{i3}^3} [(\hat{\mathbf{x}}_3 - \hat{\mathbf{x}}_i) \cdot \mathbf{e}_y] \mathbf{e}_z \delta^3 \sim O(\delta^3)$$

In the wide-separation regime, i.e., when $\delta \ll 1$, it is clear that the angular velocity of the passive sphere 3 ($\hat{\boldsymbol{\Omega}}_3 \sim O(\delta^3)$) can be neglected compared to its translational velocity $\hat{\mathbf{U}}_3 \sim O(\delta)$ or the translational velocity of PMPY ($\hat{\bar{\mathbf{U}}} \sim O(1)$).

To investigate the second reflection, we must first compute all the velocities — $\mathbf{u}_{ij}^{(1)}$ for $i, j = 1, 2, 3, i \neq j$ — that result from putting sphere j into the flow $\mathbf{u}_i^{(0)}$. Since $\mathbf{u}_3^{(0)} \equiv \mathbf{0}$ (equation (4.1)), we have $\mathbf{u}_{3j}^{(1)} \equiv \mathbf{0}$ for $j = 1, 2$. On the other hand, when we put sphere 2 or 3 into $\mathbf{u}_1^{(0)}$, the resulting flow $\mathbf{u}_{1j}^{(1)}$ is a superposition of two parts:

$$\mathbf{u}_{1j}^{(1)} = \mathbf{u}_{1j}^{(1)} \{\mathbf{F}_1\} + \mathbf{u}_{1j}^{(1)} \{\dot{\mathbf{R}}_1\}$$

where $\mathbf{u}_{1j}^{(1)} \{\mathbf{F}_1\}$ results from the drag force \mathbf{F}_1 exerted on sphere 1, and its leading term is of the order δ^4 (Kim & Karrila 1991); $\mathbf{u}_{1j}^{(1)} \{\dot{\mathbf{R}}_1\}$ results from the radial deformation of sphere 1, and its leading term is of the order δ^5 . Hence $\mathbf{u}_{1j}^{(1)} \sim O(\delta^4)$ and similarly, $\mathbf{u}_{2j}^{(1)} \sim O(\delta^4)$ as well. Thus for sphere 1:

$$\begin{aligned} \mathbf{U}_1^{(2)} &= \left(1 + \frac{R_1^2}{6} \nabla^2\right) (\mathbf{u}_{12}^{(1)} + \mathbf{u}_{13}^{(1)} + \mathbf{u}_{23}^{(1)} + \mathbf{u}_{32}^{(1)}) \Big|_{\mathbf{x}=\mathbf{x}_1} + \sim O(\delta^4) \\ \boldsymbol{\Omega}_1^{(2)} &= \frac{1}{2} \nabla \times (\mathbf{u}_{12}^{(1)} + \mathbf{u}_{13}^{(1)} + \mathbf{u}_{23}^{(1)} + \mathbf{u}_{32}^{(1)}) \Big|_{\mathbf{x}=\mathbf{x}_1} + \sim O(\delta^5) \end{aligned}$$

with similar results for sphere 2 and 3 as well. In conclusion, the results we obtained from section 4.1 are accurate up to the δ^3 term.

Finally, it is easily seen that the results obtained in section 4.1 can be applied to a system consisting of a PMPY model and N passive neutrally-buoyant spheres, as long as the spheres are separated sufficiently. We number the two spheres in the PMPY model as sphere 1 and 2, as usual, and the others from sphere 3 to sphere $N + 2$. For each of the N passive spheres, $\mathbf{u}_i^{(0)} \equiv 0$ ($i = 3, 4, \dots, N + 2$) in the zeroth reflection, from which we conclude that: up to the first reflection,

1. The PMPY model does not "see" the other spheres:

$$\mathbf{\Lambda}_i^{(1)} = \mathbf{\Lambda}_{i,j}^{(1,f)} + \mathbf{\Lambda}_{i,j}^{(1,e)} + \sum_{n=3}^{N+2} \left(\mathbf{\Lambda}_{i,n}^{(1,f)} + \mathbf{\Lambda}_{i,n}^{(1,e)} \right) = \mathbf{\Lambda}_{i,j}^{(1,f)} + \mathbf{\Lambda}_{i,j}^{(1,e)}$$

where $i, j = 1, 2$, $i \neq j$ and $\mathbf{\Lambda}$ stands for \mathbf{U} or $\mathbf{\Omega}$.

2. Each passive sphere only "sees" the PMPY model and "sees" no other spheres:

$$\mathbf{\Lambda}_n^{(1)} = \sum_{i=1,2} \left(\mathbf{\Lambda}_{n,i}^{(1,f)} + \mathbf{\Lambda}_{n,i}^{(1,e)} \right) + \sum_{\substack{m \neq n \\ 3 \leq m \leq N+2}} \left(\mathbf{\Lambda}_{n,m}^{(1,f)} + \mathbf{\Lambda}_{n,m}^{(1,e)} \right) = \sum_{i=1,2} \left(\mathbf{\Lambda}_{n,i}^{(1,f)} + \mathbf{\Lambda}_{n,i}^{(1,e)} \right)$$

where $n \in 3, 4, \dots, N + 2$ and $\mathbf{\Lambda}$ stands for \mathbf{U} or $\mathbf{\Omega}$.

4.3 Chasing an object

The scenario of a micro-swimmer swimming with a passive object has many applications. For example, can a microorganism that locates a target object (nutrient, a bacterium, etc.), capture the object within a reasonable time period? To be specific, the micro-swimmer should be able to swim fast enough to reach the target object, and the object, as it is passive, should not be pushed away faster than the micro-swimmer swims, especially when they are close.

We consider a scenario in which a PMPY swims toward a passive sphere directly in front of it, in simulating a microorganism chasing an object. As we discussed in section 3.4, a PMPY is an effective swimmer — with a translational velocity $\hat{\mathbf{U}}$ scales as $O(1)$ — and approximates the swimming behavior of *Dd amoebae* (Van Haastert 2011), which feed on bacteria. This indicates that a PMPY can swim a distance within a reasonable time period by consuming a reasonable amount of energy. For the movement of the passive sphere 3 that results from the hydrodynamic interaction with the PMPY, as we discussed in section 4.2, the leading term of $\hat{\mathbf{U}}_3$ is

$$\hat{\mathbf{U}}_3 \sim \hat{\mathbf{U}}_3^{(1)} \sim \sum_{i=1,2} \frac{3}{4} \frac{\hat{\mathbf{F}}_i + (\hat{\mathbf{F}}_i \cdot \mathbf{d}_{i3}) \mathbf{d}_{i3}}{\hat{l}_{i3}} \delta \quad (4.6)$$

Since the spheres are collinear we have $\mathbf{d}_{13} = \mathbf{d}_{23}$, and the force-free constraint of the PMPY gives $\hat{\mathbf{F}}_1 = -\hat{\mathbf{F}}_2$, both of which lie along \mathbf{d}_{13} . Therefore we have the following estimate of the translational velocity $\hat{\mathbf{U}}_3$.

$$\hat{\mathbf{U}}_3 \sim -\frac{3}{2} \hat{\mathbf{F}}_1 \left(\frac{1}{l_{13}} - \frac{1}{l_{23}} \right) \delta = -\frac{3}{2} \hat{\mathbf{F}}_1 \frac{l_{12}}{l_{13} l_{23}} \delta,$$

and by using equation (3.29) we have

$$\hat{\mathbf{U}}_3 \sim \frac{3}{2} \frac{l_{12}}{l_{13} l_{23}} \frac{R_1 R_2}{R_1 + R_2} \delta \xi. \quad (4.7)$$

From equation (4.7) we see that when the passive sphere 3 is far from the PMPY, i.e., $l_{13} \gg 1$, $l_{23} \gg 1$, \hat{U}_3 scales much less than $O(\delta)$, and only when the PMPY is close to the target can \hat{U}_3 increase to $O(\delta)$. Therefore, with the estimates of the translational velocities of the PMPY and the passive sphere giving $\hat{U} \sim O(1)$ and $\hat{U}_3 < O(\delta)$, we confirm that a PMPY can easily capture its passive target. Moreover, we note that although in problems like nutrient supply, the target objects are likely to be much smaller than the microswimmer, this size relation is not required here. As we can see from the equation (4.7), the size of the passive sphere (R_3) does not enter the leading order term of \hat{U}_3 . In fact, from equations (4.3, 4.4), R_3 only shows up in the $O(\delta^3)$ term, and as long as $R_3/l_{i3} \sim O(1)$, $i = 1, 2$, the above analysis and conclusions still hold.

To numerically investigate the effects of the PMPY on the passive sphere 3, we consider the following system (Figure 4.2a). At $t = 0$ the passive sphere 3 is at a distance d_0 from the leading sphere (i.e., sphere 2), and for $t > 0$ the PMPY swimmer executes the following cyclic deformations.

$$R_1(t) = 2 - \sin 2\pi t, \quad R_2(0) = 3, \quad R_3 \equiv 2, \quad l_{12} = l_0 + \cos 2\pi t, \quad \text{for } t \in [0, 1] \quad (4.8)$$

With this stroke the PMPY swimmer moves in the positive x direction and pushes the passive sphere in that direction. We take $l_0 = 12$, $d_0 = 20$, which allows the PMPY swimmer to execute a few cycles before it gets too close to sphere 3, that is, when $l_{23} \leq L_m$. The system profile gives $R_M \sim 3.24$, $L_m = 11$, $\delta \sim 0.29$. The translation of the PMPY is computed by equation (3.24), while that of sphere 3 is computed from equations (4.3, 4.4). After 13.5 cycles, the PMPY model swims a scaled distance of $\hat{X}_{\text{PMPY}} \sim 3.13$, while the passive sphere only moves a scaled distance $\hat{X}_3 = 0.29$ (Figure 4.2b&c). Thus $\hat{X}_3/\hat{X}_{\text{PMPY}} \sim 0.087$, which is even less than the estimated ratio $\hat{U}_3/\hat{U} \sim O(\delta)$. One sees in (b) that the trajectory of the passive sphere (blue solid line in Figure 4.2b) is only slightly tilted as compared to that of the PMPY swimmer (red solid line in Figure 4.2b). This reflects the fact that sphere 3 oscillates back and forth, and the oscillations grow as the swimmer approaches the sphere, as seen in Figure 4.2c. Thus the swimmer can easily catch up to the passive object, but lubrication effects arise when they are in close proximity.

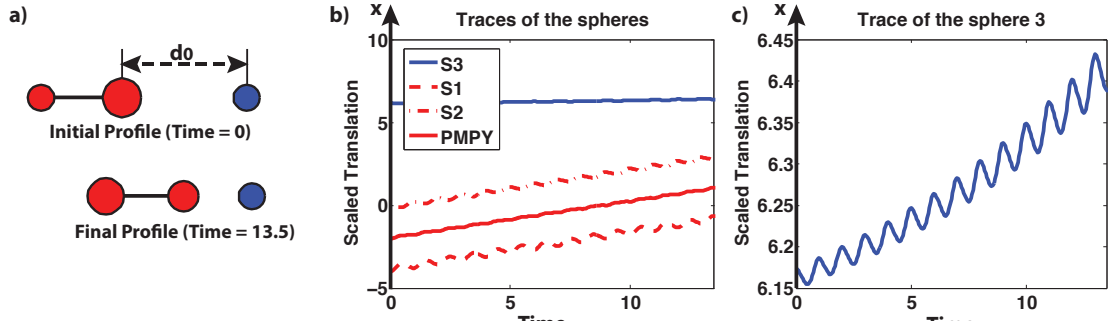


Fig. 4.2 Simulation of a PMPY swimmer and a passive sphere, arranged collinearly. (a) Initial and final profiles of the system. (b) Translation of all components in the 13.5 cycles. (c) Translation of S3 within 13.5 cycles.

4.4 Tracer trajectories

Another important application of this swimmer-object interaction problem is swimmer-tracer scattering (Dunkel *et al.* a), in which the swimming of micro-organisms stirs the surrounding fluid. This is important

in controlling and enhancing nutrient uptake, and leads to enhanced tracer diffusion observed in swimmer suspensions (Wu & Libchaber 2000, Leptos *et al.* 2009, Sokolov *et al.* 2009, Kurtuldu *et al.* 2011, Miño *et al.* 2011). Experimental observations show that trajectories of tracers in a suspension of swimmers are often nearly-closed loops (Leptos *et al.* 2009), and theoretical arguments and simulation predictions have emerged since to elucidate this phenomenon (Underhill *et al.* 2008, Rushkin *et al.* 2010, Ishikawa *et al.* 2010, Lin *et al.* 2011, Zaid *et al.* 2011). In particular, the PMPY model has been used in the study of swimmer-tracer scattering, where an asymptotic analysis based on the stroke-averaged behavior of the PMPY, together with some simulations, illustrate the near closed-loop of a triangular shape of the tracer (Dunkel *et al.* a). In this section we apply the reflection analysis elaborated in sections 4.1 and 4.2 to further investigate the tracer trajectories induced by a PMPY swimmer.

4.4.1 The instantaneous velocity of the tracer sphere

The swimmer-tracer interaction is easily found by asymptotic analysis when the swimmer and the tracer are far apart (Dunkel *et al.* a, Pushkin *et al.* 2013, Yeomans *et al.* 2014). As is the case for a PMPY swimmer, when a spherical object is far away from it, i.e., $l_{13}, l_{23} \gg 1$, the asymptotic estimate is given by equation (4.6), and the instantaneous velocity of the tracer sphere as a function of its location, is shown in Figure 4.3. In this case, the velocity field is the same as the asymptotic behavior of the velocity field generated by a single PMPY (Dunkel *et al.* a). In this snapshot the connecting rod is expanding ($\dot{l} > 0$), and one sees that

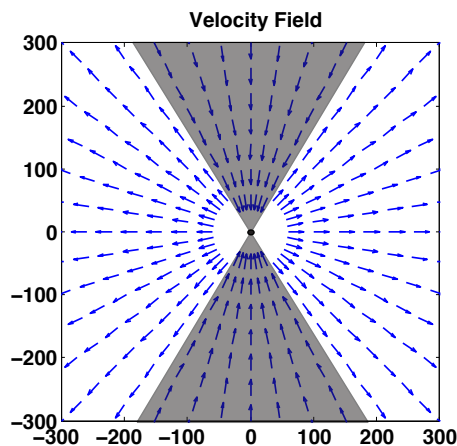


Fig. 4.3 A snapshot of the instantaneous velocity field generated by a PMPY swimmer and felt by a tracer sphere when the latter is far away from the swimmer. In this simulation the PMPY is located at the origin, with an instantaneous profile $R_1 = R_2 = 2$, $l = 6$, the connecting rod is expanding (i.e., $\dot{l} > 0$), and the expansion/contraction of the spheres in the PMPY is neglected as it only generates $O(\delta^2)$ order terms. The tracer sphere has radius $R_3 = 2.5$. Arrows only show the direction, not the magnitude, of the velocity.

the velocity field is divided into four domains. A tracer sphere located in the two shaded domains will be attracted to the PMPY and repulsed if it is located in the two white domains.

The reflection analysis allows us to observe the situation when the PMPY and the tracer sphere get close to each other, as long as $\delta < 1$ still holds. Moreover, as we showed in section 4.1, the velocity of the tracer sphere \mathbf{U}_3 consists of two parts: $\mathbf{U}_3^{(f)}$ that results from the drag forces on the two spheres in the swimmer (equation (4.3)), and $\mathbf{U}_3^{(e)}$, which results from the radial changes (equation (4.4)). To further

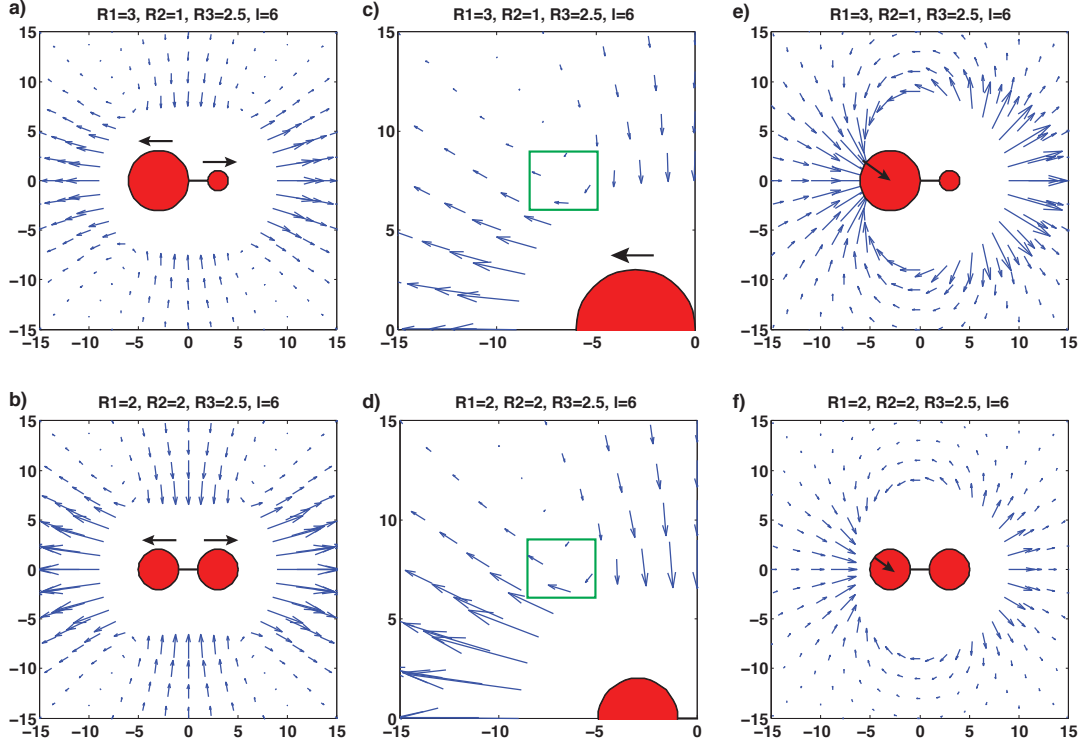


Fig. 4.4 The instantaneous velocity of a tracer sphere that results from a swimming PMPY, when the tracer sphere is close to the PMPY. The arrows in all panels are scaled uniformly, thus arrows show both direction and magnitudes. a,b) The connecting rod is instantaneously expanding at $\dot{l} = 2\pi$, and there is no expansion/contraction in the PMPY. c/d) A blown-up view of panel a/b) near sphere 1 in the PMPY. e,f) Sphere 1 is instantaneously shrinking at $\dot{R}_1 = -2\pi$ while sphere 2 is expanding. No connecting rod expansion/contraction in the PMPY.

investigate the separate effects of drag and expansion when the tracer sphere is close to the PMPY, we show the instantaneous velocity of the tracer sphere in different stages of movement of the swimmer in Figure 4.4. Figure 4.4 a&b show the velocity field when the PMPY connecting rod is expanding without radial changes, and the spheres of the PMPY are either of unequal sizes (a) or equal sizes (b). Comparing Figure 4.4 a&b with Figure 4.3 we see that even at small separations, the local velocity varies little from the far-field behaviors. The reason for this similarity is that other than the leading $O(1)$ term, the next term in $\mathbf{U}_3^{(f)}$ (equation (4.3)) is an $O(\delta^3)$ term, which decreases very rapidly as l_{13} & l_{23} increase. However, a blown-up view of the velocity fields shows that the $O(\delta^3)$ term does give rise to a tangential velocity when the tracer sphere is close to the swimmer, as it must. This is clear at the border of the shaded & white regions shown in Figure 4.3 (shown by arrows in the green boxes in Figure 4.4 c&d). This rotation of the velocity field is larger when the PMPY have unequal-sized spheres and the tracer sphere is near the larger one (Figure 4.4c). Figure 4.4 e&f show the velocity field when the PMPY undergoes radial changes without changes in the length of the connecting rod. Again we consider unequal-sized spheres (Figure 4.4e) and equal-sized spheres (Figure 4.4f) at one instant. In the asymptotic analysis (Figure 4.3) the effects on the tracer sphere that result from radial changes in the swimmer are not considered, as they only give rise to $O(\delta^2)$ terms

(equation (4.4)). However, as we can see from Figure 4.4ef, expansion and contraction of the swimmer have significant effects on the tracer sphere, and therefore should be taken into account.

Finally, when the two shape changes governed by \dot{l} and \dot{R}_1 are combined, as occurs in most of the simulations, the $O(\delta^2)$ term in the tracer's velocity clearly gives rise to a large change from the asymptotic solution when the tracer is close to the PMPY (compare Figure 4.3 and 4.5). In particular, depending on the instantaneous system profile, the effects resulting from the sphere expansion/contraction might overcome that from the rod length changes (Figure 4.5a), and therefore an asymptotic analysis is not sufficient for the study of swimmer-tracer interactions when they are close together.

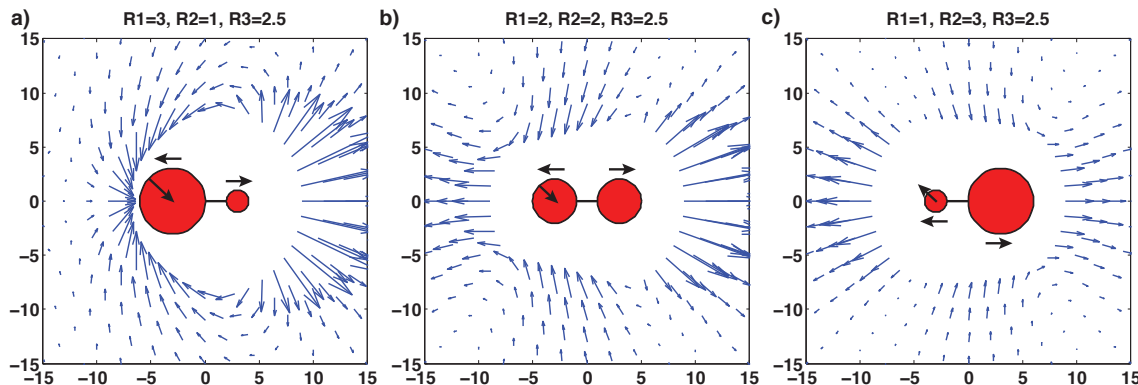


Fig. 4.5 The instantaneous velocity of a tracer sphere that results from a PMPY swimmer when the tracer sphere is close to the PMPY and higher-order effects are included. The arrows in all panels are scaled uniformly, thus arrows show both direction and magnitudes. a) The connecting rod is instantaneously expanding at $\dot{l} = 2\pi$ and sphere 1 is shrinking at $\dot{R}_1 = -2\pi$. figure. b) $\dot{l} = 2\pi$, $\dot{R}_1 = -2\pi$. c) $\dot{l} = 2\pi$, $\dot{R}_1 = 2\pi$.

4.4.2 The long-term behavior of the tracer

As we mentioned earlier, experimental observations show that trajectories of tracers in a suspension of swimmers often look loop-like (Leptos *et al.* 2009), but a loop-like trajectory will not enhance nutrient supply. In fact, simulations of *Rhodobacter sphaeroids* (Shum *et al.* 2010) have shown that when the tracer is far away from the straight path of the swimmer, the loop-like trajectory is approximately true with the net displacement between the initial and final locations considerably shorter than the characteristic trajectory size. On the other hand, when the tracer is close to the swimmer path, it is clearly pulled forward by the swimmer (Pushkin *et al.* 2013, Yeomans *et al.* 2014). Here we demonstrate a similar effect for a PMPY swimmer. The results, again with the translation of the PMPY computed by equation (3.24) and that of sphere 3 by equations (4.3, 4.4) are given in Figure 4.6a. The result is qualitatively similar to what is obtained from the simulations of *Rhodobacter sphaeroids* (Shum *et al.* 2010), that is, the tracer is pushed backwards slightly when more distant from the PMPY swimming path, and clearly pulled forward when close to the path. Its trajectory has three distinct branches, and a close-up view of a part of the trajectory shows that the tracer undergoes a spiral oscillatory motion, which is qualitatively similar to existing results (Dunkel *et al.* a, Pushkin *et al.* 2013, Yeomans *et al.* 2014). According to an asymptotic analysis (Pushkin *et al.* 2013), the tracer trajectory should approximate a closed loop, but when it is close to the PMPY Figures 4.4 and 4.5 show that the $O(\delta^2)$ term resulting from sphere expansion and contraction induces a significant distortion

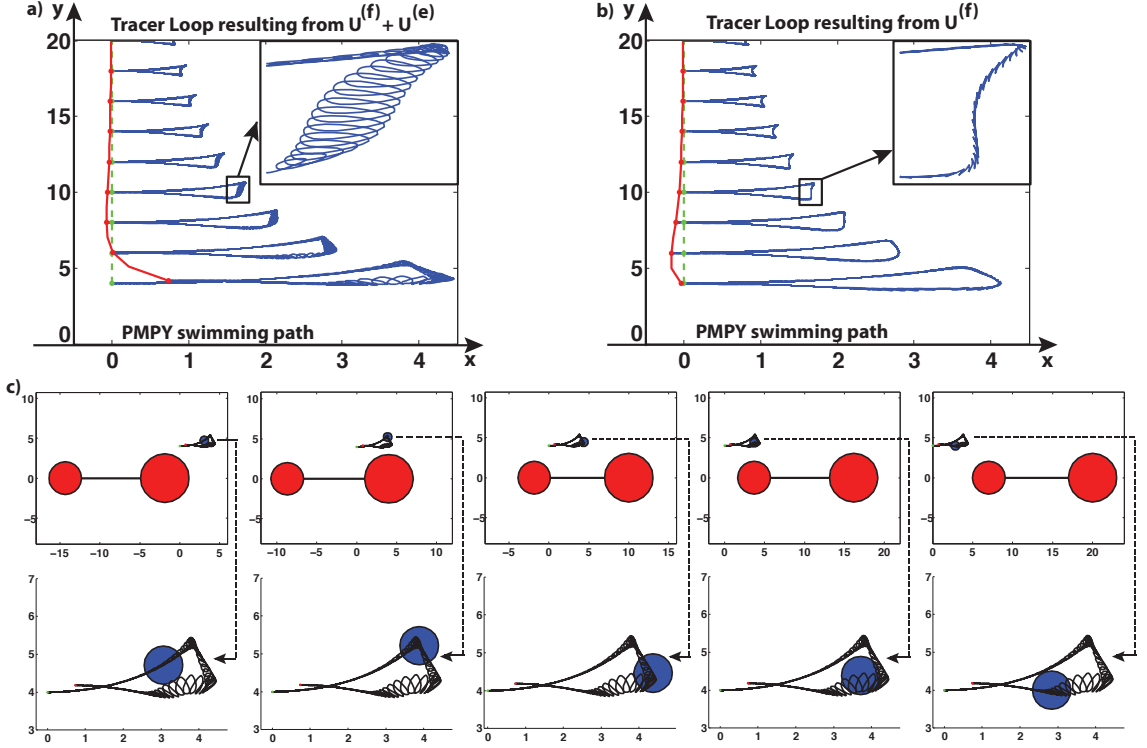


Fig. 4.6 The tracer loop when a PMPY swimmer moves in a straight line. The system profile is: $l(t) = 12 + \cos(2\pi t)$, $R_1 = 2 - \sin(2\pi t)$, $R_2(0) = 3$, $R_3 \equiv 0.5$. The swimmer moves along the x -axis, from $x = -1000$ to $x = 1000$. The tracer sphere 3 is originally located at point $(0, Y_0)$, where $Y_0 \in [4, 20]$ is the vertical distance of the tracer to the swimmer's path. The green dashed lines give the starting points of the tracer while the red solid line gives the end points. These curves are computed at increments of $\Delta Y_0 = 1$. We also show several tracer trajectories (blue solid lines), drawn for $\Delta Y_0 = 2$. a) The tracer loop of sphere 3, with $\mathbf{U}_3 = \mathbf{U}_3^{(f)} + \mathbf{U}_3^{(e)}$. b) The tracer loop of sphere 3, computed as $\mathbf{U}_3 \sim \mathbf{U}_3^{(f)}$ only. c) Snap-shots of the system in (a) with $Y_0 = 4$ and the enlarged view of sphere 3 showing its location in the loop.

to the instantaneous velocity field of the tracer. The blow-up in Figure 4.6c shows the position of the tracer sphere relative to the swimmer's position in the upper panels and the corresponding position along the quasi-loop in the lower panels. These are instantaneous snapshots, but the swimmer undergoes many cycles in the entire sequence. One sees there that the oscillations are smaller when the swimmer is approaching the tracer, during which the tracer is pushed away from the swimmer; on the other hand. Conversely, the oscillations are larger when the tracer is in the wake of the swimmer, when the tracer is being pulled toward the swimmer. While the net translation direction of the tracer per swimmer cycle is determined by its relative position to the swimmer (tracer movement: forward/downward/backward \equiv location: in front of/above/behind), the amplitude of the tracer oscillations is determined by its distance to the swimmer, as can be expected.

To investigate the effects of rod or/and sphere expansion/contraction we ran the long-term swimmer-tracer simulation again with the same strokes but with the translational velocity of the tracer computed from the flow generated by rod length changes only, i.e., $\mathbf{U}_3 \sim \mathbf{U}_3^{(f)}$ (equation (4.3)). The result is shown in Figure 4.6b, from which we see that the tracer is still pushed backward slightly, even when close to the PMPY swimming path. Thus Figure 4.6b shows that at least under the current system profile, the effect of

the drag force, which approximates the asymptotic behavior, indeed produces an essentially closed loop-like trajectory of the tracer, as was concluded in (Pushkin *et al.* 2013). On the other hand, the forward motion of the tracer (Figure 4.6a) is primarily due to the sphere expansion/contraction $O(\delta^2)$ terms. Moreover, a close-up view of the trajectory shows that the tracer still undergoes an oscillatory motion when subject only to the velocity field due to rod shortening and lengthening (Figure 4.6b, upper-right corner), but not in a spiral manner. Therefore we conclude that the spiral mode of the tracer motion is primarily due to the expansion/contraction of the PMPY spheres.

Next we investigate whether the shape of the PMPY swimmer also has an effect on the tracer scattering behavior. We consider swimmers with different rod lengths. In the following simulations we consider the system profiles

$$l(t) = L_0 + \cos(2\pi t), \quad R_1 = 2 - \sin(2\pi t), \quad R_2(0) = 3, \quad R_3 \equiv 0.5,$$

with $L_0 = 8, 12, 20, 50$. The simulation results, with $\mathbf{U}_3 = \mathbf{U}_3^{(f)} + \mathbf{U}_3^{(e)}$ calculated from equations (4.3, 4.4) are given in Figure 4.7a. There one sees that the longer the rod is, or equivalently, the further the two spheres in the swimmer are apart, the more the tracer is pulled forward, especially when it is close to the swimmer's path. Because we found earlier that the PMPY sphere expansion/contraction contributes significantly to the movement of the tracer, we repeat the simulations in Figure 4.7a but with $\mathbf{U}_3 \sim \mathbf{U}_3^{(f)}$ computed by equation (4.3) only, which approximates the asymptotic behavior. The results are shown in Figure 4.7b, from which we see that even without the sphere expansion/contraction, the tracer is still clearly dragged forward when it is close to the swimming path of a long PMPY ($L_0 = 50$). To understand this behavior, we compare two tracer trajectories, both of which result from $\mathbf{U}_3 \sim \mathbf{U}_3^{(f)}$ only. One starts with $L_0 = 12$ and $Y_0 = 10$ (Figure 4.7c), i.e., the PMPY spheres are not far apart and the tracer is not very close to the swimmer's path, and the other starts with $L_0 = 50$ and $Y_0 = 4$ (Figure 4.7d), i.e., the PMPY spheres are far apart and the tracer is close to the swimmer's path. In Figure 4.7c the trajectory of the tracer approximates an isosceles triangle and the base (side 2 in the figure) corresponds to the part of the trajectory in which the tracer is essentially directly over the swimmer. On the other hand, when L_0 is large, as in (d), the trajectory of the tracer is very different, and in particular, we see that side 2 of the triangle-like trajectory is stretched horizontally, which reflects enhanced pulling effect on the tracer. In either case, side 2 of the trajectory loop essentially reflects the tracer motion when it is above the swimmer, and therefore the comparison between Figure 4.7c and d indicates that the separation of spheres in the PMPY results in an increased pulling effect on the tracer if it is close enough to the swimmer's path.

In conclusion, we find that when the tracer is close to the infinite PMPY swimming path,

1. the $O(\delta^2)$ term that results from the PMPY sphere expansion/contraction contributes significantly to the tracer scattering;
2. increasing the sphere separation in a PMPY swimmer will enhance the tracer scattering.

5 Swimming with a friend

In this final section of analysis we consider the hydrodynamic interactions between two PMPY swimmers in an infinite fluid domain, as shown in Figure 5.1. To fix the geometry, we introduce a fixed Cartesian frame and we assign a body frame to each swimmer. $\{\mathbf{0}; \mathbf{e}_x, \mathbf{e}_y, \mathbf{e}_z\}$ is attached to PMPY I and has its origin $\mathbf{0}$ at the center \mathbf{x}_1 of sphere 1, and has \mathbf{e}_x along the direction of the connecting rod; while $\{\mathbf{0}'; \mathbf{e}_{x'}, \mathbf{e}_{y'}, \mathbf{e}_{z'}\}$ is attached to PMPY II and has its origin $\mathbf{0}$ at the center \mathbf{x}_3 of sphere 3, and $\mathbf{e}_{x'}$ along the direction of its connecting rod.

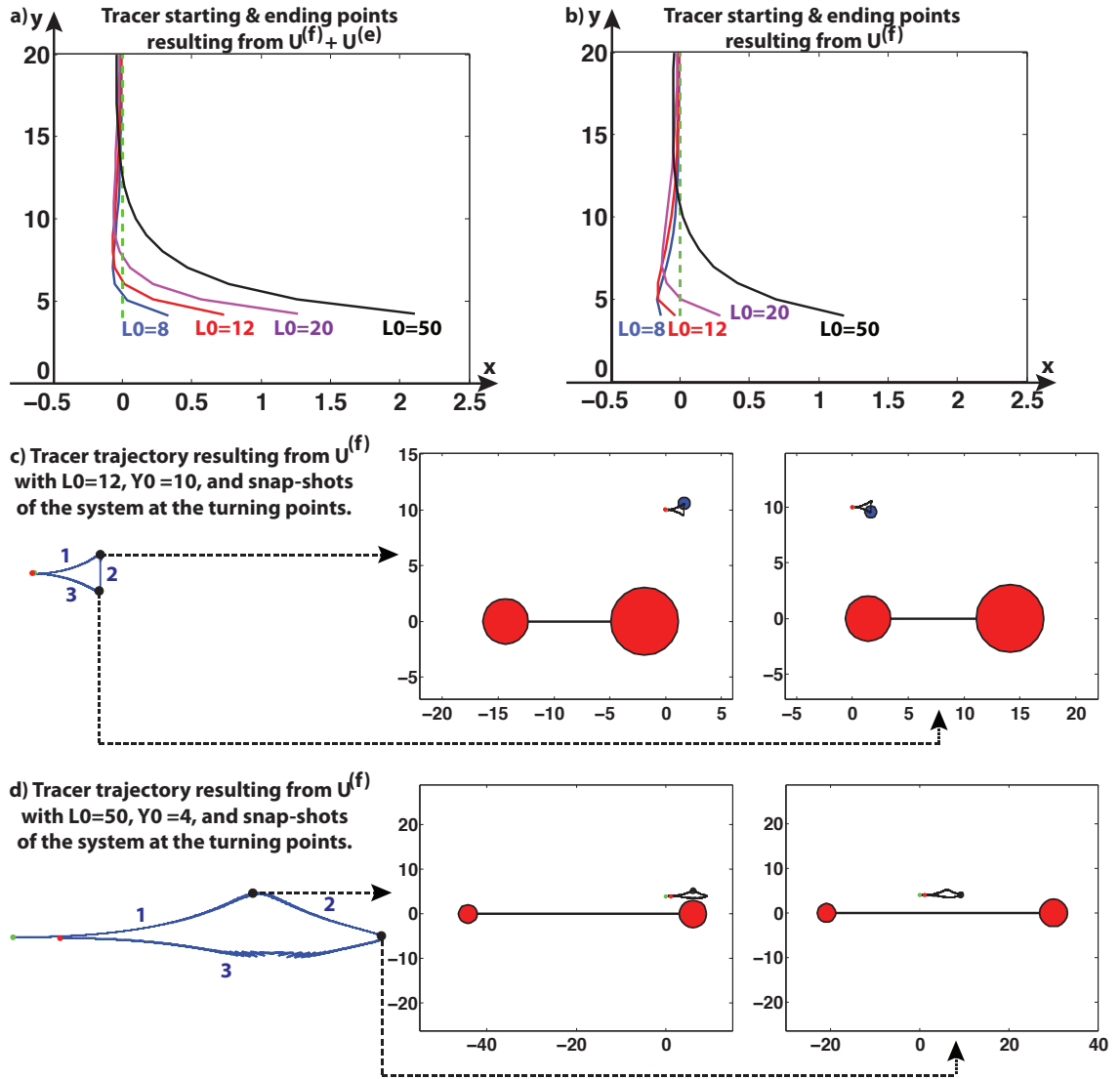


Fig. 4.7 a) The tracer sphere's starting (green dashed line) and ending points (solid lines) when a PMPY swims along the x -axis, from $x = -1000$ to $x = 1000$. The system profile is: $l(t) = L_0 + \cos(2\pi t)$, $R_1 = 2 - \sin(2\pi t)$, $R_2(0) = 3$, $R_3 \equiv 0.5$, with $L_0 = 8, 12, 20, 50$ (blue, red, magenta, and black solid lines). The tracer sphere 3 is originally located at $(0, Y_0)$, where $Y_0 \in [4, 20]$ is the vertical distance of the tracer to the PMPY swimming path. The lines are computed with $\Delta Y_0 = 1$. The translational velocity of the tracer sphere is calculated as $U_3 = U_3^{(f)} + U_3^{(e)}$. b) $U_3 \sim U_3^{(f)}$. c) The tracer trajectory with $L_0 = 12$, $Y_0 = 10$ and $U_3 \sim U_3^{(f)}$ only. Snapshots of the system at the turning points of the tracer trajectory. d) As in (c) but with $L_0 = 50$, $Y_0 = 4$.

The relationship between the two frames is given by

$$\begin{cases} \mathbf{e}_{x'} = \cos \phi \mathbf{e}_x + \sin \phi \mathbf{e}_y \\ \mathbf{e}_{y'} = -\sin \phi \mathbf{e}_x + \cos \phi \mathbf{e}_y \\ \mathbf{e}_{z'} = \mathbf{e}_z \end{cases}$$

where ϕ is the angle between the two connecting rods: $\phi = \arccos(\mathbf{d}_{12} \cdot \mathbf{d}_{34})$ and $\mathbf{d}_{ij} = (\mathbf{x}_j - \mathbf{x}_i)/|\mathbf{x}_j - \mathbf{x}_i|$.

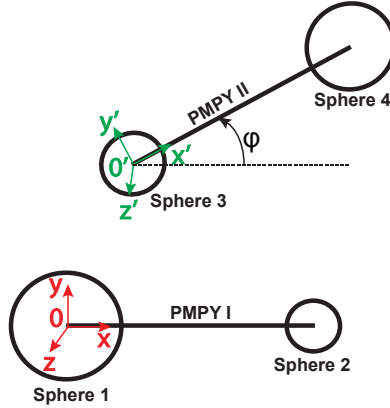


Fig. 5.1 The geometry of two PMPY swimmers in \mathbb{R}^3 .

5.1 Preliminary analysis of the two-swimmer system

The basic steps in the analysis of the two PMPY swimmer system are the same as in previous sections, and therefore we only sketch the analysis up to the first reflection. In the zeroth reflection, no hydrodynamic interactions are considered, and therefore

$$\mathbf{U}_i^{(0)} = \frac{1}{6\pi\mu R_i} \mathbf{F}_i, \quad \boldsymbol{\Omega}_i^{(0)} = \mathbf{0}. \quad (5.1)$$

The translational velocities after the first reflection are given by

$$\mathbf{U}_i^{(1)} = \sum_{j \neq i} [\mathbf{U}_{i,j}^{(1,f)} + \mathbf{U}_{i,j}^{(1,e)}] \quad (5.2)$$

$$\mathbf{U}_{i,j}^{(1,f)} = \frac{1}{8\pi\mu l_{ij}} \left[\left(1 + \frac{R_i^2 + R_j^2}{3l_{ij}^2}\right) \mathbf{F}_j + \left(1 - \frac{R_i^2 + R_j^2}{l_{ij}^2}\right) (\mathbf{F}_j \cdot \mathbf{d}_{ji}) \mathbf{d}_{ji} \right] \quad (5.3)$$

$$\mathbf{U}_{i,j}^{(1,e)} = \dot{R}_j \left(\frac{R_j}{l_{ij}}\right)^2 \mathbf{d}_{ji} \quad (5.4)$$

where $l_{ij} = |\mathbf{x}_i - \mathbf{x}_j|$ and $\mathbf{d}_{ji} = (\mathbf{x}_i - \mathbf{x}_j)/l_{ij}$. The corresponding angular velocities are

$$\boldsymbol{\Omega}_\alpha^{(1)} = \sum_{i=1,2} \frac{F_i}{8\pi\mu l_{i\alpha}^3} [(\mathbf{x}_\alpha - \mathbf{x}_i) \cdot \mathbf{e}_y] \mathbf{e}_z \quad \text{for } \alpha = 3, 4 \quad (5.5)$$

$$\boldsymbol{\Omega}_i^{(1)} = \sum_{\alpha=3,4} \frac{F_\alpha}{8\pi\mu l_{\alpha i}^3} [(\mathbf{x}_i - \mathbf{x}_\alpha) \cdot \mathbf{e}_{y'}] \mathbf{e}_{z'} \quad \text{for } i = 1, 2. \quad (5.6)$$

In addition, the system should satisfy the volume conservation condition

$$\sum_{i=1,2} R_i^3(t) \equiv \frac{3}{4\pi} V_I, \quad \sum_{\alpha=3,4} R_\alpha^3(t) \equiv \frac{3}{4\pi} V_{II} \quad (5.7)$$

and the force- and torque-free conditions

$$\begin{aligned} \text{Force-free: } & \mathbf{F}_1 + \mathbf{F}_2 = \mathbf{0}, \quad \mathbf{F}_3 + \mathbf{F}_4 = \mathbf{0} \\ \text{Torque-free: } & \mathbf{x}_1 \times \mathbf{F}_1 + \mathbf{x}_2 \times \mathbf{F}_2 = \mathbf{0}, \quad \mathbf{x}_3 \times \mathbf{F}_3 + \mathbf{x}_4 \times \mathbf{F}_4 = \mathbf{0}. \end{aligned}$$

The latter constraints require that

$$\mathbf{F}_i = F_i \mathbf{e}_x \quad (i = 1, 2), \quad \mathbf{F}_\alpha = F_\alpha \mathbf{e}_{x'} \quad (\alpha = 3, 4)$$

and

$$\sum_{i=1,2} \mathbf{F}_i = \sum_{i=1,2} F_i \mathbf{e}_x \equiv \mathbf{0}, \quad \sum_{\alpha=3,4} \mathbf{F}_\alpha = \sum_{\alpha=3,4} F_\alpha \mathbf{e}_{x'} \equiv \mathbf{0}. \quad (5.8)$$

Finally the rigid motions of the spheres in each PMPY should satisfy:

$$(\mathbf{U}_2 - \mathbf{U}_1) \cdot \mathbf{e}_x = \dot{l}_{12}, \quad (\mathbf{U}_4 - \mathbf{U}_3) \cdot \mathbf{e}_{x'} = \dot{l}_{34} \quad (5.9)$$

Equations (5.1 - 5.9) define the system that determines the swimming of the two PMPY models.

We set

$$R_M = \max_t \{R_i(t)\}_{i=1,2,3,4}, \quad L_m = \min_t \{l_{12}(t), l_{34}(t)\}, \quad \delta = \frac{R_M}{L_m},$$

we restrict the analysis to the regime that $l_{ij} > L_m$, $i = 1, 2$, $j = 3, 4$, and we use the nondimensionalization given in section 3.1. A simple analysis similar to that in section 4.2 gives the following leading order estimate

$$\mathbf{U}_i^{(0)} \sim O(1), \quad \mathbf{U}_i^{(1)} \sim O(\delta), \quad \boldsymbol{\Omega}_i^{(1)} \sim O(\delta^3)$$

From this we see that when $\delta \ll 1$, the rotation effect of the PMPYs is much smaller as compared to the translation effect.

5.2 Hydrodynamic interactions between two PMPY swimmers on a line

To proceed further we must specify how the pair moves, and we first consider the configuration in which they lie in the same line, specifically, suppose that the centers of all spheres lie along the x -axis. In addition, we place PMPY II in front of PMPY I, hence from negative to positive direction along the x -axis, the spheres are ordered from sphere 1 to sphere 4 (Figure 5.3i).

Equations (5.2, 5.3) show that the hydrodynamic interactions between the two PMPYs arise $O(\delta)$. A simple perturbation analysis gives the non-dimensionalized forces exerting on the spheres (again with hat notation omitted):

$$\begin{aligned} -F_1 = F_2 &\sim \frac{R_1 R_2}{R_1 + R_2} \xi_I + 3 \frac{\delta}{l_{12}} \left(\frac{R_1 R_2}{R_1 + R_2} \right)^2 \xi_I \\ &\quad + \frac{3}{2} \delta \frac{R_1 R_2 R_3 R_4}{(R_1 + R_2)(R_3 + R_4)} \left(\frac{1}{l_{23}} - \frac{1}{l_{24}} - \frac{1}{l_{13}} + \frac{1}{l_{14}} \right) \xi_{II} + O(\delta^2) \\ -F_3 = F_4 &\sim \frac{R_3 R_4}{R_3 + R_4} \xi_{II} + 3 \frac{\delta}{l_{34}} \left(\frac{R_3 R_4}{R_3 + R_4} \right)^2 \xi_{II} \\ &\quad + \frac{3}{2} \delta \frac{R_1 R_2 R_3 R_4}{(R_1 + R_2)(R_3 + R_4)} \left(\frac{1}{l_{23}} - \frac{1}{l_{24}} - \frac{1}{l_{13}} + \frac{1}{l_{14}} \right) \xi_I + O(\delta^2) \end{aligned}$$

where $l_{ij} = |\mathbf{x}_i - \mathbf{x}_j|$, and the translational velocities of the spheres:

$$\begin{aligned} U_1 &\sim -\frac{R_2}{R_1 + R_2} \xi_I + \delta \frac{R_1 R_2 (R_1 - R_2)}{2(R_1 + R_2)^2 l_{12}} \xi_I \\ &\quad - \frac{3}{2} \delta \frac{R_3 R_4}{(R_1 + R_2)(R_3 + R_4)} \xi_{II} \left[R_1 \left(\frac{1}{l_{13}} - \frac{1}{l_{14}} \right) + R_2 \left(\frac{1}{l_{23}} - \frac{1}{l_{24}} \right) \right] + O(\delta^2) \\ U_3 &\sim -\frac{R_4}{R_3 + R_4} \xi_{II} + \delta \frac{R_3 R_4 (R_3 - R_4)}{2(R_3 + R_4)^2 l_{34}} \xi_{II} \\ &\quad - \frac{3}{2} \delta \frac{R_1 R_2}{(R_1 + R_2)(R_3 + R_4)} \xi_I \left[R_3 \left(\frac{1}{l_{13}} - \frac{1}{l_{23}} \right) + R_4 \left(\frac{1}{l_{14}} - \frac{1}{l_{24}} \right) \right] + O(\delta^2) \end{aligned}$$

Reference to equations (3.27, 3.28), and taking into consideration the geometric condition at equation (5.9), leads to the following estimate of the hydrodynamic interaction effects on the velocities of the PMPYs.

$$U_{II \rightarrow I}^{\text{hydro}} = -\frac{3}{2} \delta \frac{R_3 R_4}{(R_1 + R_2)(R_3 + R_4)} \xi_{II} \left[R_1 \left(\frac{1}{l_{13}} - \frac{1}{l_{14}} \right) + R_2 \left(\frac{1}{l_{23}} - \frac{1}{l_{24}} \right) \right] + O(\delta^2) \quad (5.10)$$

$$U_{I \rightarrow II}^{\text{hydro}} = \frac{3}{2} \delta \frac{R_1 R_2}{(R_1 + R_2)(R_3 + R_4)} \xi_I \left[R_3 \left(\frac{1}{l_{23}} - \frac{1}{l_{13}} \right) + R_4 \left(\frac{1}{l_{24}} - \frac{1}{l_{14}} \right) \right] + O(\delta^2) \quad (5.11)$$

The geometric relations give

$$\frac{1}{l_{13}} - \frac{1}{l_{14}}, \frac{1}{l_{23}} - \frac{1}{l_{24}}, \frac{1}{l_{23}} - \frac{1}{l_{13}}, \frac{1}{l_{24}} - \frac{1}{l_{14}} > 0$$

and thus the leading order of $U_{II \rightarrow I}^{\text{hydro}}$ has the opposite sign of ξ_{II} while that of $U_{I \rightarrow II}^{\text{hydro}}$ has the same sign as ξ_I :

$$U_{II \rightarrow I}^{\text{hydro}} \xi_{II} < 0, \quad U_{I \rightarrow II}^{\text{hydro}} \xi_I > 0$$

This can be understood as follows. Since PMPY II is leading, when it lengthens it impedes the swimming of PMPY I, which follows; on the other hand, when PMPY I lengthens, it enhances the swimming of PMPY II in front of it.

The full expressions of the $O(\delta^2)$ term of $U_{II \rightarrow I}^{\text{hydro}}$, $U_{I \rightarrow II}^{\text{hydro}}$ are lengthy, however, by taking $\xi_I = \xi_{II} = 0$, we can easily obtain the hydrodynamic interactions on the sphere velocities that result from the sphere expansion/contraction of the other PMPY only (Appendix E.2):

$$\begin{aligned} U_{II \rightarrow I}^{\text{hydro}} \{\dot{R}\} &= -R_3^2 \zeta_3 \delta^2 \left[\frac{R_1}{R_1 + R_2} \left(\frac{1}{l_{13}^2} - \frac{1}{l_{14}^2} \right) + \frac{R_2}{R_1 + R_2} \left(\frac{1}{l_{23}^2} - \frac{1}{l_{24}^2} \right) \right] + O(\delta^3) \\ U_{I \rightarrow II}^{\text{hydro}} \{\dot{R}\} &= -R_1^2 \zeta_1 \delta^2 \left[\frac{R_3}{R_3 + R_4} \left(\frac{1}{l_{23}^2} - \frac{1}{l_{13}^2} \right) + \frac{R_4}{R_3 + R_4} \left(\frac{1}{l_{24}^2} - \frac{1}{l_{14}^2} \right) \right] + O(\delta^3) \end{aligned}$$

The geometry of the system also dictates that the leading order term of $U_{II \rightarrow I}^{\text{hydro}} \{\dot{R}\}$ has the opposite sign of ζ_3 , while that of $U_{I \rightarrow II}^{\text{hydro}} \{\dot{R}\}$ has the opposite sign of ζ_1 :

$$(U_{II \rightarrow I}^{\text{hydro}} \{\dot{R}\}) \zeta_3 < 0, \quad (U_{I \rightarrow II}^{\text{hydro}} \{\dot{R}\}) \zeta_1 < 0$$

The first relation is easy to understand: the expansion of sphere 3, which is the closer of 3 and 4 to PMPY I, will impede the swimming of PMPY I, which follows PMPY II. For the second relation, recall that the volume conservation constraint gives $R_1^2 \zeta_1 = -R_2^2 \zeta_2$, thus we have $(U_{I \rightarrow II}^{\text{hydro}} \{\dot{R}\}) \zeta_2 > 0$, that is, the leading order of $U_{I \rightarrow II}^{\text{hydro}} \{\dot{R}\}$ has the same sign as ζ_2 . In another words, the expansion of sphere 2 which is the sphere in PMPY I that is near PMPY II, will enhance the swimming of PMPY II.

When $\delta \ll 1$ the hydrodynamic effect that results from sphere expansion/contraction ($U^{\text{hydro}} \{\dot{R}\} \sim O(\delta^2)$) can certainly be neglected compared to the total hydrodynamic effect due to expansion/contraction of the rod, which is $U^{\text{hydro}} \sim O(\delta)$. Here we consider the hydrodynamic effects when the spheres are allowed to come closer, i.e., $\delta < 1$ but not too small. We first consider the instantaneous behavior of the system, and then the period-average behavior. For example, we consider an instantaneous system configuration in which $R_1 = R_2 = R_3 = R_4 = R$ and $l_{12} = l_{23} = l_{34} = L$, and for this we have for the leading order terms

$$|U_{II \rightarrow I}^{\text{hydro}}| = \frac{R}{4L} \delta |\xi_{II}|, \quad |U_{II \rightarrow I}^{\text{hydro}} \{\dot{R}\}| = \frac{4R^2}{9L^2} \delta^2 |\zeta_3|.$$

Recalling that the non-dimensionalization of our system guarantees that $R \leq 1$, $L \geq 1$ (equation (3.6)), in the case of $R = L = 1$, we have the relation

$$\frac{|U_{II \rightarrow I}^{\text{hydro}} \{\dot{R}\}|}{|U_{II \rightarrow I}^{\text{hydro}}|} \sim \frac{16}{9} \delta \left| \frac{\zeta_3}{\xi_{II}} \right|.$$

For a system with $\delta \sim 0.5$ where the spheres are close to each other, the coefficient of the above equation is $8/9$, and in this case the hydrodynamic effects that result from sphere expansion/contraction must be included, together with higher order terms in U^{hydro} .

Figure 5.2 gives the instantaneous fluid velocity field around a system of two linear PMPYs, where the instantaneous system profile is $R_1 = R_2 = R_3 = R_4 = 2$, $l_{12} = l_{34} = 6$, $l_{23} = 8$. Figure 5.2a & b give the velocity fields when only the rod lengths vary, while in Figure 5.2c-f we include both rod and sphere changes. A comparison of the two cases shows that for a linear system in which δ is not too small, the $O(\delta^2)$ terms that result from the sphere changes give rise to a large perturbation of the surrounding fluid near the swimmers.

To obtain some insight into the swimming behavior of a linear system of two PMPYs over a period, we consider the following two systems.

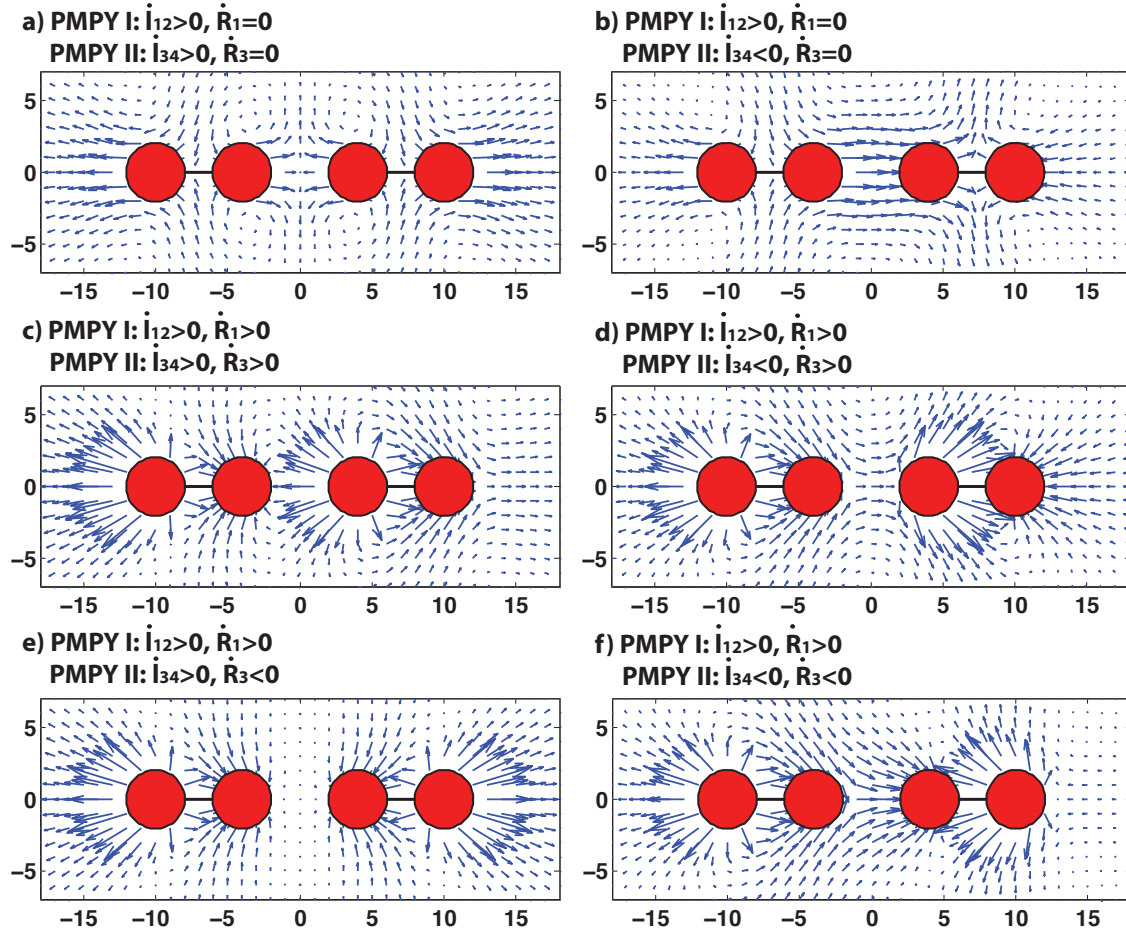


Fig. 5.2 The instantaneous fluid velocity field around two linear PMPYs, with $R_1 = R_2 = R_3 = R_4 = 2$, $l_{12} = l_{34} = 6$, $l_{23} = 8$. (a) Both swimmers undergo expansion and contraction of their connecting rods, but no volume changes. For I, $\dot{l}_{12} = 2\pi$, $\dot{R}_1 = 0$, and for II $\dot{l}_{34} = 2\pi$, $\dot{R}_3 = 0$; (b) As in (a), but with $\dot{l}_{34} = -2\pi$; (c) For I, $\dot{l}_{12} = 2\pi$, and $\dot{R}_1 = 2\pi$, and for II $\dot{l}_{34} = 2\pi$, $\dot{R}_3 = 2\pi$; (d) As in (c), but with $\dot{l}_{34} = -2\pi$; (e) For I, $\dot{l}_{12} = 2\pi$, $\dot{R}_1 = 2\pi$, and for II $\dot{l}_{34} = 2\pi$, $\dot{R}_3 = -2\pi$; (f) As in (e) but with $\dot{l}_{34} = -2\pi$, $\dot{R}_3 = -2\pi$.

– System i:

$$\begin{aligned} \text{PMPY I: } R_1(t) &= 2 - \sin 2\pi t, & R_2(0) &= 3, & l_{12} &= l_0 + \cos 2\pi t \\ \text{PMPY II: } R_3(t) &= 2 - \sin(2\pi t + \psi_0), & l_{34} &= l_0 + \cos(2\pi t + \psi_0) \end{aligned}$$

– System ii:

$$\begin{aligned} \text{PMPY I: } R_1(0) &= 3, & R_2(t) &= 2 + \sin 2\pi t, & l_{12} &= l_0 + \cos 2\pi t \\ \text{PMPY II: } R_4(t) &= 2 + \sin(2\pi t + \psi_0), & l_{34} &= l_0 + \cos(2\pi t + \psi_0), \end{aligned}$$

both with the following constraint and initial condition:

$$\begin{aligned} \text{Equal volume conservation: } & \frac{4\pi}{3}(R_1^3 + R_2^3) = \frac{4\pi}{3}(R_3^3 + R_4^3) \equiv \text{Const.} \\ \text{Initial distance between the two PMPY models: } & l_{23}(0) = d_0 \end{aligned}$$

In either the system, the two PMPYs undergo the same loop in the control space (\dot{l}, \dot{R}_1) except for a phase difference ψ_0 .

We solve the linear system equations (5.1 - 5.9), with equations (5.5, 5.6) for the angular motions removed due to the linear geometry (Appendix D). We take $l_0 = 8$, thus $R_M \sim 3.24$, $l_m = 7$, $\delta \sim 0.46$. Simulation results of the two systems for the translation and performance are shown in Figure 5.3, and for comparison we show the results for a single swimmer undergoing the same cyclic deformations (black dotted line in Figure 5.3a-f&jk, and black solid line in Figure 5.3gh). From these results we can draw the following conclusions.

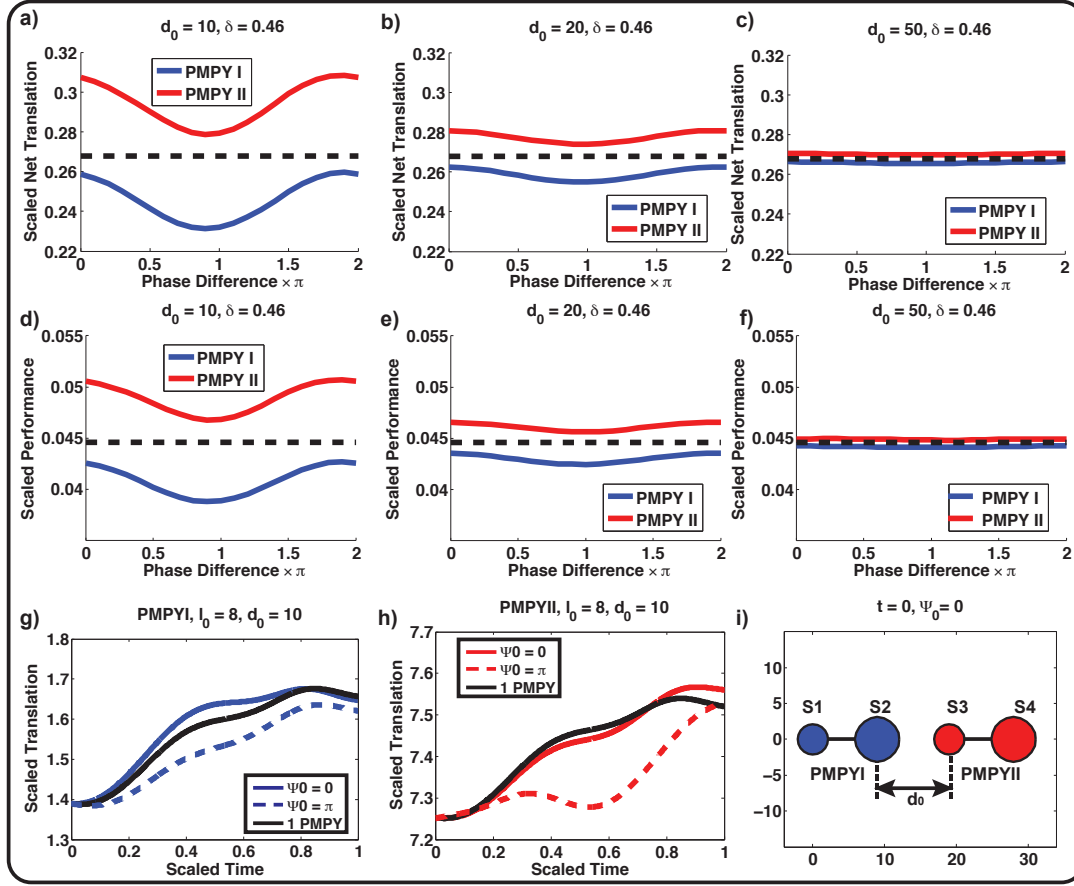
1. Figure 5.3a-c show that in system i the one in front (PMPY II) gets pushed forward (red line), while the one that follows (PMPY I, blue line) gets pushed backward, and Figure 5.3d-f show that the performance of the PMPY in front increased while that of the one that follows is decreased. On the other hand, in system ii we observe the reverse effect: the one in front gets pulled back and its performance decreased, while the one that follows gets pushed forward and its performance enhanced (Figure 5.3j,k). Therefore we see that in system i the two PMPYs are repelling one another, while in system ii they are attracting each other. In short, *when two PMPYs that are identical except for a phase difference in their shape deformations swim in a line, they may repel or attract each other with a small amplitude, depending on their initial configuration and shape deformations.*
2. Regarding the phase difference, in the repelling system i, when $\psi_0 = 0$, PMPY II gets the maximum increase while PMPY I gets the minimum decrease in both net translation and performance; on the other hand when $\psi = \pi$, PMPY II gets the minimum increase while PMPY I gets the maximum decrease in both net translation and performance (Figure 5.3a,d). In the attracting system ii we observe the similar effect (Figure 5.3j,k).

Finally, we compute the scaled distance change $\hat{l}_{23}(1) - \hat{l}_{23}(0)$ between the two PMPYs after one period for systems with different values of l_0 and d_0 . If there is no hydrodynamic interaction between them, due either to length changes in the rod or volume changes in the spheres, then this difference is identically zero. On the other hand, with hydrodynamic interactions the difference will generally be non-zero, and will reflect the strength of the interaction. This raises the question as to how accurately the asymptotic approximation can capture this interaction. In simulations to examine this, we allow $l_{23} < L_m$ as long as all spheres are always kept separated. Figure 5.4 shows the results for $l_0 = 8$ or 20, and $d_0 \in [8, 40]$, with the translation either calculated up to the first reflection (equations (5.1 - 5.4), Figure 5.4 solid lines), or by asymptotic approximation to $O(\delta)$ (Figure 5.4 dashed lines). From this we see that when l_0 and d_0 are both small, i.e., the spheres are close, there is a clear difference in magnitude between the asymptotic solution and the solution that results from one reflection, although they are qualitatively similar. This and the foregoing results show that the higher-order terms have a significant effect on both the instantaneous and long-term translation and performance of the swimmers.

5.3 Hydrodynamic interaction between two PMPY models swimming in a plane

To conclude the analysis of interacting swimmers, we consider the scenario in which the swimmers are swimming parallel to one another (Figure 5.1). To simplify the computation, we approximate the equations

System i: PMPYs repel each other



System ii: PMPYs attract each other

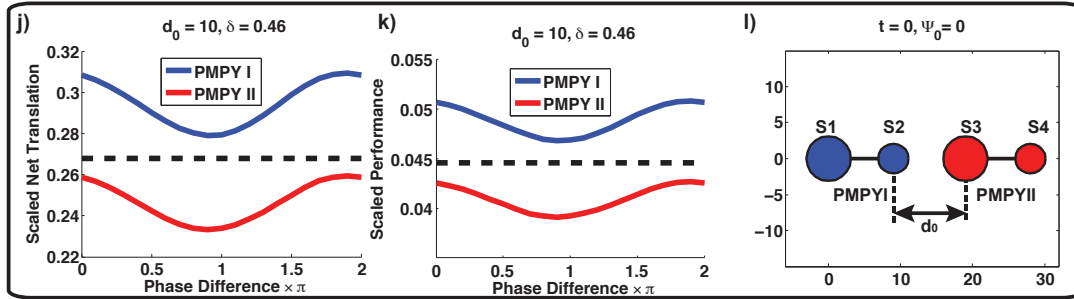


Fig. 5.3 Two PMPYs swim in a line. In panels (a-f) and (j,k) the dashed black line gives either the scaled net translation \hat{X} or the scaled performance $\hat{\mathcal{P}}$ of a single PMPY undergoing the same sequence of shape changes. (a-i) Simulation results for system i – (j-k) simulation results for system ii. (a-c,j) The relation between the scaled net translations of the two PMPYs (\hat{X}_I , PMPY I, blue line; \hat{X}_{II} , PMPY II, red line) and the phase difference Ψ_0 for $d_0 = 10, 20, 50$ and $l_0 = 8$. (d-f,k) The relation between the scaled performance of the two PMPYs ($\hat{\mathcal{P}}_I$, PMPY I, blue line; $\hat{\mathcal{P}}_{II}$, PMPY II, red line) and the phase difference Ψ_0 for $d_0 = 10, 20, 50$ and $l_0 = 8$. (g) The scaled trajectory $\hat{X}_I(0 \leq t \leq 1)$ of PMPY I with $l_0 = 8, d_0 = 10$ and phase difference $\Psi_0 = 0$ (blue solid line) or π (blue dashed line), comparing to the scaled trajectory of a single PMPY undergoing the same sequence of shape deformations (black solid line). (h) As in (g), but for PMPYII. (i,l) The initial profile of the system with $l_0 = 8, d_0 = 10, \Psi_0 = 0$.

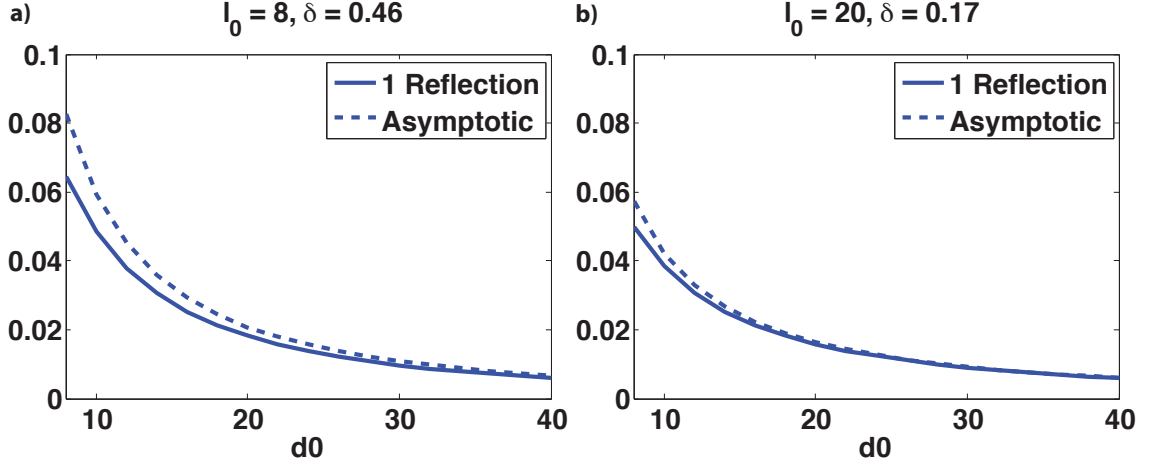


Fig. 5.4 $\hat{l}_{23}(1) - \hat{l}_{23}(0)$ for system i, with different values of l_0 and d_0 , where the translation is either calculated up to the first reflection (solid lines), or by asymptotic approximation to $O(\delta)$ (dashed lines).

5.1 - 5.9 to order δ^2 , hence for the rigid motions we have the following approximations.

$$\hat{\mathbf{U}}_i \sim \frac{\hat{\mathbf{R}}_i}{\hat{R}_i} + \sum_{j \neq i} \left[\frac{3}{4\hat{l}_{ij}} \delta \left(\hat{\mathbf{F}}_j + (\hat{\mathbf{F}}_j \cdot \hat{\mathbf{d}}_{ji}) \hat{\mathbf{d}}_{ji} \right) + \hat{\zeta}_j \left(\frac{\hat{R}_j}{\hat{l}_{ij}} \right)^2 \delta^2 \mathbf{d}_{ji} \right] + O(\delta^3) \quad (5.12)$$

$$\hat{\boldsymbol{\Omega}}_i \sim O(\delta^3) \quad (5.13)$$

This allows us to neglect the angular motion of the PMPYs. Again, we see that the hydrodynamic interactions contribute from the $O(\delta)$ term. The algorithm for the computational scheme is given in Appendix D. The complexity of the geometry makes it difficult to gain insight from an asymptotic analysis, but the velocity field shown in Figure 4.4 may help in understanding the behavior of the hydrodynamic interactions between the two PMPYs. For example, when one of the PMPYs is expanding its connecting rod and the other PMPY is right above or below it, they will be attracted to each other. Also, when the PMPYs are short (i.e., small l_I, l_{II}) and close to each other, the $O(\delta^2)$ terms that result from sphere expansion/contraction may have significant effects and have to be incorporated (Figure 4.4 e & f).

We suppose that the two swimmers start from parallel initial positions – both lie along the x -direction, with sphere 3 located directly above sphere 1 (Figure 5.5a). Again we consider the two protocols specified in section 5.2, with the initial vertical distance between sphere 1 and 3 $l_{13}(0) = 10$ and $l_0 = 8$. Thus the systems have scales $R_M \sim 3.24$, $l_m = 7$ and $\delta \sim 0.46$. In system i, the scaled distance between the sphere 1 and 3 decreases from $\hat{l}_{13}(0) \sim 3.086$ to $\hat{l}_{13}(1) \sim 3.0491 \pm 0.003$ (Figure 5.5b). That is, the hydrodynamic interaction between the swimmers leads to an attraction effect of scaled distance ~ 0.037 , which is of the same order as what was obtained for the linear system in section 5.2. The attraction effect is also slightly affected by the phase difference ψ_0 , as shown by Figure 5.5b: when $\psi_0 = 0$ it reaches its maximum while at $\psi_0 = \pi$ it is at the minimum. On the other hand, in system ii, within one cycle, the scaled distance between spheres 1 and 3 increases from $\hat{l}_{13}(0) = 3.086$ to $\hat{l}_{13} \sim 3.124 \pm 0.002$ (Figure 5.5c), indicating a small repulsion between the two PMPYs resulting from the hydrodynamic interaction. What is interesting is that prior analysis shows that when laid collinear, the repelling system i becomes attracting, while the attracting system ii then becomes repelling, when subjected to the cyclic protocol in section 5.2.

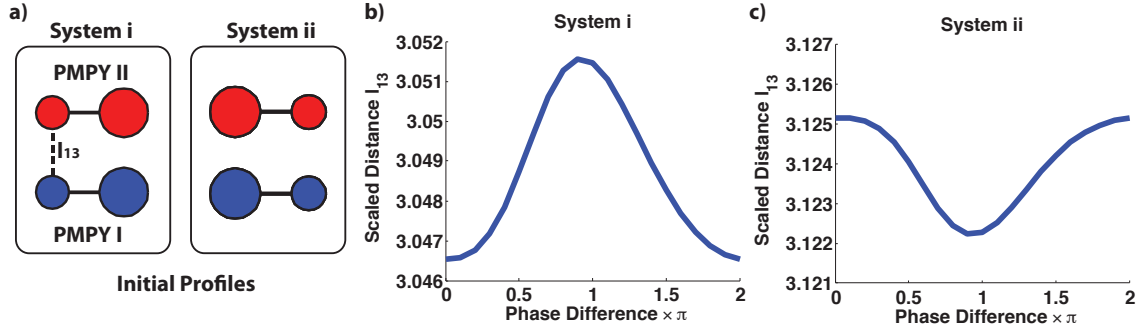


Fig. 5.5 Two PMPYs swim from a parallel initial position. (a) With $l_0 = 8$, $l_{13}(0) = 10$, $\psi_0 = 0$, the initial profiles of system i and ii. (b) The relation between the scaled distance in the vertical direction between sphere 1 and 3 in system i after one cycle ($l_{13}(1)$) and the phase difference ψ_0 . (c) As in (b) but for system ii.

6 Extended scallop theorem and mixed controls

A widely-quoted principle in LRN swimming is that *any reciprocal stroke gives no net motion*, which is known as the "scallop theorem" (Purcell 1977). An immediate corollary of this theorem is: if a self-propulsion swimmer has only one degree of freedom in its shape deformations, any cyclic stroke must be reciprocal and hence it cannot swim at LRN. However, a group of reciprocal swimmers, none of which can swim in isolation, may coordinate their shape deformations such that the aggregate shape deformations of the group are not reciprocal. Thus, by taking advantage of the hydrodynamic interactions, they may swim. This phenomenon is referred to as "no many scallop theorem" in the existing literature (Koiller *et al.* 1996, Lauga & Bartolo 2008, Alexander & Yeomans 2008, Lauga 2011). We quote from (Lauga 2011): "Although a body undergoing reciprocal motion cannot swim, two bodies undergoing reciprocal motion with nontrivial phase differences are able to take advantage of the unsteady hydrodynamic flows they create to undergo nonzero collective and relative dynamics; there is thus no many-scallop theorem."

In previous sections each PMPY could swim by itself, but here we modify the PMPY model into a scallop-type swimmer and study the collective behavior. In particular, we focus on how well the collection can swim by taking advantage of hydrodynamic interactions. As we discussed earlier, a PMPY has two degrees of freedom in its shape deformations, namely \dot{l} and \dot{R}_1 , and to make it a scallop-type swimmer, we can disable either of them. Thus for two hobbled PMPYs swimming together, there are three possibilities for their controls: $(\dot{l}_I, \dot{l}_{II})$, $(\dot{R}_{I,1}, \dot{R}_{II,1})$, or a mixed control $(\dot{l}_I, \dot{R}_{II,1})$. The first case, i.e., $(\dot{l}_I, \dot{l}_{II})$, in which each PMPY is a simple dumb-bell with an extensible connecting rod, has been studied previously (Lauga & Bartolo 2008, Alexander & Yeomans 2008), while the other combinations of controls have not. Recall that for a single active LRN swimmer, three linked-sphere models have been designed according to these three different combinations of controls: Najafi-Golestanian three-sphere model in (\dot{l}_1, \dot{l}_2) (Alexander *et al.* 2009, Najafi & Golestanian 2004), PMPY in (\dot{l}, \dot{R}_1) (Avron *et al.* 2005) and the three-sphere volume-exchange model (\dot{R}_1, \dot{R}_3) (Wang *et al.* 2012). It was shown that a PMPY adopting the mixed control is superior than the other two by order $O(L^2)$ in both net translation and performance, where L is the typical length of the swimmers (Wang & Othmer 2015). Here we ask the question: will a mixed control strategy of deformations lead to better LRN swimming for two hobbled PMPYs, as it does for a single active swimmer?

Again we consider two PMPYs lying along the x -axis, with PMPY II in front. We design three systems according to different types of controls.

– System A in $(\dot{l}_I, \dot{l}_{II})$ (two dumb-bells):

$$R_1 = R_2 = R_3 = R_4 = 3.24, \quad l_{12} = l_0 + \cos(2\pi t), \quad l_{34} = l_0 + \sin(2\pi t)$$

– System B in $(\dot{R}_{I,1}, \dot{R}_{II,1})$:

$$R_1(t) = 2 + \cos(2\pi t), \quad R_2(0) = 2, \quad R_3(t) = 2 + \sin(2\pi t), \quad R_4(0) = 3 \quad l_{12} = l_{34} = l_0 - 1$$

– System C in $(\dot{l}_I, \dot{R}_{II,1})$:

$$R_1 = R_2 = 3, \quad R_3(t) = 2 + \sin(2\pi t), \quad R_4(0) = 3, \quad l_{12}(t) = l_0 + \cos(2\pi t), \quad l_{34} = l_0$$

– Initial condition: $l_{23}(0) = d_0$

Therefore the three systems have the same scales: $R_M \sim 3.24$, $L_m = l_0 - 1$. We perform simulation with $l_0 = d_0 = 12$, which gives $\delta \sim 0.29$, and the scaled net translations \hat{X}_I, \hat{X}_{II} and scaled performances $\hat{\mathcal{P}}_I, \hat{\mathcal{P}}_{II}$ are given in Table 1.

Table 1 Simulation results of the three systems of two degraded PMPYs.

	\hat{X}_I	\hat{X}_{II}	$\hat{\mathcal{P}}_I$	$\hat{\mathcal{P}}_{II}$
System A	-0.8×10^{-3}	-1.1×10^{-3}	5.25×10^{-4}	6.94×10^{-4}
System B	3.3×10^{-3}	4.0×10^{-3}	6.66×10^{-4}	7.84×10^{-4}
System C	0.5×10^{-3}	-17.5×10^{-3}	3.39×10^{-4}	34×10^{-4}

First, from Table 1 we see that all three systems can swim, although none is as effective as one single active PMPY, which typically swims a scaled net translation of $\hat{X} \sim O(10^{-1})$ and with a scaled performance of $\hat{\mathcal{P}} \sim O(10^{-2})$ under this protocol (see section 3.4). Next, we find that the swimming behaviors of systems A and B, i.e., the two with the same type of shape deformations, are quite similar: both PMPYs in both systems have scaled net translations and scaled performances of the orders $\hat{X} \sim O(10^{-3})$ and $\hat{\mathcal{P}} \sim O(10^{-4})$. On the other hand, system C, which adopts the mixed controls, behaves very differently. The PMPY with shape deformations in \dot{l} (i.e., PMPY I) swims much less effectively than the one using an \dot{R} control (PMPY II), with scaled net translations and scaled performance ratios $\hat{X}_{II}/\hat{X}_I \sim 35$ and $\hat{\mathcal{P}}_{II}/\hat{\mathcal{P}}_I \sim 10$. Also, PMPY II in system C clearly swims better than either of the two PMPYs in system A or B, while the poorer one (PMPY I) swims slightly worse than the two PMPYs in system A or B. A detailed asymptotic analysis of the three systems is given in Appendix E.

The reasons for this difference in outcome for different control choices are: 1) \dot{l} gives rise to lower-order terms in the translational velocity than does \dot{R} (equation 3.23); 2) to guarantee that the lower-order terms resulting from \dot{l} do not vanish in the net translation, it is necessary that the coefficients that depend on the radii be time-dependent, otherwise the temporal integral will become an exact integral, or at best only result in higher order terms. To be more specific:

1. Controls in $(\dot{R}_{I,1}, \dot{R}_{II,1})$ will result in terms no lower than $O(\delta^2)$ in velocity and net translation.
2. Controls in $(\dot{l}_I, \dot{l}_{II})$ will result in leading order term of $O(1)$ or $O(\delta)$ in velocity, depending on the geometry of the model. However, their coefficients are either of the form $\Phi(R_{1,2,3,4})$ or $\Phi(R_{1,2,3,4})/l(t)$, where the radii are all constants. In the former case, it gives rise to an exact integral when computing the net translation; in the latter case, when integrated, it only gives higher order terms. For details, see the discussion in Appendix E.1.

3. Only with mixed controls in $(\dot{l}_I, \dot{R}_{II,1})$ and for the PMPY with shape deformation \dot{R} , the leading order in velocity is of $O(\delta)$ order and of the form $\Phi(R_{1,2,3,4}(t))/l(t)$, which neither vanishes nor degrades when integrated.

Finally we summarize previous studies on the *scallop theorem* (Purcell 1977, Lauga 2011) together with our discussions from section 4,5 into the following *extended scallop principle*:

Principle 1 (Extended Scallop Principle) *In an LRN Newtonian flow,*

1. *a scallop cannot swim;*
2. *a living scallop surrounded by a few dead scallops cannot swim;*
3. *a group of living scallops can swim, but in an energy-inefficient manner.*

The precise mathematical interpretation of Principle 1 is as follows. At low Reynolds number,

1. a self-deformable swimmer with only one degree of freedom cannot swim — which is the statement of the original scallop theorem.
2. A self-deformable swimmer with only one degree of freedom cannot swim efficiently in the presence of passive rigid objects. This can be seen from section 4, as the presence of a rigid object that cannot deform itself has no effect on the swimmer up to the first reflection. When further reflections are considered, the presence of the rigid objects nearby will indeed affect the swimmer, but the effect would be too small to have a significant effect on the swimmer.
3. A group of self-deformable swimmers, all with only one degree of freedom, can swim by taking advantage of hydrodynamic interactions. However, both the translation and performance are much worse than one swimmer with multiple degrees of freedom.

7 Discussion

Herein we used a basic PMPY model to study the LRN swimming characteristics of both single and multiple swimmers, so as to understand the effect of hydrodynamic interactions on the translation and efficiency of such swimmers. One significant result is that the PMPY model is an efficient LRN swimmer whose swimming behavior approximates that of swimming *Dd amoebae*. This suggests that the PMPY model may provide a good first-order model for the study of microorganisms swimming at LRN. As was shown, to better approximate the characteristics of LRN swimming microorganisms one must allow the spheres to approach more closely than in previous analyses, in which case the asymptotic solution for $\delta = 0$ is inadequate and higher-terms in the interactions must be included. When a PMPY is swimming with a passive object, the swimming PMPY has a clear effect on the passive object, while the existence of the latter has little effect on the PMPY, as long as the size of this object is comparable to or less than the spheres in the PMPY. If the passive object is directly ahead of the PMPY, the PMPY can catch up with it within a few cycles, using a reasonable amount of energy. If the freely buoyant object is not directly in the PMPY's path, its long-term trajectory approximates a closed-triangle when it is far away from the PMPY's swimming path, or it will be pushed forward if it is close to the PMPY's swimming path. In this case the higher-order terms in the solution of the translational velocity of the PMPY contribute significantly to this entrainment effect, and again, an asymptotic solution does not capture this effect. Moreover, a longer PMPY will enhance the entrainment effect.

When there are two PMPYs swimming together, either collinearly or not, the hydrodynamic interactions among them may cause some attraction or repulsion between them, depending on the stroke. However, this effect is small compared with the net translation of the PMPYs, but again, higher-order terms should be

taken into consideration, particularly if one is interested in either the instantaneous or long-term behavior of the system. A scallop-type swimmer cannot swim at LRN on its own or in the presence of non-deformable bouyant objects, but by cleverly coordinating their strokes, two or more of them can swim by taking advantage of hydrodynamic interactions. Although swimming in this manner is generally not efficient, a pair of scallop-type swimmers that use a mixed (\dot{l}, \dot{R}) control may enhance the swimming of one of the pair as compared to pairs in which both use either a pure (\dot{l}) or (\dot{R}) control.

In the biological context the surrounding material may be non-Newtonian, and in particular, is often viscoelastic. Some results for this case are known, (Qiu *et al.* 2014, Curtis & Gaffney 2013), but much remains to be done.

Appendices

A Newtonian flow produced by the translation and radial expansion of a sphere

Here we derive the velocity field $\mathbf{u}(\mathbf{x})$ of a LRN flow produced by a sphere of radius R , pulled by a force \mathbf{F} and expanding radially at a rate $\dot{R} = dR/dt$. Due to the linearity of LRN flows, the velocity field is the sum of two terms: that resulting from the drag force — $\mathbf{u}\{\mathbf{F}\}$, and that resulting from the radial expansion — $\mathbf{u}\{\dot{R}\}$:

$$\mathbf{u} = \mathbf{u}\{\mathbf{F}\} + \mathbf{u}\{\dot{R}\} \quad (\text{A.1})$$

The flow produced by the translation of a solid sphere is a classical result (Pozrikidis 1992). It can be represented in terms of a Stokeslet and dipole with poles at the center of the sphere that are given by

$$\mathbf{G} = \frac{\delta}{r} + \frac{\mathbf{r}\mathbf{r}}{r^3} \quad (\text{A.2})$$

$$\mathbf{D} = -\frac{\delta}{r^3} + 3\frac{\mathbf{r}\mathbf{r}}{r^5} \quad (\text{A.3})$$

where \mathbf{x}_0 is the center of the sphere, $\mathbf{r} = \mathbf{x} - \mathbf{x}_0$ and $r = |\mathbf{r}|$. \mathbf{G} is called the Oseen tensor. The velocity field is then

$$u_i(\mathbf{x}) = G_{ij}(\mathbf{x}, \mathbf{x}_0) \left(\frac{3}{4} R U_j \right) - D_{ij}(\mathbf{x}, \mathbf{x}_0) \left(\frac{1}{4} R^3 U_j \right). \quad (\text{A.4})$$

Here \mathbf{U} is the translational velocity of the sphere, i.e., $\mathbf{U}(t) = \dot{\mathbf{x}}_0(t)$. The relation between the drag force \mathbf{F} and \mathbf{U} is

$$\mathbf{F} = 6\pi\mu R \mathbf{U} \quad (\text{A.5})$$

Using the above one obtains the fluid velocity

$$\begin{aligned} u_i &= \frac{1}{24\pi\mu} \left[3 \left(\frac{\delta_{ij}}{r} + \frac{r_i r_j}{r^3} \right) F_j - \left(-\frac{\delta_{ij}}{r^3} + 3 \frac{r_i r_j}{r^5} \right) R^2 F_j \right] \\ &= \frac{1}{24\pi\mu} \left[3 \left(\frac{F_i}{r} + \frac{(\mathbf{F} \cdot \mathbf{r}) r_i}{r^3} \right) + \left(\frac{F_i}{r^3} - 3 \frac{(\mathbf{F} \cdot \mathbf{r}) r_i}{r^5} \right) R^2 \right] \\ &= \frac{1}{24\pi\mu r} \left[\left(3 + \frac{R^2}{r^2} \right) F_i + 3 \left(\frac{1}{r^2} - \frac{R^2}{r^4} \right) (\mathbf{F} \cdot \mathbf{r}) r_i \right] \end{aligned}$$

or alternatively

$$\mathbf{u}\{\mathbf{F}\} = \frac{1}{24\pi\mu r} \left[\left(3 + \frac{R^2}{r^2} \right) \mathbf{F} + 3 \left(1 - \frac{R^2}{r^2} \right) (\mathbf{F} \cdot \hat{\mathbf{r}}) \hat{\mathbf{r}} \right] \quad (\text{A.6})$$

where $\hat{\mathbf{r}} = \mathbf{r}/|\mathbf{r}|$.

The velocity field $\mathbf{u}\{\dot{R}\}$ of the flow produced by a radially expanding sphere can be represented by a point source with pole at the center \mathbf{x}_0 of the sphere, and thus has the form

$$\mathbf{u} = \alpha \frac{\hat{\mathbf{r}}}{r^2} \quad (\text{A.7})$$

where the strength of the source (α) is a constant to be determined. The no-slip boundary condition on the sphere surface implies that

$$\mathbf{u}(\mathbf{x}) = \frac{dR}{dt} \hat{\mathbf{r}}. \quad (\text{A.8})$$

From (A.7,A.8) we find that $\alpha = \dot{R}R^2$, and therefore

$$\mathbf{u}\{\dot{R}\} = \dot{R} \left(\frac{R}{r}\right)^2 \hat{\mathbf{r}}. \quad (\text{A.9})$$

If we represent it in terms of the sphere volume $v = 4\pi R^3/3$ this reads

$$\mathbf{u}\{\dot{R}\} = \frac{\dot{v}}{4\pi r^2} \hat{\mathbf{r}} \quad (\text{A.10})$$

This leads to the combined flow \mathbf{u} (3.12):

$$\mathbf{u}(\mathbf{r}; R, \mathbf{F}, \dot{R}) = \frac{1}{24\pi\mu r} \left[\left(3 + \frac{R^2}{r^2}\right) \mathbf{F} + 3 \left(1 - \frac{R^2}{r^2}\right) (\mathbf{F} \cdot \hat{\mathbf{r}}) \hat{\mathbf{r}} \right] + \dot{R} \left(\frac{R}{r}\right)^2 \hat{\mathbf{r}}.$$

B Accuracy of $U_i^{(e)}$ after incorporating the second reflection

Next we determine how a second reflection \mathbf{l} contributes to the rigid motions of two radially expanding spheres.

0th Reflection. We consider two spheres with radii $R_1(t)$ and $R_2(t)$ resp., centered at $\mathbf{x}_1(t)$ and $\mathbf{x}_2(t)$ so that $\mathbf{x}_2 - \mathbf{x}_1$ points in the \mathbf{e}_x direction. The radial expansion of the i th sphere alone generates a flow

$$\mathbf{u}_i^{(0)}(\mathbf{x}) = R_i^2 \dot{R}_i \frac{\mathbf{x} - \mathbf{x}_i}{|\mathbf{x} - \mathbf{x}_i|^3} \quad (\text{B.1})$$

and the rigid motion of the sphere vanishes

$$\mathbf{U}_i^{(0)} = \mathbf{0}, \quad \boldsymbol{\omega}_i^{(0)} = \mathbf{0}. \quad (\text{B.2})$$

1st Reflection. Next we put sphere 1 into the flow \mathbf{u}_2 generated by the radially expanding sphere 2. We calculate the resulting translational velocity $\mathbf{U}_1^{(1)}$, angular velocity $\boldsymbol{\omega}_1^{(1)}$, and the stresslet $\mathbf{S}_1^{(1)}$, from which we obtain the velocity field $\mathbf{u}_{21}(\mathbf{x})$.

Translational velocity $\mathbf{U}_1^{(1)}$.

$$\mathbf{U}_1^{(1)} = \left(1 + \frac{R_1^2}{6} \nabla^2\right) \mathbf{u}_2^{(0)} \Big|_{\mathbf{x}=\mathbf{x}_1} = R_2^2 \dot{R}_2 \left[\frac{\mathbf{x}_1 - \mathbf{x}_2}{|\mathbf{x}_1 - \mathbf{x}_2|^3} + \frac{R_1^2}{6} \nabla^2 \left(\frac{\mathbf{x} - \mathbf{x}_2}{|\mathbf{x} - \mathbf{x}_2|^3} \right) \Big|_{\mathbf{x}=\mathbf{x}_1} \right] = R_2^2 \dot{R}_2 \left[-\frac{\mathbf{e}_x}{l^2} + \frac{R_1^2}{6} \nabla^2 \left(\frac{\mathbf{x} - \mathbf{x}_2}{|\mathbf{x} - \mathbf{x}_2|^3} \right) \Big|_{\mathbf{x}=\mathbf{x}_1} \right]$$

Letting $\mathbf{r} = \mathbf{x} - \mathbf{x}_2$ and $r = |\mathbf{r}|$, we must calculate

$$\nabla^2 \left(\frac{\mathbf{r}}{r^3} \right) = \partial_k \partial_k \frac{r_i}{r^3}$$

Since

$$\partial_k \left(\frac{1}{r^n} \right) = -\frac{nr_k}{r^{n+2}}$$

we have

$$\begin{aligned} \partial_k \left(\frac{r_i}{r^3} \right) &= \frac{\delta_{ik}}{r^3} - \frac{3r_i r_k}{r^5} \\ \partial_k \partial_k \left(\frac{r_i}{r^3} \right) &= -\frac{3\delta_{ik} r_k}{r^5} - \frac{3\delta_{ik} r_k}{r^5} - \frac{3r_i \partial_k y_k}{r^5} + \frac{15r_i r_k r_k}{r^7} = 0. \end{aligned}$$

Thus

$$\nabla^2 \left(\frac{\mathbf{r}}{r^3} \right) = \mathbf{0}$$

and

$$\mathbf{U}_1^{(1)} = -\frac{R_2^2 \dot{R}_2}{l^2} \mathbf{e}_x \quad (\text{B.3})$$

Angular velocity $\boldsymbol{\omega}_1^{(1)}$.

$$\boldsymbol{\omega}_1^{(1)} = \frac{1}{2} \nabla \times \mathbf{u}_2^{(0)} \Big|_{\mathbf{x}=\mathbf{x}_1} = \mathbf{0} \quad (\text{B.4})$$

Stresslet $\mathbf{S}_1^{(1)}$. The rate of deformation that results from \mathbf{u}_2 is

$$\mathbf{E}_2^{(0)} = \frac{1}{2} \left[\nabla \mathbf{u}_2^{(0)} + (\nabla \mathbf{u}_2^{(0)})^T \right] - \frac{1}{3} \mathbf{I} (\nabla \cdot \mathbf{u}_2^{(0)}) = \dot{R}_2 R_2^2 \left[\frac{1}{2} \left(\nabla \frac{\hat{\mathbf{r}}}{r^2} + (\nabla \frac{\hat{\mathbf{r}}}{r^2})^T \right) - \frac{1}{3} \mathbf{I} \left(\nabla \cdot \frac{\hat{\mathbf{r}}}{r^2} \right) \right]$$

where $\hat{\mathbf{r}} = \mathbf{r}/r$. Using spherical coordinates, we have

$$\begin{aligned} \nabla \frac{\hat{\mathbf{r}}}{r^2} &= \left(\hat{\mathbf{r}} \frac{\partial}{\partial r} + \frac{1}{r} \hat{\boldsymbol{\theta}} \frac{\partial}{\partial \theta} + \frac{1}{r \sin \theta} \hat{\boldsymbol{\phi}} \frac{\partial}{\partial \phi} \right) \left(\frac{\hat{\mathbf{r}}}{r^2} \right) = \left(\frac{\partial}{\partial r} \frac{1}{r^2} \right) \hat{\mathbf{r}} = -\frac{2}{r^3} \hat{\mathbf{r}} \\ \nabla \cdot \frac{\hat{\mathbf{r}}}{r^2} &= \frac{\partial}{\partial r} \frac{1}{r^2} + \frac{2}{r} \frac{1}{r^2} = 0. \end{aligned}$$

Thus

$$\mathbf{E}_2^{(0)} = -\frac{2R_2^2 \dot{R}_2}{r^3} \hat{\mathbf{r}} \hat{\mathbf{r}} = -\frac{2R_2^2 \dot{R}_2}{r^5} \mathbf{r} \mathbf{r}, \quad (\text{B.5})$$

and the stresslet is given by

$$\mathbf{S}_1^{(1)} = \frac{20}{3} \pi \mu R_1^3 \left(1 + \frac{R_1^2}{10} \nabla^2 \right) \mathbf{E}_2^{(0)} \Big|_{\mathbf{x}=\mathbf{x}_1} = -\frac{40}{3} \pi \mu R_1^3 R_2^2 \dot{R}_2 \left[\frac{\mathbf{e}_x \mathbf{e}_x}{l^3} + \frac{R_1^2}{10} \nabla^2 \left(\frac{\mathbf{r} \mathbf{r}}{r^5} \right) \Big|_{\mathbf{x}=\mathbf{x}_1} \right]$$

We need to calculate

$$\nabla^2 \left(\frac{\mathbf{r} \mathbf{r}}{r^5} \right) = \partial_k \partial_k \left(\frac{r_i r_j}{r^5} \right)$$

$$\begin{aligned} \partial_k \left(\frac{r_i r_j}{r^5} \right) &= \frac{\delta_{ik} r_j}{r^5} + \frac{\delta_{jk} r_i}{r^5} - \frac{5 r_i r_j r_k}{r^7} \\ \partial_k \partial_k \left(\frac{r_i r_j}{r^5} \right) &= \left(\frac{\delta_{ik} \delta_{jk}}{r^5} - \frac{5 \delta_{ik} r_j r_k}{r^7} \right) + \left(\frac{\delta_{jk} \delta_{ik}}{r^5} - \frac{5 \delta_{jk} r_i r_k}{r^7} \right) + \left(-\frac{5 \delta_{ik} r_j r_k}{r^7} - \frac{5 \delta_{jk} r_i r_k}{r^7} - \frac{5 r_i r_j \partial_k r_k}{r^7} + \frac{35 r_i r_j r_k r_k}{r^9} \right) = \frac{2 \delta_{ij}}{r^5} \end{aligned}$$

Thus

$$\mathbf{S}_1^{(1)} = -\frac{40}{3} \pi \mu R_1^3 R_2^2 \dot{R}_2 \left[\frac{\mathbf{e}_x \mathbf{e}_x}{l^3} + \frac{R_1^2}{5 l^3} \mathbf{I} \right] \quad (\text{B.6})$$

Finally, the velocity field $\mathbf{u}_{21}^{(1)}(\mathbf{x})$ is given by

$$\mathbf{u}_{21}(\mathbf{x}) = \left(\mathbf{S}_1^{(1)} \cdot \nabla \right) \cdot \frac{\mathbf{G}(\mathbf{x} - \mathbf{x}_1)}{8 \pi \mu} + \dots \quad (\text{B.7})$$

From equations (B.6, A.2) we have that near \mathbf{x}_1 ,

$$\mathbf{S}_1^{(1)} \sim O\left(\frac{1}{l^3}\right), \quad \mathcal{G} \sim O\left(\frac{1}{l}\right)$$

and thus the velocity near \mathbf{x}_1 scales as $\mathbf{u}_{21}^{(1)} \sim O(l^{-5})$.

2nd Reflection. Now we reflect once again and consider sphere 1 immersed in the flow $\mathbf{u}_{12}^{(1)}$. The translational velocity $\mathbf{U}_1^{(2)}$ that results is given by

$$\mathbf{U}_1^{(2)} = \left(1 + \frac{R_1^2}{6} \nabla^2 \right) \mathbf{u}_{12}^{(1)} \Big|_{\mathbf{x}=\mathbf{x}_1} \quad (\text{B.8})$$

From the discussion of the first reflection we know that near \mathbf{x}_1 the velocity field $\mathbf{u}_{12}^{(1)}$ is $O(l^{-5})$, and thus $\mathbf{U}_1^{(2)} \sim O(l^{-5})$ as well.

C Calculation of $\boldsymbol{\Omega}_{3,i}^{(1)}$

The angular velocity of sphere 3 (i.e., the free-floating sphere) $\boldsymbol{\Omega}_{3,i}^{(1)}$ consists of two parts: $\boldsymbol{\Omega}_{3,i}^{(1,f)}$ that results from the drag force on sphere i , and $\boldsymbol{\Omega}_{3,i}^{(1,e)}$ that results from the expansion of sphere i . Here we calculate them separately.

First, $\boldsymbol{\Omega}_{3,i}^{(1,e)}$, which results from the flow generated by the expansion of sphere i is:

$$\mathbf{u}_i^{(0,e)} = R_i^2 \dot{R}_i \frac{\mathbf{x} - \mathbf{x}_i}{|\mathbf{x} - \mathbf{x}_i|^3},$$

and therefore

$$\boldsymbol{\Omega}_{3,i}^{(1,e)} = \frac{1}{2} \nabla \times \mathbf{u}_i^{(e)} \Big|_{\mathbf{x}=\mathbf{x}_3} = \frac{R_i^2 \dot{R}_i}{2} \nabla \times \left(\frac{\mathbf{x} - \mathbf{x}_i}{|\mathbf{x} - \mathbf{x}_i|^3} \right) \Big|_{\mathbf{x}=\mathbf{x}_3}. \quad (\text{C.1})$$

Let $\mathbf{r} = \mathbf{x} - \mathbf{x}_i$ and $r = |\mathbf{x} - \mathbf{x}_i|$ – then the antisymmetric part in equation C.1 is

$$\partial_j \left(\frac{r_k}{r^3} \right) - \partial_k \left(\frac{r_j}{r^3} \right) = \left(\frac{\delta_{jk}}{r^3} - \frac{3r_j r_k}{r^5} \right) - \left(\frac{\delta_{kj}}{r^3} - \frac{3r_k r_j}{r^5} \right) = 0$$

and therefore $\boldsymbol{\Omega}_{3,i}^{(1,e)} = 0$.

Next, $\boldsymbol{\Omega}_{3,i}^{(1,f)}$, which results from the flow generated by the drag force $\mathbf{F}_i = F_i \mathbf{e}_x$ on sphere i , is given by

$$\begin{aligned} \boldsymbol{\Omega}_{3,i}^{(1,f)} &= \frac{1}{2} \nabla \times \mathbf{u} \{ \mathbf{F}_i \} \Big|_{\mathbf{x}=\mathbf{x}_3} \\ &= \frac{1}{16\pi\mu} \nabla \times \left[\left(\frac{1}{r} + \frac{1}{3r^3} \right) F_i \mathbf{e}_x + \left(\frac{1}{r} - \frac{1}{r^3} \right) (F_i \mathbf{e}_x \cdot \frac{\mathbf{r}}{r}) \frac{\mathbf{r}}{r} \right] \Big|_{\mathbf{x}=\mathbf{x}_3} \\ &= \frac{F_i}{16\pi\mu} \nabla \times \left[\left(\frac{1}{r} + \frac{1}{3r^3} \right) \mathbf{e}_x + \left(\frac{1}{r} - \frac{1}{r^3} \right) \frac{r_x \mathbf{r}}{r^2} \right]. \end{aligned}$$

Since

$$\begin{aligned} \nabla \times \left(\frac{1}{r^n} \mathbf{e}_x \right) &= -\frac{nr_z}{r^{n+2}} \mathbf{e}_y + \frac{nr_y}{r^{n+2}} \mathbf{e}_z \\ \nabla \times \left(\frac{r_x \mathbf{r}}{r^n} \right) &= -\frac{r_z}{r^n} \mathbf{e}_y + \frac{r_y}{r^n} \mathbf{e}_z \end{aligned}$$

we have

$$\boldsymbol{\Omega}_{3,i}^{(1,f)} = \frac{F_i}{8\pi\mu r^3} \left[-r_z \mathbf{e}_y + r_y \mathbf{e}_z \right] \Big|_{\mathbf{r}=\mathbf{x}_3 - \mathbf{x}_i} = \frac{F_i}{8\pi\mu l_{i3}^3} (\mathbf{x}_3 - \mathbf{x}_i)_y \mathbf{e}_z \quad (\text{C.2})$$

and therefore

$$\boldsymbol{\Omega}_3^{(1)} = \sum_{i=1,2} \boldsymbol{\Omega}_{3,i}^{(1,f)} + \boldsymbol{\Omega}_{3,i}^{(1,e)} = \sum_{i=1,2} \frac{F_i}{8\pi\mu l_{i3}^3} (\mathbf{x}_3 - \mathbf{x}_i)_y \mathbf{e}_z. \quad (\text{C.3})$$

D Numerical scheme of two PMPY models

The following numerical scheme is written in terms of unscaled variables.

When the two PMPY models both lie along the x -axis, and the spheres are numbered 1, 2, 3, 4 from the negative to the positive x -direction, the equations (5.1 - 5.9) reduce to

$$\begin{pmatrix} A_{11} & A_{12} \\ A_{21} & A_{22} \end{pmatrix} \begin{pmatrix} \mathbf{U} \\ \mathbf{F} \end{pmatrix} = \begin{pmatrix} \mathbf{B}_1 \\ \mathbf{B}_2 \end{pmatrix} \quad (\text{D.1})$$

where

$$\mathbf{U} = \begin{pmatrix} U_1 \\ U_2 \\ U_3 \\ U_4 \end{pmatrix}, \quad \mathbf{F} = \mu^{-1} \begin{pmatrix} F_1 \\ F_2 \\ F_3 \\ F_4 \end{pmatrix}.$$

Here $A_{11} = -I_4$, where I_4 is the 4×4 identity matrix, $A_{12} = (a_{ij})$ is a symmetric 4×4 matrix, with

$$a_{ii} = \frac{1}{6\pi R_i}, \quad a_{ij} = \frac{1}{4\pi l_{ij}} \left(1 - \frac{R_i^2 + R_j^2}{3l_{ij}^2} \right)$$

and

$$(A_{21} \ A_{22}) = \begin{pmatrix} 1 & -1 & 0 & 0 & 0 & 0 & 0 \\ 0 & 0 & 1 & -1 & 0 & 0 & 0 \\ 0 & 0 & 0 & 0 & 1 & 1 & 0 \\ 0 & 0 & 0 & 0 & 0 & 0 & 1 \end{pmatrix}.$$

$\mathbf{B}_1 \in \mathbb{R}^4$, is given by

$$(\mathbf{B}_1)_i = - \sum_{j \neq i} \text{sign}(i-j) \dot{R}_j \left(\frac{R_j}{l_{ij}} \right)^2$$

and

$$\mathbf{B}_2 = \begin{pmatrix} -l_{12} \\ -l_{34} \\ 0 \\ 0 \end{pmatrix}.$$

On the other hand, when the two PMPY models swim in a plane, we approximate the scaled system to $O(\delta^2)$, hence the rigid motions of the spheres can be approximated by equations (5.12, 5.13). Returning to the unscaled equations, to further simplify the system, from equations (5.8) we know that $\mathbf{F}_1, \mathbf{F}_2$ are directed along \mathbf{e}_x and $\mathbf{F}_3, \mathbf{F}_4$ are directed along \mathbf{e}_y . Moreover,

$$F_2 = -F_1, \quad F_4 = -F_3$$

Hence the equation system (5.1 - 5.9) can be reduced to a system with unknowns

$$U_{1x}, U_{1y}, U_{2x}, U_{2y}, U_{3x'}, U_{3y'}, U_{3x''}, U_{3y''}, F_1, F_3$$

where $U_{1x} = \mathbf{U}_1 \cdot \mathbf{e}_x$, $U_{3x'} = \mathbf{U}_3 \cdot \mathbf{e}_{x'}$, and so on. Taking into account the fact that $\mathbf{e}_x = \mathbf{d}_{12}$ and $\mathbf{e}_{x'} = \mathbf{d}_{34}$, the nondimensional form of (D.1) can be simplified to

$$\begin{aligned}
& -U_{1x} + \left(\frac{1}{6\pi R_1} - \frac{1}{4\pi l_{12}} \right) \frac{F_1}{\mu} + \frac{1}{8\pi} \left[\frac{\mathcal{F}(\mathbf{d}_{31}; \mathbf{e}_{x'}, \mathbf{e}_x)}{l_{13}} - \frac{\mathcal{F}(\mathbf{d}_{41}; \mathbf{e}_{x'}, \mathbf{e}_x)}{l_{14}} \right] \frac{F_3}{\mu} \\
& = \dot{R}_2 \left(\frac{R_2}{l_{12}} \right)^2 - \dot{R}_3 \left(\frac{R_3}{l_{13}} \right)^2 (\mathbf{e}_x \cdot \mathbf{d}_{31}) - \dot{R}_4 \left(\frac{R_4}{l_{14}} \right)^2 (\mathbf{e}_x \cdot \mathbf{d}_{41}) \\
& -U_{1y} + \frac{1}{8\pi} \left[\frac{\mathcal{F}(\mathbf{d}_{31}; \mathbf{e}_{x'}, \mathbf{e}_y)}{l_{13}} - \frac{\mathcal{F}(\mathbf{d}_{41}; \mathbf{e}_{x'}, \mathbf{e}_y)}{l_{14}} \right] \frac{F_3}{\mu} = -\dot{R}_3 \left(\frac{R_3}{l_{13}} \right)^2 (\mathbf{e}_y \cdot \mathbf{d}_{31}) - \dot{R}_4 \left(\frac{R_4}{l_{14}} \right)^2 (\mathbf{e}_y \cdot \mathbf{d}_{41}) \\
& -U_{2x} + \left(-\frac{1}{6\pi R_2} + \frac{1}{4\pi l_{21}} \right) \frac{F_1}{\mu} + \frac{1}{8\pi} \left[\frac{\mathcal{F}(\mathbf{d}_{32}; \mathbf{e}_{x'}, \mathbf{e}_x)}{l_{23}} - \frac{\mathcal{F}(\mathbf{d}_{42}; \mathbf{e}_{x'}, \mathbf{e}_x)}{l_{24}} \right] \frac{F_3}{\mu} \\
& = -\dot{R}_1 \left(\frac{R_1}{l_{21}} \right)^2 - \dot{R}_3 \left(\frac{R_3}{l_{23}} \right)^2 (\mathbf{e}_x \cdot \mathbf{d}_{32}) - \dot{R}_4 \left(\frac{R_4}{l_{24}} \right)^2 (\mathbf{e}_x \cdot \mathbf{d}_{42}) \\
& -U_{2y} + \frac{1}{8\pi} \left[\frac{\mathcal{F}(\mathbf{d}_{32}; \mathbf{e}_{x'}, \mathbf{e}_y)}{l_{23}} - \frac{\mathcal{F}(\mathbf{d}_{42}; \mathbf{e}_{x'}, \mathbf{e}_y)}{l_{24}} \right] \frac{F_3}{\mu} = -\dot{R}_3 \left(\frac{R_3}{l_{23}} \right)^2 (\mathbf{e}_y \cdot \mathbf{d}_{32}) - \dot{R}_4 \left(\frac{R_4}{l_{24}} \right)^2 (\mathbf{e}_y \cdot \mathbf{d}_{42}) \\
& -U_{3x'} + \left(\frac{1}{6\pi R_3} - \frac{1}{4\pi l_{34}} \right) \frac{F_3}{\mu} + \frac{1}{8\pi} \left[\frac{\mathcal{F}(\mathbf{d}_{13}; \mathbf{e}_x, \mathbf{e}_{x'})}{l_{31}} - \frac{\mathcal{F}(\mathbf{d}_{23}; \mathbf{e}_x, \mathbf{e}_{x'})}{l_{32}} \right] \frac{F_1}{\mu} \\
& = -\dot{R}_1 \left(\frac{R_1}{l_{31}} \right)^2 (\mathbf{e}_{x'} \cdot \mathbf{d}_{13}) - \dot{R}_2 \left(\frac{R_2}{l_{32}} \right)^2 (\mathbf{e}_{x'} \cdot \mathbf{d}_{23}) + \dot{R}_4 \left(\frac{R_4}{l_{34}} \right)^2 \\
& -U_{3y'} + \frac{1}{8\pi} \left[\frac{\mathcal{F}(\mathbf{d}_{13}; \mathbf{e}_x, \mathbf{e}_{y'})}{l_{31}} - \frac{\mathcal{F}(\mathbf{d}_{23}; \mathbf{e}_x, \mathbf{e}_{y'})}{l_{32}} \right] \frac{F_1}{\mu} = -\dot{R}_1 \left(\frac{R_1}{l_{31}} \right)^2 (\mathbf{e}_{y'} \cdot \mathbf{d}_{13}) - \dot{R}_2 \left(\frac{R_2}{l_{32}} \right)^2 (\mathbf{e}_{y'} \cdot \mathbf{d}_{23}) \\
& -U_{4x'} + \left(-\frac{1}{6\pi R_4} + \frac{1}{4\pi l_{43}} \right) \frac{F_3}{\mu} + \frac{1}{8\pi} \left[\frac{\mathcal{F}(\mathbf{d}_{14}; \mathbf{e}_x, \mathbf{e}_{x'})}{l_{41}} - \frac{\mathcal{F}(\mathbf{d}_{24}; \mathbf{e}_x, \mathbf{e}_{x'})}{l_{42}} \right] \frac{F_1}{\mu} \\
& = -\dot{R}_1 \left(\frac{R_1}{l_{41}} \right)^2 (\mathbf{e}_{x'} \cdot \mathbf{d}_{14}) - \dot{R}_2 \left(\frac{R_2}{l_{42}} \right)^2 (\mathbf{e}_{x'} \cdot \mathbf{d}_{24}) - \dot{R}_3 \left(\frac{R_3}{l_{43}} \right)^2 \\
& -U_{4y'} + \frac{1}{8\pi} \left[\frac{\mathcal{F}(\mathbf{d}_{14}; \mathbf{e}_x, \mathbf{e}_{y'})}{l_{41}} - \frac{\mathcal{F}(\mathbf{d}_{24}; \mathbf{e}_x, \mathbf{e}_{y'})}{l_{42}} \right] \frac{F_1}{\mu} = -\dot{R}_1 \left(\frac{R_1}{l_{41}} \right)^2 (\mathbf{e}_{y'} \cdot \mathbf{d}_{14}) - \dot{R}_2 \left(\frac{R_2}{l_{42}} \right)^2 (\mathbf{e}_{y'} \cdot \mathbf{d}_{24}) \\
& U_{2x} \quad -U_{1x} = \dot{l}_{12} \\
& U_{4x'} \quad -U_{3x'} = \dot{l}_{34}
\end{aligned}$$

where

$$\mathcal{F}(\mathbf{d}; \mathbf{e}_\alpha, \mathbf{e}_\beta) = (\mathbf{e}_\alpha \cdot \mathbf{e}_\beta) + (\mathbf{e}_\alpha \cdot \mathbf{d})(\mathbf{e}_\beta \cdot \mathbf{d}).$$

E Asymptotic analysis of the three systems consisting of two hobbled PMPYs

For simplicity, we denote the distance between any two spheres i and j by l_{ij} . For example, $l_{13} = l_{12} + l_{23}$.

E.1 System A (two dumb-bells) with controls in $(\dot{l}_I, \dot{l}_{II})$

The asymptotic behavior of the velocity of the spheres is

$$\begin{aligned}
U_1 & \sim \frac{F_1}{6\pi\mu R_1} + \frac{F_2}{4\pi\mu l_{12}} + \frac{F_3}{4\pi\mu l_{13}} + \frac{F_4}{4\pi\mu l_{14}} \\
U_2 & \sim \frac{F_1}{4\pi\mu l_{12}} + \frac{F_2}{6\pi\mu R_2} + \frac{F_3}{4\pi\mu l_{23}} + \frac{F_4}{4\pi\mu l_{24}} \\
U_3 & \sim \frac{F_1}{4\pi\mu l_{13}} + \frac{F_2}{4\pi\mu l_{23}} + \frac{F_3}{6\pi\mu R_3} + \frac{F_4}{4\pi\mu l_{34}} \\
U_4 & \sim \frac{F_1}{4\pi\mu l_{14}} + \frac{F_2}{4\pi\mu l_{24}} + \frac{F_3}{4\pi\mu l_{34}} + \frac{F_4}{6\pi\mu R_4}
\end{aligned}$$

with relations and constraints

$$\begin{aligned} U_2 - U_1 = \dot{l}_{12} = \xi_I, \quad U_4 - U_3 = \dot{l}_{34} = \xi_{II} \\ F_1 + F_2 = 0, \quad F_3 + F_4 = 0. \end{aligned}$$

After scaling with hat notation omitted, the system becomes

$$\begin{aligned} U_1 &\sim \frac{F_1}{R_1} + \frac{3}{2} \left[\frac{F_2}{l_{12}} + \frac{F_3}{l_{13}} + \frac{F_4}{l_{14}} \right] \delta \\ U_2 &\sim \frac{F_2}{R_2} + \frac{3}{2} \left[\frac{F_1}{l_{12}} + \frac{F_3}{l_{23}} + \frac{F_4}{l_{24}} \right] \delta \\ U_3 &\sim \frac{F_3}{R_3} + \frac{3}{2} \left[\frac{F_1}{l_{13}} + \frac{F_2}{l_{23}} + \frac{F_4}{l_{34}} \right] \delta \\ U_4 &\sim \frac{F_4}{R_4} + \frac{3}{2} \left[\frac{F_1}{l_{14}} + \frac{F_2}{l_{24}} + \frac{F_3}{l_{34}} \right] \delta \\ U_2 - U_1 = \dot{l}_{12} = \xi_I, \quad U_4 - U_3 = \dot{l}_{34} = \xi_{II} \\ F_1 + F_2 = 0, \quad F_3 + F_4 = 0. \end{aligned}$$

With $F_2 = -F_1$, $F_4 = -F_3$, the system is simplified to

$$\begin{aligned} U_1 &\sim F_1 \left(\frac{1}{R_1} - \frac{3\delta}{2l_{12}} \right) + \frac{3}{2} F_3 \delta \left(\frac{1}{l_{13}} - \frac{1}{l_{14}} \right) \\ U_2 &\sim F_1 \left(\frac{3\delta}{2l_{12}} - \frac{1}{R_2} \right) + \frac{3}{2} F_3 \delta \left(\frac{1}{l_{23}} - \frac{1}{l_{24}} \right) \\ U_3 &\sim \frac{3}{2} F_1 \delta \left(\frac{1}{l_{13}} - \frac{1}{l_{23}} \right) + F_3 \left(\frac{1}{R_3} - \frac{3\delta}{2l_{34}} \right) \\ U_4 &\sim \frac{3}{2} F_1 \delta \left(\frac{1}{l_{14}} - \frac{1}{l_{24}} \right) + F_3 \left(\frac{3\delta}{2l_{34}} - \frac{1}{R_3} \right). \end{aligned}$$

When $R_1 = R_2 = R_3 = R_4 = R$,

$$\begin{aligned} \xi_I = U_2 - U_1 &\sim -F_1 \left(\frac{1}{R_1} + \frac{1}{R_2} \right) \Rightarrow F_1 = -\frac{R}{2} \xi_I \\ \xi_{II} = U_4 - U_3 &\sim -F_3 \left(\frac{1}{R_3} + \frac{1}{R_4} \right) \Rightarrow F_3 = -\frac{R}{2} \xi_{II}. \end{aligned}$$

Velocities of the PMPYs:

$$\begin{aligned} \bar{U}_I &= \frac{1}{2} (U_1 + U_2) = \frac{1}{2} F_1 \left(\frac{1}{R_1} - \frac{1}{R_2} \right) + \frac{3}{4} F_3 \delta \left(\frac{1}{l_{13}} - \frac{1}{l_{14}} + \frac{1}{l_{23}} - \frac{1}{l_{24}} \right) \sim -\frac{3}{8} R \xi_{II} \delta \left(\frac{1}{l_{13}} - \frac{1}{l_{14}} + \frac{1}{l_{23}} - \frac{1}{l_{24}} \right) \\ \bar{U}_{II} &= \frac{1}{2} (U_3 + U_4) = \frac{3}{4} F_1 \delta \left(\frac{1}{l_{13}} - \frac{1}{l_{23}} + \frac{1}{l_{14}} - \frac{1}{l_{24}} \right) + \frac{1}{2} F_3 \left(\frac{1}{R_3} - \frac{1}{R_4} \right) \sim -\frac{3}{8} R \xi_I \delta \left(\frac{1}{l_{13}} - \frac{1}{l_{23}} + \frac{1}{l_{14}} - \frac{1}{l_{24}} \right) \end{aligned}$$

Power of the PMPYs:

$$\begin{aligned} P_I &= F_1 U_1 + F_2 U_2 = F_1 (U_1 - U_2) = -F_1 \xi_I = \frac{R}{2} \xi_I^2 \\ P_{II} &= F_3 U_3 + F_4 U_4 = F_3 (U_3 - U_4) = -F_3 \xi_{II} = \frac{R}{2} \xi_{II}^2 \end{aligned}$$

However, we observe that although \bar{U}_I, \bar{U}_{II} scale like $O(\delta)$, the net translations X_I, X_{II} do not. Without loss of generality, we consider the first integral term in X_I :

$$\int \bar{U}_I dt = -\frac{3}{8} R \delta \int_0^1 \frac{\xi_{II}(t)}{l_{13}(t)} dt$$

l_{13} can be written as $l_{13} = l_{12} + l_{23} = 2 + \Delta l_{12} + \Delta l_{23}$, where $\Delta l_{12}, \Delta l_{23} \sim O(\delta)$, thus

$$\frac{1}{l_{13}} = \frac{1}{2 + \Delta l_{12} + \Delta l_{23}} = \frac{1}{2} - \frac{\Delta l_{12} + \Delta l_{23}}{4} + O(\delta^2)$$

and

$$\begin{aligned} -\frac{3}{8}R\delta \int_0^1 \frac{\xi_{II}(t)}{l_{13}(t)} dt &= -\frac{3}{8}R\delta \int_0^1 \xi_{II} \left(\frac{1}{2} - \frac{\Delta l_{12} + \Delta l_{23}}{4} \right) dt + O(\delta^3) \\ &= -\frac{3}{16}R\delta \int_0^1 \xi_{II} dt + \frac{3}{32}R\delta \int_0^1 \xi_{II} (\Delta l_{12} + \Delta l_{23}) dt + O(\delta^3). \end{aligned}$$

The first integral vanishes since it is an exact integral, the second one is an $O(\delta^2)$ term, hence

$$-\frac{3}{8}R\delta \int_0^1 \frac{\xi_{II}(t)}{l_{13}(t)} dt \sim O(\delta^2).$$

A similar argument applies to all other integrals in X_I, X_{II} , thus at most $X_I, X_{II} \sim O(\delta^2)$.

When the radii are not all equal, the leading order term of \bar{U}_I, \bar{U}_{II} scales as $O(1)$, but this does not contribute to the net translations and we still have $X_I, X_{II} \sim O(\delta^2)$. This is because the leading order terms are of the form $\Phi \xi(t)$, where the coefficient Φ depends on the radii only, thus $\int \Phi \xi dt$ is again an exact integral. Also this case, the $O(\delta)$ terms in \bar{U}_I, \bar{U}_{II} become more complicated, but they are still of the form $\Phi \xi/l_{ij}$, where Φ depends on the radii only, and the same argument above applies, thus in the end we have $X_I, X_{II} \sim O(\delta^2)$.

E.2 System B with controls in (\dot{R}_1, \dot{R}_3)

The asymptotic behavior of the velocity of each sphere is

$$\begin{aligned} U_1 &\sim \frac{F_1}{6\pi\mu R_1} + \left[\frac{F_2}{4\pi\mu l_{12}} - \left(\frac{R_2}{l_{12}} \right)^2 \dot{R}_2 \right] + \left[\frac{F_3}{4\pi\mu l_{13}} - \left(\frac{R_3}{l_{13}} \right)^2 \dot{R}_3 \right] + \left[\frac{F_4}{4\pi\mu l_{14}} - \left(\frac{R_4}{l_{14}} \right)^2 \dot{R}_4 \right] \\ U_2 &\sim \frac{F_2}{6\pi\mu R_2} + \left[\frac{F_1}{4\pi\mu l_{12}} + \left(\frac{R_1}{l_{12}} \right)^2 \dot{R}_1 \right] + \left[\frac{F_3}{4\pi\mu l_{23}} - \left(\frac{R_3}{l_{23}} \right)^2 \dot{R}_3 \right] + \left[\frac{F_4}{4\pi\mu l_{24}} - \left(\frac{R_4}{l_{24}} \right)^2 \dot{R}_4 \right] \\ U_3 &\sim \frac{F_3}{6\pi\mu R_3} + \left[\frac{F_1}{4\pi\mu l_{13}} + \left(\frac{R_1}{l_{13}} \right)^2 \dot{R}_1 \right] + \left[\frac{F_2}{4\pi\mu l_{23}} + \left(\frac{R_2}{l_{23}} \right)^2 \dot{R}_2 \right] + \left[\frac{F_4}{4\pi\mu l_{34}} - \left(\frac{R_4}{l_{34}} \right)^2 \dot{R}_4 \right] \\ U_4 &\sim \frac{F_4}{6\pi\mu R_4} + \left[\frac{F_1}{4\pi\mu l_{14}} + \left(\frac{R_1}{l_{14}} \right)^2 \dot{R}_1 \right] + \left[\frac{F_2}{4\pi\mu l_{24}} + \left(\frac{R_2}{l_{24}} \right)^2 \dot{R}_2 \right] + \left[\frac{F_3}{4\pi\mu l_{34}} + \left(\frac{R_3}{l_{34}} \right)^2 \dot{R}_3 \right] \end{aligned}$$

with relations

$$\begin{aligned} U_2 - U_1 &= 0, & U_4 - U_3 &= 0 \\ F_1 + F_2 &= 0, & F_3 + F_4 &= 0 \\ R_1^2 \dot{R}_1 + R_2^2 \dot{R}_2 &= 0 & \Rightarrow & R_2^2 \zeta_2 = -R_1^2 \zeta_1 \\ R_3^2 \dot{R}_3 + R_4^2 \dot{R}_4 &= 0 & \Rightarrow & R_4^2 \zeta_4 = -R_3^2 \zeta_3. \end{aligned}$$

After scaling with hat notation omitted

$$\begin{aligned} U_1 &\sim \frac{F_1}{R_1} + \left[\frac{3F_2}{2l_{12}} \delta - \left(\frac{R_2}{l_{12}} \right)^2 \zeta_2 \delta^2 \right] + \left[\frac{3F_3}{2l_{13}} \delta - \left(\frac{R_3}{l_{13}} \right)^2 \zeta_3 \delta^2 \right] + \left[\frac{3F_4}{2l_{14}} \delta - \left(\frac{R_4}{l_{14}} \right)^2 \zeta_4 \delta^2 \right] \\ U_2 &\sim \frac{F_2}{R_2} + \left[\frac{3F_1}{2l_{12}} \delta + \left(\frac{R_1}{l_{12}} \right)^2 \zeta_1 \delta^2 \right] + \left[\frac{3F_3}{2l_{23}} \delta - \left(\frac{R_3}{l_{23}} \right)^2 \zeta_3 \delta^2 \right] + \left[\frac{3F_4}{2l_{24}} \delta - \left(\frac{R_4}{l_{24}} \right)^2 \zeta_4 \delta^2 \right] \\ U_3 &\sim \frac{F_3}{R_3} + \left[\frac{3F_1}{2l_{13}} \delta + \left(\frac{R_1}{l_{13}} \right)^2 \zeta_1 \delta^2 \right] + \left[\frac{3F_2}{2l_{23}} \delta + \left(\frac{R_2}{l_{23}} \right)^2 \zeta_2 \delta^2 \right] + \left[\frac{3F_4}{2l_{34}} \delta - \left(\frac{R_4}{l_{34}} \right)^2 \zeta_4 \delta^2 \right] \\ U_4 &\sim \frac{F_4}{R_4} + \left[\frac{3F_1}{2l_{14}} \delta + \left(\frac{R_1}{l_{14}} \right)^2 \zeta_1 \delta^2 \right] + \left[\frac{3F_2}{2l_{24}} \delta + \left(\frac{R_2}{l_{24}} \right)^2 \zeta_2 \delta^2 \right] + \left[\frac{3F_3}{2l_{34}} \delta + \left(\frac{R_3}{l_{34}} \right)^2 \zeta_3 \delta^2 \right]. \end{aligned}$$

With $F_2 = -F_1, F_4 = -F_3$, the system becomes

$$\begin{aligned} U_1 &\sim F_1 \left(\frac{1}{R_1} - \frac{3\delta}{2l_{12}} \right) + \frac{3F_3}{2} \delta \left(\frac{1}{l_{13}} - \frac{1}{l_{14}} \right) + \delta^2 \left[- \left(\frac{R_2}{l_{12}} \right)^2 \zeta_2 - \left(\frac{R_3}{l_{13}} \right)^2 \zeta_3 - \left(\frac{R_4}{l_{14}} \right)^2 \zeta_4 \right] \\ U_2 &\sim F_1 \left(-\frac{1}{R_2} + \frac{3\delta}{2l_{12}} \right) + \frac{3F_3}{2} \delta \left(\frac{1}{l_{23}} - \frac{1}{l_{24}} \right) + \delta^2 \left[\left(\frac{R_1}{l_{12}} \right)^2 \zeta_1 - \left(\frac{R_3}{l_{23}} \right)^2 \zeta_3 - \left(\frac{R_4}{l_{24}} \right)^2 \zeta_4 \right] \\ U_3 &\sim \frac{3F_1}{2} \delta \left(\frac{1}{l_{13}} - \frac{1}{l_{23}} \right) + F_3 \left(\frac{1}{R_3} - \frac{3\delta}{2l_{34}} \right) + \delta^2 \left[\left(\frac{R_1}{l_{13}} \right)^2 \zeta_1 + \left(\frac{R_2}{l_{23}} \right)^2 \zeta_2 - \left(\frac{R_4}{l_{34}} \right)^2 \zeta_4 \right] \\ U_4 &\sim \frac{3F_1}{2} \delta \left(\frac{1}{l_{14}} - \frac{1}{l_{24}} \right) + F_3 \left(-\frac{1}{R_4} + \frac{3\delta}{2l_{34}} \right) + \delta^2 \left[\left(\frac{R_1}{l_{14}} \right)^2 \zeta_1 + \left(\frac{R_2}{l_{24}} \right)^2 \zeta_2 + \left(\frac{R_3}{l_{34}} \right)^2 \zeta_3 \right]. \end{aligned}$$

Expand F_1, F_3 as

$$F_1 = F_1^0 + \delta F_1^1 + \delta^2 F_1^2 + O(\delta^3), \quad F_3 = F_3^0 + \delta F_3^1 + \delta^2 F_3^2 + O(\delta^3);$$

then

$$\begin{aligned} U_1 &\sim \frac{F_1^0}{R_1} + \delta \frac{F_1^1}{R_1} - \delta \frac{3F_1^0}{2l_{12}} + \delta^2 \frac{F_1^2}{R_1} - \delta^2 \frac{3F_1^1}{2l_{12}} + \frac{3}{2} \delta F_3^0 \left(\frac{1}{l_{13}} - \frac{1}{l_{14}} \right) + \frac{3}{2} \delta^2 F_3^1 \left(\frac{1}{l_{13}} - \frac{1}{l_{14}} \right) \\ &\quad + \delta^2 \left[- \left(\frac{R_2}{l_{12}} \right)^2 \zeta_2 - \left(\frac{R_3}{l_{13}} \right)^2 \zeta_3 - \left(\frac{R_4}{l_{14}} \right)^2 \zeta_4 \right] + O(\delta^3) \\ U_2 &\sim -\frac{F_1^0}{R_2} - \delta \frac{F_1^1}{R_2} + \delta \frac{3F_1^0}{2l_{12}} - \delta^2 \frac{F_1^2}{R_2} + \delta^2 \frac{3F_1^1}{2l_{12}} + \frac{3}{2} \delta F_3^0 \left(\frac{1}{l_{23}} - \frac{1}{l_{24}} \right) + \frac{3}{2} \delta^2 F_3^1 \left(\frac{1}{l_{23}} - \frac{1}{l_{24}} \right) \\ &\quad + \delta^2 \left[\left(\frac{R_1}{l_{12}} \right)^2 \zeta_1 - \left(\frac{R_3}{l_{23}} \right)^2 \zeta_3 - \left(\frac{R_4}{l_{24}} \right)^2 \zeta_4 \right] + O(\delta^3) \\ U_3 &\sim \frac{F_3^0}{R_3} + \delta \frac{F_3^1}{R_3} - \delta \frac{3F_3^0}{2l_{34}} + \delta^2 \frac{F_3^2}{R_3} - \delta^2 \frac{3F_3^1}{2l_{34}} + \frac{3}{2} \delta F_1^0 \left(\frac{1}{l_{13}} - \frac{1}{l_{23}} \right) + \frac{3}{2} \delta^2 F_1^1 \left(\frac{1}{l_{13}} - \frac{1}{l_{23}} \right) \\ &\quad + \delta^2 \left[\left(\frac{R_1}{l_{13}} \right)^2 \zeta_1 + \left(\frac{R_2}{l_{23}} \right)^2 \zeta_2 - \left(\frac{R_4}{l_{34}} \right)^2 \zeta_4 \right] + O(\delta^3) \\ U_4 &\sim -\frac{F_3^0}{R_4} - \delta \frac{F_3^1}{R_4} + \delta \frac{3F_3^0}{2l_{34}} - \delta^2 \frac{F_3^2}{R_4} + \delta^2 \frac{3F_3^1}{2l_{34}} + \frac{3}{2} \delta F_1^0 \left(\frac{1}{l_{14}} - \frac{1}{l_{24}} \right) + \frac{3}{2} \delta^2 F_1^1 \left(\frac{1}{l_{14}} - \frac{1}{l_{24}} \right) \\ &\quad + \delta^2 \left[\left(\frac{R_1}{l_{14}} \right)^2 \zeta_1 + \left(\frac{R_2}{l_{24}} \right)^2 \zeta_2 + \left(\frac{R_3}{l_{34}} \right)^2 \zeta_3 \right] + O(\delta^3). \end{aligned}$$

Compare the $O(1)$ terms:

$$U_1^0 = U_2^0 \Rightarrow \frac{F_1^0}{R_1} = -\frac{F_1^0}{R_2} \Rightarrow F_1^0 = 0, \quad \text{similarly,} \quad F_3^0 = 0.$$

Compare the $O(\delta)$ terms:

$$U_1^1 = U_2^1 \Rightarrow \frac{F_1^1}{R_1} = -\frac{F_1^1}{R_2} \Rightarrow F_1^1 = 0, \quad \text{similarly,} \quad F_3^1 = 0.$$

Compare the $O(\delta^2)$ terms:

$$\begin{aligned} U_1^2 &= \frac{F_1^2}{R_1} + \left[- \left(\frac{R_2}{l_{12}} \right)^2 \zeta_2 - \left(\frac{R_3}{l_{13}} \right)^2 \zeta_3 - \left(\frac{R_4}{l_{14}} \right)^2 \zeta_4 \right] \\ U_2^2 &= -\frac{F_1^2}{R_2} + \left[\left(\frac{R_1}{l_{12}} \right)^2 \zeta_1 - \left(\frac{R_3}{l_{23}} \right)^2 \zeta_3 - \left(\frac{R_4}{l_{24}} \right)^2 \zeta_4 \right] \\ U_1^2 = U_2^2 &\Rightarrow F_1^2 = \frac{R_1 R_2}{R_1 + R_2} \left(\frac{1}{l_{13}^2} - \frac{1}{l_{23}^2} - \frac{1}{l_{14}^2} + \frac{1}{l_{24}^2} \right) R_3^2 \zeta_3 \end{aligned}$$

and similarly,

$$\begin{aligned} U_3^2 &= \frac{F_3^2}{R_3} + \left[\left(\frac{R_1}{l_{13}} \right)^2 \zeta_1 + \left(\frac{R_2}{l_{23}} \right)^2 \zeta_2 - \left(\frac{R_4}{l_{34}} \right)^2 \zeta_4 \right] \\ U_4^2 &= -\frac{F_3^2}{R_4} + \left[\left(\frac{R_1}{l_{14}} \right)^2 \zeta_1 + \left(\frac{R_2}{l_{24}} \right)^2 \zeta_2 + \left(\frac{R_3}{l_{34}} \right)^2 \zeta_3 \right] \\ U_3^2 = U_4^2 &\Rightarrow F_3^2 = \frac{R_3 R_4}{R_3 + R_4} \left(\frac{1}{l_{14}^2} - \frac{1}{l_{13}^2} - \frac{1}{l_{24}^2} + \frac{1}{l_{23}^2} \right) R_1^2 \zeta_1. \end{aligned}$$

Velocities of the PMPYs:

$$\begin{aligned} U_I = U_1 = U_2 &= \frac{R_1^2}{l_{12}^2} \zeta_1 \delta^2 + R_3^2 \zeta_3 \delta^2 \left[\frac{R_1}{R_1 + R_2} \left(\frac{1}{l_{14}^2} - \frac{1}{l_{13}^2} \right) + \frac{R_2}{R_1 + R_2} \left(\frac{1}{l_{24}^2} - \frac{1}{l_{23}^2} \right) \right] \\ U_{II} = U_3 = U_4 &= \frac{R_3^2}{l_{34}^2} \zeta_3 \delta^2 + R_1^2 \zeta_1 \delta^2 \left[\frac{R_3}{R_3 + R_4} \left(\frac{1}{l_{13}^2} - \frac{1}{l_{23}^2} \right) + \frac{R_4}{R_3 + R_4} \left(\frac{1}{l_{14}^2} - \frac{1}{l_{24}^2} \right) \right] \end{aligned}$$

Power of the PMPYs:

$$P_I = \frac{8}{3}(R_1\zeta_1^2 + R_2\zeta_2^2) = \frac{8}{3}R_1\frac{R_1^3 + R_2^3}{R_2^3}\zeta_1^2$$

$$P_{II} = \frac{8}{3}(R_3\zeta_3^2 + R_4\zeta_4^2) = \frac{8}{3}R_3\frac{R_3^3 + R_4^3}{R_4^3}\zeta_3^2$$

E.3 System C with controls in (\dot{I}_I, \dot{R}_3)

The asymptotic behavior of the velocity of each sphere is

$$U_1 \sim \frac{F_1}{6\pi\mu R_1} + \frac{F_2}{4\pi\mu l_{12}} + \left[\frac{F_3}{4\pi\mu l_{13}} - \left(\frac{R_3}{l_{13}}\right)^2 \dot{R}_3 \right] + \left[\frac{F_4}{4\pi\mu l_{14}} - \left(\frac{R_4}{l_{14}}\right)^2 \dot{R}_4 \right]$$

$$U_2 \sim \frac{F_2}{6\pi\mu R_2} + \frac{F_1}{4\pi\mu l_{12}} + \left[\frac{F_3}{4\pi\mu l_{23}} - \left(\frac{R_3}{l_{23}}\right)^2 \dot{R}_3 \right] + \left[\frac{F_4}{4\pi\mu l_{24}} - \left(\frac{R_4}{l_{24}}\right)^2 \dot{R}_4 \right]$$

$$U_3 \sim \frac{F_3}{6\pi\mu R_3} + \frac{F_1}{4\pi\mu l_{13}} + \frac{F_2}{4\pi\mu l_{23}} + \left[\frac{F_4}{4\pi\mu l_{34}} - \left(\frac{R_4}{l_{34}}\right)^2 \dot{R}_4 \right]$$

$$U_4 \sim \frac{F_4}{6\pi\mu R_4} + \frac{F_1}{4\pi\mu l_{14}} + \frac{F_2}{4\pi\mu l_{24}} + \left[\frac{F_3}{4\pi\mu l_{34}} + \left(\frac{R_3}{l_{34}}\right)^2 \dot{R}_3 \right]$$

with relations

$$U_2 - U_1 = \dot{I}_{12} = \xi_I, \quad U_4 - U_3 = 0$$

$$F_1 + F_2 = 0, \quad F_3 + F_4 = 0$$

$$R_3^2\zeta_3 + R_4^2\zeta_4 = 0 \Rightarrow R_4^2\zeta_4 = -R_3^2\zeta_3.$$

After scaling

$$U_1 \sim \frac{F_1}{R_1} + \frac{3F_2}{2l_{12}}\delta + \left[\frac{2F_3}{2l_{13}}\delta - \left(\frac{R_3}{l_{13}}\right)^2\zeta_3\delta^2 \right] + \left[\frac{3F_4}{2l_{14}}\delta - \left(\frac{R_4}{l_{14}}\right)^2\zeta_4\delta^2 \right]$$

$$U_2 \sim \frac{F_2}{R_2} + \frac{3F_1}{2l_{12}}\delta + \left[\frac{2F_3}{2l_{23}}\delta - \left(\frac{R_3}{l_{23}}\right)^2\zeta_3\delta^2 \right] + \left[\frac{3F_4}{2l_{24}}\delta - \left(\frac{R_4}{l_{24}}\right)^2\zeta_4\delta^2 \right]$$

$$U_3 \sim \frac{F_3}{R_3} + \frac{3F_1}{2l_{13}}\delta + \frac{3F_2}{2l_{23}}\delta + \left[\frac{3F_4}{2l_{34}}\delta - \left(\frac{R_4}{l_{34}}\right)^2\zeta_4\delta^2 \right]$$

$$U_4 \sim \frac{F_4}{R_4} + \frac{3F_1}{2l_{14}}\delta + \frac{3F_2}{2l_{24}}\delta + \left[\frac{3F_3}{2l_{34}}\delta + \left(\frac{R_3}{l_{34}}\right)^2\zeta_3\delta^2 \right].$$

With $F_2 = -F_1$, $F_4 = -F_3$, the system is simplified to

$$U_1 \sim \frac{F_1}{R_1} - \frac{3F_1}{2l_{12}}\delta + \left[\frac{3F_3}{2l_{13}}\delta - \left(\frac{R_3}{l_{13}}\right)^2\zeta_3\delta^2 \right] + \left[-\frac{3F_3}{2l_{14}}\delta + \left(\frac{R_3}{l_{14}}\right)^2\zeta_3\delta^2 \right]$$

$$U_2 \sim -\frac{F_1}{R_2} + \frac{3F_1}{2l_{12}}\delta + \left[\frac{3F_3}{2l_{23}}\delta - \left(\frac{R_3}{l_{23}}\right)^2\zeta_3\delta^2 \right] + \left[-\frac{3F_3}{2l_{24}}\delta + \left(\frac{R_3}{l_{24}}\right)^2\zeta_3\delta^2 \right]$$

$$U_3 \sim \frac{F_3}{R_3} + \frac{3F_1}{2l_{13}}\delta - \frac{3F_1}{2l_{23}}\delta + \left[-\frac{3F_3}{2l_{34}}\delta + \left(\frac{R_3}{l_{34}}\right)^2\zeta_3\delta^2 \right]$$

$$U_4 \sim -\frac{F_3}{R_4} + \frac{3F_1}{2l_{14}}\delta - \frac{3F_1}{2l_{24}}\delta + \left[\frac{3F_3}{2l_{34}}\delta + \left(\frac{R_3}{l_{34}}\right)^2\zeta_3\delta^2 \right].$$

For PMPY I,

$$\xi_I = U_2 - U_1 \sim -F_1\left(\frac{1}{R_1} + \frac{1}{R_2}\right) \Rightarrow F_1 = -\frac{R_1 R_2}{R_1 + R_2}\xi_I,$$

thus for PMPY II,

$$\begin{aligned} U_3 &\sim \frac{F_3}{R_3} - \frac{3}{2} \frac{R_1 R_2}{R_1 + R_2} \xi_I \delta \left(\frac{1}{l_{13}} - \frac{1}{l_{23}} \right) - \frac{3F_3}{2l_{34}} \delta + \left(\frac{R_3}{l_{34}} \right)^2 \zeta_3 \delta^2 \\ U_4 &\sim -\frac{F_3}{R_4} - \frac{3}{2} \frac{R_1 R_2}{R_1 + R_2} \xi_I \delta \left(\frac{1}{l_{14}} - \frac{1}{l_{24}} \right) + \frac{3F_3}{2l_{34}} \delta + \left(\frac{R_3}{l_{34}} \right)^2 \zeta_3 \delta^2. \end{aligned}$$

Expand F_3 as $F_3 = F_3^0 + \delta F_3^1 + \delta^2 F_3^2 + O(\delta^3)$,

$$\begin{aligned} U_3 &\sim \frac{F_3^0}{R_3} + \delta \frac{F_3^1}{R_3} + \delta^2 \frac{F_3^2}{R_3} - \frac{3}{2} \frac{R_1 R_2}{R_1 + R_2} \xi_I \delta \left(\frac{1}{l_{13}} - \frac{1}{l_{23}} \right) - \frac{3F_3^0}{2l_{34}} \delta - \frac{3F_3^1}{2l_{34}} \delta^2 + \left(\frac{R_3}{l_{34}} \right)^2 \zeta_3 \delta^2 \\ U_4 &\sim -\frac{F_3^0}{R_4} - \delta \frac{F_3^1}{R_4} - \delta^2 \frac{F_3^2}{R_4} - \frac{3}{2} \frac{R_1 R_2}{R_1 + R_2} \xi_I \delta \left(\frac{1}{l_{14}} - \frac{1}{l_{24}} \right) + \frac{3F_3^0}{2l_{34}} \delta + \frac{3F_3^1}{2l_{34}} \delta^2 + \left(\frac{R_3}{l_{34}} \right)^2 \zeta_3 \delta^2 \end{aligned}$$

Compare the $O(1)$ terms

$$U_3^0 = U_4^0 \Rightarrow \frac{F_3^0}{R_3} = -\frac{F_3^0}{R_4} \Rightarrow F_3^0 = 0.$$

Compare the $O(\delta)$ terms

$$U_3^1 = U_4^1 \Rightarrow F_3^1 = \frac{3}{2} \frac{R_1 R_2}{R_1 + R_2} \frac{R_3 R_4}{R_3 + R_4} \xi_I \left(\frac{1}{l_{13}} - \frac{1}{l_{23}} - \frac{1}{l_{14}} + \frac{1}{l_{24}} \right)$$

Velocities of the PMPYs:

$$\begin{aligned} \bar{U}_I &= \frac{1}{2}(U_1 + U_2) \\ &= \frac{9}{8} \frac{R_1 R_2 R_3 R_4}{(R_1 + R_2)(R_3 + R_4)} \xi_I \delta^2 \left(\frac{1}{l_{13}} - \frac{1}{l_{14}} + \frac{1}{l_{23}} - \frac{1}{l_{24}} \right)^2 + \frac{1}{2} R_3^2 \zeta_3 \delta^2 \left(\frac{1}{l_{14}^2} - \frac{1}{l_{13}^2} + \frac{1}{l_{24}^2} - \frac{1}{l_{23}^2} \right) \\ \bar{U}_{II} &= U_3 = U_4 \\ &\sim \frac{3}{2} \frac{R_1 R_2}{R_1 + R_2} \xi_I \delta \left[\frac{R_3}{R_3 + R_4} \left(\frac{1}{l_{23}} - \frac{1}{l_{13}} \right) + \frac{R_4}{R_3 + R_4} \left(\frac{1}{l_{24}} - \frac{1}{l_{14}} \right) \right] \end{aligned}$$

Power of the PMPYs:

$$\begin{aligned} P_I &= F_1 U_1 + F_2 U_2 = F_1 (U_1 - U_2) = -F_1 \xi_I = \frac{R_1 R_2}{R_1 + R_2} \xi_I^2 \\ P_{II} &= \frac{8}{3} (R_3 \zeta_3^2 + R_4 \zeta_4^2) = \frac{8}{3} R_3 \frac{R_3^3 + R_4^3}{R_3^2} \zeta_3^2 \end{aligned}$$

References

- Alexander, G., Pooley, C., & Yeomans, J. (2009). *Journal of Physics: Condensed Matter*, **21** (20), 204108.
 Alexander, G. P. & Yeomans, J. M. (2008). *EPL (Europhysics Letters)*, **83** (3), 34006.
 Avron, J., Kenneth, O., & Oaknin, D. (2005). *New Journal of Physics*, **7**, 234.
 Barry, N. P. & Bretscher, M. S. (2010). *Proceedings of the National Academy of Sciences*, **107** (25), 11376.
 Bergert, M., Chandradoss, S. D., Desai, R. A., & Paluch, E. (2012). *Proceedings of the National Academy of Sciences*, **109** (36), 14434–14439.
 Binamé, F., Pawlak, G., Roux, P., & Hibner, U. (2010). *Mol. BioSyst.* **6** (4), 648–661.
 Brennen, C. E. (2013). *Cavitation and Bubble Dynamics*. Cambridge University Press.
 Brenner, H. (1961). *Chemical Engineering Science*, **16** (3-4), 242–251.
 Charras, G. & Paluch, E. (2008). *Nature Reviews Molecular Cell Biology*, **9** (9), 730–736.
 Childress, S. (1977). *Mechanics of swimming and flying*. Courant Institute of Mathematical Sciences.
 Cooley, M. & O'Neill, M. (1969a). *Mathematika*, **16** (01), 37–49.
 Cooley, M. & O'Neill, M. (1969b). In: *Mathematical Proceedings of the Cambridge Philosophical Society* volume 66 pp. 407–415, Cambridge Univ Press.

- Curtis, M. P. & Gaffney, E. A. (2013). *Physical Review E*, **87** (4), 043006.
- Dunkel, J., Putz, V. B., Zaid, I. M., & Yeomans, J. M. (a). *Soft Matter*, (17), 4268–4276.
- Elgeti, J., Winkler, R. G., & Gompper, G. (2015). *Reports on Progress in Physics*, **78** (5), 056601.
- Fackler, O. T. & Grosse, R. (2008). *The Journal of Cell Biology*, **181** (6), 879–884.
- Friedl, P. & Alexander, S. (2011). *Cell*, **147** (5), 992–1009.
- Friedl, P. & Wolf, K. (2003). *Nat. Rev. Cancer*, **3** (5), 362–74.
- Hancock, G. (1953). *Proceedings of the Royal Society of London. Series A. Mathematical and Physical Sciences*, **217** (1128), 96–121.
- Higdon, J. J. L. (1979). , **94**, 331–351.
- Ishikawa, T., Locsei, J., & Pedley, T. (2010). *Physical Review E*, **82** (2), 021408.
- Kim, S. & Karrila, S. J. (1991). *Microhydrodynamics: Principles and Selected Applications*. New York: Butterworth-Heinemann.
- Koiller, J., Ehlers, K., & Montgomery, R. (1996). *Journal of Nonlinear Science*, **6** (6), 507–541.
- Kurtuldu, H., Guasto, J. S., Johnson, K. A., & Gollub, J. P. (2011). *Proceedings of the National Academy of Sciences*, **108** (26), 10391–10395.
- Lämmermann, T., Bader, B. L., Monkley, S. J., Worbs, T., Wedlich-Söldner, R., Hirsch, K., Keller, M., Förster, R., Critchley, D. R., Fässler, R., *et al.* (2008). *Nature*, **453** (7191), 51–55.
- Lauga, E. (2011). *Soft Matter*, **7** (7), 3060–3065.
- Lauga, E. & Bartolo, D. (2008). *Physical Review E*, **78** (3), 030901.
- Leptos, K. C., Guasto, J. S., Gollub, J. P., Pesci, A. I., & Goldstein, R. E. (2009). *Physical Review Letters*, **103** (19), 198103.
- Liang, Z., Gimbutas, Z., Greengard, L., Huang, J., & Jiang, S. (2013). *Journal of Computational Physics*, **234**, 133–139.
- Lin, Z., Thiffeault, J.-L., & Childress, S. (2011). *Journal of Fluid Mechanics*, **669**, 167–177.
- Luke, J. H. (1989). *SIAM Journal on Applied Mathematics*, **49** (6), 1635–1651.
- Maiuri, P., Rupprecht, J.-F., Wieser, S., Rupprecht, V., Bénichou, O., Carpi, N., Coppey, M., Beco, S. D., Gov, N., Heisenberg, C.-P., *et al.* (2015). *Cell*, **161** (2), 374–386.
- Miño, G., Mallouk, T. E., Darnige, T., Hoyos, M., Dauchet, J., Dunstan, J., Soto, R., Wang, Y., Rousselet, A., & Clement, E. (2011). *Physical review letters*, **106** (4), 048102.
- Najafi, A. & Golestanian, R. (2004). *Physical Review E*, **69** (6), 062901.
- Phan-Thien, N., Tran-Cong, T., & Ramia, M. (1987). *Journal of Fluid Mechanics*, **184**, 533–549.
- Pozrikidis, C. (1992). *Boundary integral and singularity methods for linearized viscous flow*. Number 8. Cambridge Univ Pr.
- Purcell, E. M. (1977). *Am. J. Phys.*, **45** (1), 3–11.
- Pushkin, D. O., Shum, H., & Yeomans, J. M. (2013). *Journal of Fluid Mechanics*, **726**, 5–25.
- Qiu, T., Lee, T.-C., Mark, A. G., Morozov, K. I., Münster, R., Mierka, O., Turek, S., Leshansky, A. M., & Fischer, P. (2014). *Nature Communications*, **5**.
- Renkawitz, J., Schumann, K., Weber, M., Lämmermann, T., Pflücke, H., Piel, M., Polleux, J., Spatz, J. P., & Sixt, M. (2009). *Nature Cell Biology*, **11** (12), 1438–1443.
- Renkawitz, J. & Sixt, M. (2010). *EMBO reports*, **11** (10), 744–750.
- Rupprecht, V., Wieser, S., Callan-Jones, A., Smutny, M., Morita, H., Sako, K., Barone, V., Ritsch-Marte, M., Sixt, M., Voituriez, R., *et al.* (2015). *Cell*, **160** (4), 673–685.
- Rushkin, I., Kantsler, V., & Goldstein, R. E. (2010). *Physical review letters*, **105** (18), 188101.
- Shum, H., Gaffney, E., & Smith, D. (2010). In: *Proceedings of the Royal Society of London A: Mathematical, Physical and Engineering Sciences* volume 466 pp. 1725–1748, The Royal Society.
- Sokolov, A., Goldstein, R. E., Feldchtein, F. I., & Aranson, I. S. (2009). *Physical Review E*, **80** (3), 031903.
- Stimson, M. & Jeffery, G. (1926). *Proceedings of the Royal Society of London. Series A, Containing Papers of a Mathematical and Physical Character*, **111** (757), 110–116.
- Stone, H. A. & Samuel, A. D. T. (1996). *Physical Review Letters*, **77** (19), 4102–4104.
- Taylor, G. (1952). *Proceedings of the Royal Society of London. Series A, Mathematical and Physical Sciences*, , 225–239.
- Underhill, P. T., Hernandez-Ortiz, J. P., & Graham, M. D. (2008). *Physical Review Letters*, **100** (24), 248101.
- Van Haastert, P. J. (2011). *PLoS one*, **6** (11), e27532.
- van Zijl, F., Krupitza, G., & Mikulits, W. (2011). *Mutation Research/Reviews in Mutation Research*, **728** (1), 23–34.
- Wajnryb, E., Mizerski, K. A., Zuk, P. J., & Szymczak, P. (2013). *Journal of Fluid Mechanics*, **731**, R3.
- Wang, Q., Hu, J., & Othmer, H. (2012). In: *Natural Locomotion in Fluids and on Surfaces* pp. 185–195. Springer.
- Wang, Q. & Othmer, H. G. (2015). *Mathematical Biosciences and Engineering*, **12** (6), 1303–1320.
- Wang, Q. & Othmer, H. G. (2016). *Journal of mathematical biology*, **72** (7), 1893–1926.
- Welch, M. D. (2015). *Cell*, **160** (4), 581–582.
- Wolf, K., Mazo, I., Leung, H., Engelke, K., Andrian, U. H. V., Deryugina, E. I., Strongin, A. Y., Bröcker, E. B., & Friedl, P. (2003). *The Journal of Cell Biology*, **160** (2), 267–277.
- Wu, X.-L. & Libchaber, A. (2000). *Physical Review Letters*, **84** (13), 3017.
- Yamakawa, H. (1970). *The Journal of Chemical Physics*, **53** (1), 436–443.
- Yeomans, J. M., Pushkin, D. O., & Shum, H. (2014). *The European Physical Journal Special Topics*, **223** (9), 1771–1785.

-
- Zaid, I. M., Dunkel, J., & Yeomans, J. M. (2011). *Journal of The Royal Society Interface*, **8** (62), 1314–1331.
- Zatulovskiy, E., Tyson, R., Bretschneider, T., & Kay, R. R. (2014). *J. Cell Biol.* **204** (6), 1027–1044.
- Zuk, P., Wajnryb, E., Mizerski, K., & Szymczak, P. (2014). *Journal of Fluid Mechanics*, **741**, R5.